SANDIA REPORT

SAND2014-3136
Unlimited Release
Printed May 2014

Effects of Increasing Tip Velocity on Wind Turbine Rotor Design

Brian R. Resor, David C. Maniaci, Jonathan C. Berg, Phillip Richards

Prepared by
Sandia National Laboratories
Albuquerque, New Mexico 87185 and Livermore, California 94550

Sandia National Laboratories is a multi-program laboratory managed and operated by Sandia Corporation, a wholly owned subsidiary of Lockheed Martin Corporation, for the U.S. Department of Energy's National Nuclear Security Administration under contract DE-AC04-94AL85000.

Issued by Sandia National Laboratories, operated for the United States Department of Energy by Sandia Corporation.

Available to DOE and DOE contractors from
U.S. Department of Energy
Office of Scientific and Technical Information
P.O. Box 62
Oak Ridge, TN 37831

Telephone: (865) 576-8401
Facsimile: (865) 576-5728
E-Mail: reports@adonis.osti.gov
Online ordering: http://www.osti.gov/bridge

Available to the public from
U.S. Department of Commerce
National Technical Information Service
5285 Port Royal Rd.
Springfield, VA 22161

Telephone: (800) 553-6847
Facsimile: (703) 605-6900
E-Mail: orders@ntis.fedworld.gov
Online order: http://www.ntis.gov/help/ordermethods.asp?loc=7-4-0#online

SAND2014-3136
Unlimited Release
Printed May 2014

Effects of Increasing Tip Velocity on Wind Turbine Rotor Design

Brian R. Resor, David C. Maniaci, Jonathan C. Berg, Phillip Richards
Wind Energy Technologies Department
Sandia National Laboratories
P.O. Box 5800
Albuquerque, New Mexico 87185-1124

Abstract

A reduction in cost of energy from wind is anticipated when maximum allowable tip velocity is allowed to increase. Rotor torque decreases as tip velocity increases and rotor size and power rating are held constant. Reduction in rotor torque yields a lighter weight gearbox, a decrease in the turbine cost, and an increase in the capacity for the turbine to deliver cost competitive electricity. The high speed rotor incurs costs attributable to rotor aero-acoustics and system loads. The increased loads of high speed rotors drive the sizing and cost of other components in the system. Rotor, drivetrain, and tower designs at 80 m/s maximum tip velocity and 100 m/s maximum tip velocity are created to quantify these effects. Component costs, annualized energy production, and cost of energy are computed for each design to quantify the change in overall cost of energy resulting from the increase in turbine tip velocity. High fidelity physics based models rather than cost and scaling models are used to perform the work. Results provide a quantitative assessment of anticipated costs and benefits for high speed rotors. Finally, important lessons regarding full system optimization of wind turbines are documented.

ACKNOWLEDGMENTS

The authors thank the members of the NREL systems engineering team who worked closely with Sandia authors to execute the investigation: Katherine Dykes, Yi Guo, Andrew Ning, Andrew Platt, and Paul Veers.

CONTENTS

FIGURES

TABLES

NOMENCLATURE

AEP	Annual Energy Production
c	Chord length
C	Single cycle material strength
C_p	Rotor power coefficient
C_T	Rotor thrust coefficient
CFD	Computational Fluid Dynamics
CRP	Carbon Reinforced Polyester
d	Distance from the elastic center to the mid-thickness of blade skin
DB	Double-Bias material
DLC	Design Load Case
DOE	Department of Energy
DOWEC	Dutch Offshore Wind Energy Converter
E	Young's modulus
ECD	Extreme Coherent gust with Direction change
EI	Section stiffness
ETM	Extreme Turbulence Model
EWM	Extreme Wind Model
EWS	Extreme Wind Shear
FE	Finite Element
G	Shear modulus
GRP	Glass Reinforced Polyester
GUI	Graphical User Interface
IEC	International Electro-technical Commission
LCOE	Levelized Cost of Energy
LE	Leading edge
M	Bending moment
NACA	National Advisory Committee for Aeronautics
NREL	National Renewable Energy Laboratory
NTM	Normal Turbulence Model
S	Material stress
SNL	Sandia National Laboratories
t/c	Airfoil thickness to chord ratio
TE	Trailing edge
TSR	Tip speed ratio
UCS	Ultimate Compressive Strength
UD	Uni-Directional material
UTS	Ultimate Tensile Strength
ε	Strain
ν	Poisson ratio

EXECUTIVE SUMMARY

Modern land-based wind turbine rotors operate up to tip velocities of 75 to 80 meters per second because noise from aero-acoustic sources on the blade typically constrains the maximum tip velocity. Some modern rotors are able to operate within adequate noise constraints at even higher tip speeds when development of aero-acoustic noise mitigation technologies are successful or when the rotors are intended for farms offering minimal public exposure to noise, such as an offshore farm.

System benefits of high speed rotors have been the subject of discussion over many years. In general, rotor torque decreases as tip velocity increases and rotor size and power rating are held constant. A reduction in rotor torque translates into a gearbox that is lighter weight and less expensive. If all other components remain unchanged as rotor tip velocity increases, the less expensive gearbox yields a decrease in the turbine cost and ultimately an improvement in the ability for the turbine to deliver cost competitive electricity. However, resulting changes in loads on the rotor, as well as the rest of the turbine system, can have a strong effect on the sizing and cost of other components in the system.

The magnitude of these costs and benefits are not well quantified. The NREL 5MW reference turbine model was used to initialize design concepts for rotor, drivetrain, and tower at 80 m/s maximum tip velocity and 100 m/s maximum tip velocity. Component costs, AEP, and then LCOE were computed for each design to quantify the change in overall LCOE as a result of changing the turbine tip velocity. High fidelity, physics based models instead of more common, empirical cost and scaling models were used to perform the work. The detailed component designs were guided by standard design practices. The quantified change in system LCOE resulting from increasing tip velocity can be used to motivate investments in research to overcome barriers related to aero-acoustics.

This investigation combined core competencies of the National Renewable Energy Laboratory and Sandia National Laboratories. Technical tasks were defined as follows:

- NREL
    - Full aeroelastic system loads analysis
    - Drivetrain design
    - Tower design
    - Aero-acoustic noise estimation
    - Cost modeling, including computation of component costs and AEP
- SNL
    - Rotor design (aerodynamics and structures)

The present Sandia report includes detailed documentation of the Sandia rotor design methods and results. A joint NREL-Sandia report includes a high-level summary of the rotor designs and documents results of the full system study [1].

Rotor designs were created in a two-step process. First, an aero-structural optimization process was used to identify the blade geometry which yielded the highest annual energy production

(AEP) for the lightest blade structural design. Second, the promising generic blade structural designs were used to initialize a detailed structural optimization in which spar cap, panels and trailing edge reinforcements are sized such that the blades meet the intent of design standards. The outcomes were rotor aerodynamic-structural designs which

- were as light as possible (assuming weight is directly related to cost),
- met a consistent set of design criteria, and
- captured as much energy as possible.

Optimized designs for 80 and 100 m/s tip velocity rotors were used in the full system loads and cost model to arrive at overall COE estimates which quantified the expected system benefits of increased tip velocity designs.

Results of the rotor investigation show that an increase of the maximum allowable tip speed leads to decreased rotor torque, increased rotor thrust loads, increased blade mass and increased blade cost. Rotor torque decreased by 20% as a direct result of the increase in rotor operating speed. The decrease in rotor torque has a strong beneficial effect on the cost of a gearbox. The rotor thrust load increased approximately 13-23%, depending on the approach used for increasing the tip velocity to 100 m/s from 80 m/s. Rotor loads drive the cost and sizing of other components in the turbine system: bearings, shafts, gearbox, bedplate and tower. Blade mass and cost increased approximately 2-9%, depending on the approach used for increasing the tip velocity to 100 m/s. Rotor loads and blade mass increases will lead to increased component costs within the larger system [1].

Important lessons regarding coupling of rotor design and full system design were demonstrated. The optimization found two approaches for design of the high speed rotor. The first strategy led to the lightest and cheapest blades but highest rotor loads as well as highest increases in balance of turbine system costs (with the exception of the gearbox). The second led to a smaller increase in rotor loads but highest blade cost because a decrease in blade chord and absolute thickness commands significant additional reinforcing material to enable sufficient blade flapwise and edgewise stiffness. The heavier blade was shown to be more beneficial in terms of the full system design and cost analysis. The lower system cost is driven by lower system loads.

Tower clearance criteria causes conventional designs to be stiffness driven. Final design examples previewed the system benefits of elimination of the tower clearance design driver. A high speed rotor which is not stiffness driven is approximately representative of either an upwind rotor including a large amount of upwind prebend or coning, or a downwind rotor which has no downwind tower clearance constraint. These designs are frequency and/or fatigue driven. The investigation showed an additional decrease in blade mass as much as 17% for a high speed flexible rotor.

1. BACKGROUND

In the early days of modern wind turbines (circa 1980), blade tip velocities were capped in the vicinity of 60 m/s and noise levels were in the vicinity of 100dB. In the 1990's, blade designers moved from square tips to more pointed "shark fin" tips. The innovation enabled blade tip velocities to increase to approximately 65 m/s while maintaining noise levels under 100dB. Land-based wind project development recently has constrained turbine designs to operate at blade tip velocities in the range of 75 to 80 m/s, or slightly higher. A proprietary "noise mode" of operation is used to mitigate noise by reducing rotor speeds at night. Figure 1 depicts the estimated maximum tip speeds that are determined by review of current online wind turbine product literature.

Turbine noise levels are usually dominated by blade tip noise when appropriate measures have been taken to mitigate sound emissions and audible tones from the tower head machinery within the nacelle and the power electronic converters often located within the tower base. The blade tip velocity constraint arises largely from blade tip aero-acoustic noise generation. Several components of aerodynamic noise are important:

- Turbulent inflow noise
- Tip vortex noise
- Airfoil boundary layer noise
- Trailing edge noise
- Separation noise

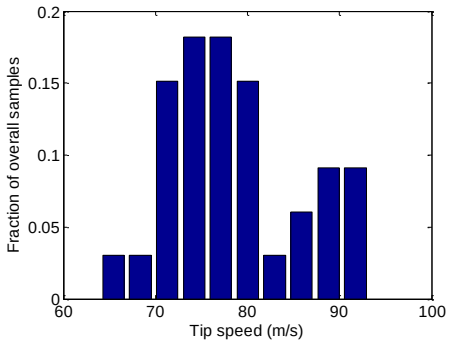

Figure 1: Estimated tip speeds for a collection of currently available turbine models

The opportunity to reduce drivetrain cost is realized via a proportionate reduction in drivetrain torque capacity if the acoustic (tip velocity) constraint is removed. The reduction in drivetrain torque capacity may lead to cheaper and lighter gearboxes as well as lighter and cheaper balance of turbine components as a result of a lighter drivetrain. However, the problem is more complex. Design tip speed ratio for the ideal aerodynamic rotor increases as tip velocity increases. As design tip speed ratio is increased, for any given airfoil selection, the solidity of an optimum rotor decreases as the square of tip speed ratio. Reduced solidity leads to reduced blade absolute thickness and leads to reduced bending moduli of the blade sections, i.e. more flexible blades. Blade flexibility is a challenge for upwind rotor designs which are stiffness driven based on tower clearance requirements.

Jamieson [2] investigated the effects of increased rotor tip velocity. A 120 m/s tip velocity rotor was designed and compared to a baseline 80 m/s rotor. In his work, an upwind, three bladed high speed rotor design was not discussed due to expected loss of stiffness for lower chord required for higher tip speed ratio. However, a two bladed rotor at any given design tip speed ratio has a similar solidity to a three bladed rotor. It is much easier to realize stiff blades when each blade section is 50% wider. Jamieson concluded that a two bladed upwind configuration should be feasible and would realize the expected cost benefit in the drivetrain from reduced rated torque. Whilst a two bladed upwind high speed rotor is feasible, such a design, in striving for sufficient blade stiffness to allow safe tower clearance, defeats many of the potential benefits of a flexible rotor system and cannot realize much weight reduction in the rotor system. Jamieson showed that the high speed, downwind flexible rotor was promising and makes good sense as an integrated design concept. The main added cost for the high speed rotor design was in up-rating the mechanical brake for emergency braking. High upwind blade deflections are expected when pitch control is used for braking. In the end, Jamieson estimates the overall cost impact of the high speed rotor design be a 15% to 20% reduction in wind turbine capital cost.

Additional consequences of high speed rotors in terms of blade erosion or surface damage are important. Jamieson [2] as well as Keegan [3] discussed the impact of velocity on blade erosion. The energy of impinging particles (dust, rain, and/or hail) on the operational blade increases dramatically as relative velocity between the blade and the particle increase.

2. APPROACH

The scope of work was controlled. Two primary reasons drove the single focus on tip velocity increase: 1) to demonstrate of a preliminary rotor optimization framework on a relatively simple multidisciplinary design problem and 2) to provide a preliminary quantitative assessment of tip speed increase effects. Singular focus on tip velocity meant the following considerations were outside the scope of work. Inclusion of these considerations as design variables or intermediate variables required more verification and validation of the integrated tools than was available at the time of the investigation. Each is an important area for ongoing investigation.

- **Rotor size.** A complete investigation would include effects of rotor size. Tip speed increases on commercial turbines are driven by the need for larger swept area while allowing minimal changes to the rest of the turbine system. In these cases, increases in rotor cost attributed to increased blade size are offset by increased energy capture by the larger swept rotor area.
- **Turbine wind speed class.** Turbine wind speed class was not changed. The Turbine class for these designs is IEC I-B. Investigations at lower turbine classes could exhibit different results.
- **Blade materials.** Comparison studies on the use of carbon fiber or glass fiber in the construction of the blades was not included. All blade designs were made of glass fiber, foam core panels, and carbon fiber spar caps.
- **Innovative airfoils.** Innovative airfoils, i.e. flatback airfoils, were not included as design options. Airfoils are summarized in Table 1. They are representative of airfoils commonly used in modern commercial rotors.
- **Aeroelastic tailoring.** Aeroelastic tailoring, i.e. bend-twist coupling, was not considered. Aeroelastic tailoring is a rotor design feature that enables larger swept area and minimal cost to the system in terms of increased rotor loads. The implementation of aeroelastic tailoring requires more verification and validation than was completed by the tools at the time of the investigation.
- **Two-bladed rotor.** Individual blade thickness, thus structural efficiency, is higher for a two-bladed rotor than a three-bladed rotor of equal solidity.
- **Controls.** Rotor controls are an important element of turbine loads mitigation during dynamic loading scenarios. The investigation includes tuning of the Region 2 control constant. Region 2 control is primarily driven by torque constant meant to govern the rotor speed in a manner that tracks the desired rotor performance. Implementation of tuned constants for Region 2.5 and Region 3 are more complicated and were not automated in the optimization framework.

The results of the investigation were not meant to be the ultimate determination of system benefits of increasing tip speed. Instead, the work leads to future studies performed by an improved integrated framework of higher fidelity models which take advantage of more design variables.

80 m/s Tip Velocity (Design 80)

The first turbine variant used all of the 5MW NREL reference model components with the exception of the rotor. The baseline rotor blade was redesigned to find optimal airfoil schedule, chord distribution and twist distribution for a three bladed rotor. The redesign included tightly coupled effects of blade aerodynamic geometry and structural design. The generator speed control constants were recomputed according to the new rotor performance but the blade pitch controller remained unchanged from the 5MW reference model. The fine pitch setting in Region 2 as well as the Region 3 time constants for the pitch controller were unchanged from baseline values.

100 m/s Tip Velocity (Design 100 low TSR & Design high TSR)

The second turbine variant used all of the 5MW NREL reference model components with the exception of the rotor and modified gearbox ratio. The baseline rotor blade was redesigned to find the optimal airfoil schedule, chord distribution and twist distribution for tip velocity increase of 25% to 100 m/s for a three bladed rotor. Generator speed control constants were recomputed according to the new rotor performance but the blade pitch controller remained unchanged from the 80 m/s 5MW reference model. The fine pitch setting in Region 2 as well as the Region 3 time constants for the pitch controller were unchanged from baseline values. The drivetrain input speed increased accordingly and the torque capacity was reduced by a proportionate amount. A significant cost saving for the drivetrain was anticipated for the high speed configuration by virtue of the torque reduction.

In performing these designs, two different approaches were pursued. One optimal design, Design 100 low TSR, was essentially the same as Design 80, in terms of solidity and TSR. The design operated at higher rotor speeds than the 80 m/s counterpart. The other design, Design 100 high TSR, was based on a higher design TSR and lower solidity. Both designs are included here because they demonstrate important lessons regarding rotor designs done in isolation versus rotor designs which include system considerations.

100 m/s Tip Velocity, Flexible Blade (Design 100 Flexible)

The third turbine configuration used the same aerodynamic design and controllers as Designs 100, but removed the blade deflection constraint in the design of the layup components. The configuration was crudely representative of a downwind rotor or of an upwind rotor designed with high pre-bend and/or coning. No tower shadow or upwind blade deflection was considered for either case.

3. BLADE BACKGROUND

The starting point for rotor designs was the Sandia 61.5 meter blade concept [4]. The blade concept represents the aerodynamic design of the NREL 5MW reference turbine and includes a layup concept that was created to meet basic IEC design standards while matching the basic mass properties of the original NREL 5MW reference turbine blades. The current work improved upon the previous design by seeking a more optimal aerodynamic and structural design.

Airfoils

A combination of DU and NACA airfoils is used in the original NREL 5MW reference rotor design. The same airfoil family, shapes and polar data were used in newly optimized rotors. However, newly optimized rotors allow relocation of the airfoils to achieve the appropriate thickness distribution as determined by the optimization tool. The reported NREL 5MW airfoils and nominal airfoil thicknesses are shown in Table 1.

Table 1: Airfoil names and maximum thickness ratios

Airfoil Name	t/c ratio
DU99-W-405	40%
DU99-W-350	35%
DU97-W-300	30%
DU91-W2-250	25%
DU93-W-210	21%
NACA 64-618	18%

Aerodynamic Polar Data

Figure 2 shows corrected airfoil polar data from the official NREL 5MW reference turbine file archive. AirfoilPrep was used to compute lift and drag coefficient values corrected for rotational stall delay [5]. AirfoilPrep was used to compute drag coefficient values corrected by the Viterna method for 0 to 90 deg angle of attack. Polar data were not recomputed for the change in Reynolds numbers attributed to the rotor speed increase. The polar data are based on Re = 7 million. Computation of polar data at additional Reynolds numbers was outside the scope of work.

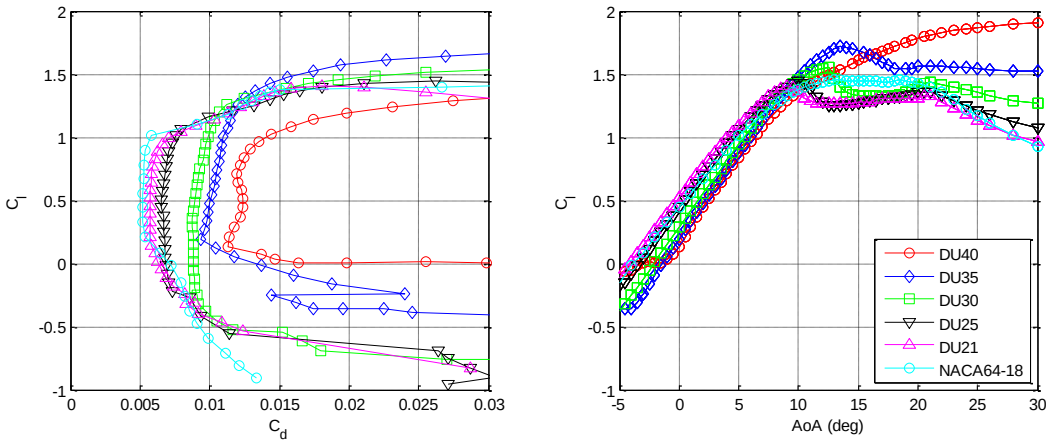

Figure 2: Corrected airfoil polar data from the NREL 5MW reference turbine model

Blade Tip Design

Reference [6] contains discussions of the relationship between aero-acoustic noise and blade tip design. Tip noise is highly dependent upon the strength of the vortex shed at the tip. The more dramatic the spanwise lift gradient approaching the tip, the stronger the vortex shed from the tip. A stronger vortex directly correlates to a louder tip noise prediction. Use of square tips adds significantly to the low-frequency noise, but reduces high-frequency noise. As stated earlier, pointed tips have been responsible in recent decades for lowering of aero-acoustic noise generation.

Optimal blade tip design for minimum aero-acoustic noise production is a complex topic and the subject of specific research. Aero-acoustically optimized tip designs were beyond the scope of the study. Tips were intentionally square. Square tips are not used on modern rotors because they are noisy, especially at high tip velocities. They were used as a means to provide consistency across the designs. Innovative tip designs should be the topic of additional work.

Materials

Material properties used in the blade model were the same as those used in the Sandia 100m Blade design [7] and in the Sandia 61.5m structural concept [4]. Those reports contain a detailed record of material choices and derivation of mechanical properties. Material properties are summarized in Table 2 and were the properties used in the investigation.

Out-of-plane blade tip deflection, panel buckling, and fatigue damage are drivers for blade design. Choice of materials and mechanical properties of the materials are important to the blades. An investigation into the use of different combinations of materials was beyond the scope of work. Materials properties shown here were used consistently across rotor designs so that in a relative sense, comparisons between designs were meaningful.

Table 2: Summary of material properties

	Layer Thickness	Ex	Ey	Gxy	Prxy	Dens.	UTS	UCS
	[mm]	[MPa]	[MPa]	[MPa]	[-]	[kg/m3]	[MPa]	[MPa]
Gelcoat	0.05	3440		1380	0.3	1235	-	-

E-LT-5500(UD)	0.47	41,800	14,000	2630	0.28	1920	972	702
SNL(Triax)	0.94	27,700	13,650	7200	0.39	1850	700[a]	-
Saertex(DB)	1	13,600	13,300	11,800	0.49	1780	144	213
FOAM	1	256			0.3	200	-	-
Carbon(UD)	0.47	114,500	8,390	5990	0.27	1220	1546	1047

Blade Root Hardware

Blade root hardware (e.g. carrots, t-bolts, embedded studs) were not included in the structural model. The root diameter and root buildup material and layer schedule were the same for all designs.

[a] The estimated strength for the triax material is set to 700 MPa by examination of similar triax materials from the SNL/MSU materials database having similarly high modulus of elasticity.

4. AERO-STRUCTURAL WIND BLADE DESIGN TOOLS

A process combining three publicly available tools from the wind energy community was used for the initial aero-structural optimization:

- HARP_Opt [8] is an aero-structural rotor design optimization suite which is based on the use of genetic algorithms to find rotor designs exhibiting the effective combinations of rotor loads, which translate to blade weight, and energy captured.
- Co-Blade [9] is a cross section based structural analysis tool which is ideally suited for integration into wind blade optimization
- NuMAD [10] brings a framework for managing blade layup components during optimization as well as performing high fidelity wind blade structural analyses

HARP_Opt

HARP_Opt (Horizontal Axis Rotor Performance Optimization) is a MATLAB® script that utilizes a multiple-objective genetic algorithm and blade-element momentum (BEM) theory flow model to design horizontal-axis wind and hydrokinetic turbine rotors.

Genetic algorithms solve optimization problems by mimicking the principles of biological evolution. Rules modeled on biological reproduction and gene modification are used in genetic algorithms to repeatedly modify a population of individuals to create subsequent generations of superior individuals. HARP_Opt utilizes the MATLAB® Genetic Algorithm solver to perform the optimization, and the WT_Perf [11] BEM theory code to predict rotor performance metrics.

HARP_Opt optimizes a rotor's performance for steady and uniform flows (no sheared or yawed flows). HARP_Opt can be used to design a variety of rotor control configurations, including fixed or variable rotor speed and fixed or variable pitch rotor configurations. HARP_Opt can be used to design blades containing circular or non-circular roots.

HARP_Opt can function as a single- or multiple-objective optimization code. The primary optimization objective is to maximize the turbine's AEP. Rayleigh, Weibull, or user-defined wind speed distributions can be used to compute annual energy production. An additional objective can be activated, in which HARP_Opt performs a structural optimization to minimize the blade mass. For the structural analysis, the blade is modeled as a thin shell of bulk isotropic material; maximum allowable strain is used as a constraint while the blade mass is minimized. Maximizing energy production and minimizing blade mass are conflicting objectives, thus HARP_Opt will identify the set of Pareto optimal solutions. To meet these objectives, HARP_Opt calculates an optimal blade shape (twist, chord, and airfoil distributions) and optimal control of the rotor speed and blade pitch.

Co-Blade

Co-Blade is open source software that can be used for the structural analysis and design of composite blades for wind and hydrokinetic turbines. The objective of Co-Blade is to help designers accelerate the preliminary design phase by providing the capabilities to quickly analyze alternative composite layups and to study their effects on composite blade properties, deformations, and material stresses and strains.

Co-Blade enables realistic modeling of composite blades exibiting nearly arbitrary topology and material properties. Co-blade is used for computation of structural properties such as

- offsets: center-of-mass, tension-center, & shear-center
- inertias: mass & mass moments of inertia
- stiffnesses: axial, bending, & torsional
- principal axes: inertial, centroidal, & elastic principal axes
- modal analysis: coupled mode shapes & frequencies (via integration w/ BModes [12])

Co-Blade is used to perform structural analysis including applied aerodynamic forces and moments, computation of body forces (centrifugal, and weight), computation of load induced blade deflections, lamina-level stresses and strains and panel buckling stresses. Co-Blade can be used for optimization of composite layups. For a given external blade shape and design load, Co-Blade can determine an optimal composite layup which minimizes blade mass while simultaneously satisfying constraints on maximum stress, buckling, deflection and placement of natural frequencies.

Co-Blade performs a linear buckling analysis to predict the critical buckling stresses following the engineering approaches. Co-Blade idealizes the top and bottom surfaces of the blade as curved plates subjected to the combined conditions of compression and shear. The shear webs are idealized as flat plates subjected to the combined conditions of bending and shear. The plates are idealized as isotropic and having simply-supported (pinned) boundary conditions on all four sides (which is a conservative approach). The plate stiffness (effective stiffness from classical laminate theory), thickness, curvature, and width dimensions therefore contribute to the prediction of critical buckling stresses.

NuMAD

NuMAD v2.0 is a tool developed and used at Sandia National Laboratories for the creation of high fidelity wind blade structural models. NuMAD helps the wind blade structural designer manage material properties, materials placement, and blade geometry. Blade models are converted by NuMAD into ANSYS finite element shell models. The ANSYS shell elements contain all the information to effectively capture the complex layup of the blade structure.

An improved version of NuMAD is under development and is used to execute the investigation. The primary advance is a new approach to wind blade structures modeling based on layup components.

Additional NuMAD features include:

- Simple representation of layup components in a “blade object” framework
- Easy access to blade object data during optimizations
- Detailed blade schedule of layers output

Layup component objects are defined by their spanwise extent, chordwise extent, fabric composition, and a schedule of fabric layers versus span. Chordwise extent of layup components are defined by key points LE, a, b, c, d, and TE in Figure 4. The locations of these key points are computed from the specification of three blade surface lengths: LE band width, Spar cap width

and TE band width. Additionally, the spar cap is automatically centered at the point of maximum airfoil thickness to take advantage of the airfoil shape for structural efficiency. More discussion of the usage of the approach is found later in this report under the heading of "Structures Optimization".

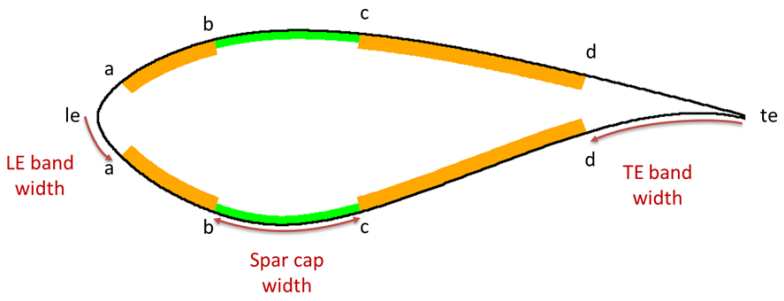

Figure 3: Blade cross section showing keypoints between chordwise regions

Assembly of an Aero-Structural Optimization Tool

Table 3 summarizes the strengths and weaknesses of the three codes with respect to factors that are important to efficient and accurate aero-structural optimization. Each of the three tools brings a valuable capability to the overall blade design process. They are combined in a way to include analysis fidelity where accuracy is needed but to utilize computationally fast tools where efficiency is needed.

The NuMAD blade object, which includes detailed layup definitions, replaced the thin shell representation of blades in HARP_Opt. A tool that converts NuMAD blade objects to Co-Blade models was created so that fast turnaround Co-Blade structural analyses can support the aero-structural optimization in HARP_Opt by providing blade deflection in response to the aerodynamic load. HARP_Opt includes design variables for airfoil locations, chord distributions and twist distributions. Additional design variables were added to affect the blade spar cap design. Spar cap design (as well as airfoil thickness distribution) was the primary driver for blade flapwise stiffness, and therefore, blade tip deflection for a given aerodynamic load. Figure 4 highlights the modifications to HARP_Opt inputs.

Table 3: Strengths and weaknesses of individual codes

Publicly available code	Strength	Weakness
HARP_Opt v2.00.00	A multi-objective rotor optimization tool geared to maximize AEP while minimizing blade mass.	Structural representation of blades is limited to a shell of uniform wall thickness.
Co-Blade v1.23.00	A computationally efficient structural design and analysis tool based on 2D cross section analysis.	Buckling computations are fast, but uncertainty on the level of conservatism may be high.
NuMAD v2.1	A blade structure design tool that includes abilities to represent blade layup and architecture parametrically in an optimization framework and to use ANSYS for high fidelity buckling analysis.	Requires time intensive buckling computations in ANSYS.

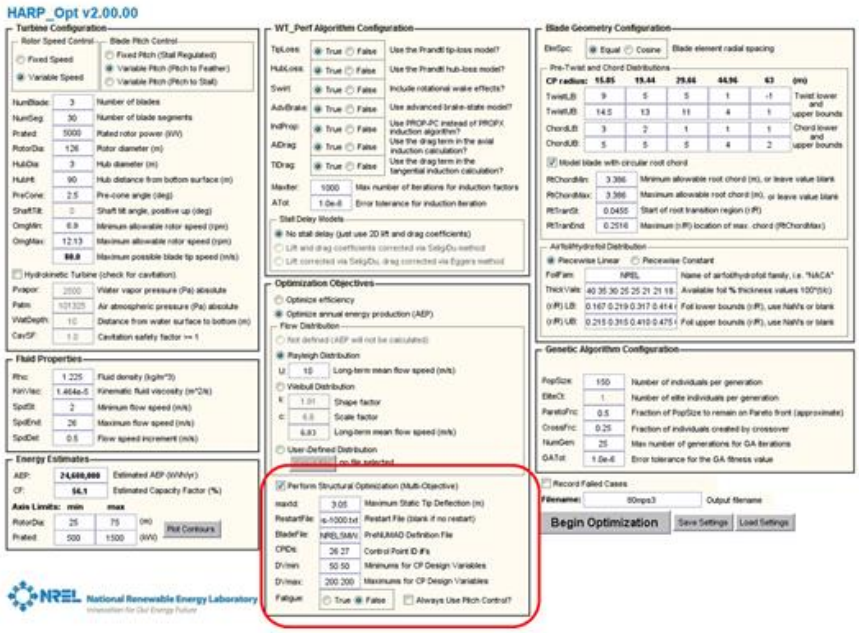

Figure 4: Modified HARP_Opt GUI; modifications in red

5. AERO-STRUCTURAL OPTIMIZATION

Design Variables

Twenty total design variables were available to the multi-objective genetic algorithm. Bounds of these design variables were set by the user; narrow bounds enable quicker convergence on solutions; wide bounds enable exploration of a larger design space.

- 5 points shaped the entire chord distribution
- 5 points shaped the entire twist distribution
- 8 airfoil locations; a variable representing airfoil location for each of the following airfoil thicknesses was used: 18, 21, 21, 25, 25, 30, 35 and 40%
- 2 points shaped the distribution of materials in the spar caps

Details of how the chord, twist and thickness distributions were defined can be found in documentation for HARP_Opt. Five control points were used to define Bezier functions that described smooth distributions of chord and twist. Spanwise location of these chord and twist control points was fixed. Magnitudes of the control points were specified by design variables. Thickness distribution was determined by placement of airfoils at spanwise locations given by design variables. Note that the user must decide beforehand what airfoil family and what thicknesses to use.

Bounds on the design variables were set by the user. The bounds on chord design variables were set such that it is not possible for the maximum chord to be greater than the maximum chord of the original baseline blade. Large values of maximum chord were not allowed during because of the potential effects on transportation logistics, which was outside the scope of the study.

Appendix A contains a complete listing of input parameters used for each of the rotor optimizations.

Fitness Function

The genetic algorithm used a two-objective fitness function, F(x), to assess the quality of the blade design represented by the set of design variables.

$$F(x) = [F_1(x), F_2(x)] \qquad \text{Eq.(5.1)}$$

In general, the relative importance of the objectives is not known until the system's best capabilities are determined and tradeoffs between the objectives are fully understood. Otherwise, two objectives can be combined into one, thus eliminating the need for multi-objective optimization. One might use a metric such as blade mass per AEP, blade cost per AEP, or even system cost per AEP as a single objective for minimization. Each of these metrics drives toward low LCOE. It can be useful to keep objectives separate to learn about the characteristics of all candidates on the Pareto front and even to consider designs in the interior space near the Pareto Front that may have desirable traits.

$F_1(x)$ and $F_2(x)$ were minimized during the optimization. The two dimensions of the fitness function follows:

$$F_1(x) = AEP(x) * (-1) \qquad \text{Eq.(5.2)}$$

$$F_2(x) = M(x) * P \qquad \text{Eq.(5.3)}$$

$$P = \begin{cases} \frac{\delta(x)}{\delta_{target}}, & if\ \delta(x) > \delta_{target} \\ 1, & otherwise \end{cases} \qquad \text{Eq.(5.4)}$$

where x is the set of design variables, AEP is the product of the power curve and wind speed distribution, M is the blade mass and P is a penalty. The quantity M*P is referred to as the penalized blade mass. The penalty (P>1) arises when the target blade deflection, δ_{target}, is exceeded by the computed deflection for the design $\delta(x)$. For example, if blade tip deflection is to be no greater than 3 meters and a 15,000 kg blade design exhibits a maximum deflection under load of 3.3 meters, then the penalty, P, is computed as 1.1 and the objective $F_2(x)$, penalized blade mass, is 16,500 kg. Designs which violate tip deflection criteria are not simply thrown away, but are used to help guide the optimizer toward a better solution where P is close to one.

Optimization Results

Approximately 30,000 designs were evaluated for each rotor (population 150 for each of 200 generations). Results are summarized by Pareto fronts shown in Figure 5. A Pareto front represents the collection of noninferior designs that are identified in the space of design variables. A noninferior design is one which cannot experience improvement in one design objective without degradation of another design objective. The collection of noninferior designs is known as the Pareto optima, Pareto frontier or simply the Pareto front.

High AEP candidates exhibit high blade mass, which is indicative of high loading required to capture higher AEP. Low AEP candidates exhibit lower blade mass, which is indicative of less loading.

Manipulation of the design variable bounds related to chord distribution and setting of the tip deflection target leads the optimization toward two different high velocity rotor strategies:

1) Maintain the same operating tip speed ratio and rotor solidity as the 80 m/s rotor (low TSR rotor) or
2) Increase the operating tip speed ratio and decrease the rotor solidity from the 80 m/s rotor (high TSR rotor).

Note that the rotor TSR is not a design variable. The rotor TSR is an outcome of the overall design optimization variables described above.

Later analyses will show that the first strategy leads to the lightest and cheapest blades but leads to the highest rotor loads as well as highest increases in balance of turbine system costs (with the exception of the gearbox). Under the first approach, Design 80 and Design 100 low TSR rotors were practically the same. The second leads to a smaller increase in rotor loads but leads to the highest blade cost; a decrease in blade chord and absolute thickness commands significant additional spar cap material to enable sufficient blade flap wise stiffness. The best strategy was not determined until the full system design and cost analysis was performed and final LCOE values computed. Therefore, each of the design strategies carry forward.

Crude assumptions regarding system cost per kilowatt rating and blade cost per kilogram were used to convert from blade mass to approximate system cost in Figure 6. The smallest slope tangent line passing from the plot origin to candidates on the Pareto front are used to locate candidates for lowest cost of energy. The intersection of the line and the Pareto candidates shows graphically that the higher AEP candidates were preferred to the lowest cost design candidates.

Table 4 summarizes assumptions used to provide a conversion from blade mass to system cost.

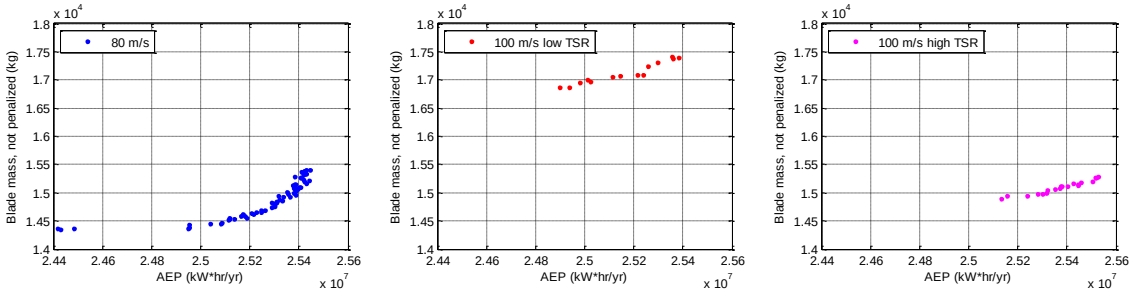

Figure 5: Pareto fronts showing the sets of noninferior designs. Points shown for designs that meet tip deflection requirement, *P*<1

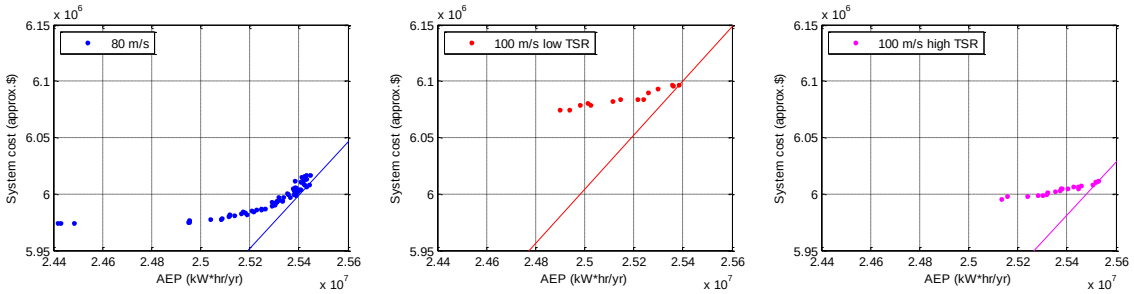

Figure 6: Pareto fronts expressed in terms of approximate system cost versus AEP

Table 4: Assumptions used to estimate blade and system cost

		Reference
Baseline single blade weight (kg)	15,000	From this work
Expected system capital cost ($/kW)	$1,200	Figure 19 in Ref.[13]
Turbine rating (kW)	5,000	
S_{80}, System cost ($M)	$6.0	
Blades percentage of capital cost	14%	Table 2 in Ref.[14]
B_{80}, Cost of blade set	$840,000	
Non-rotor components ($M)	$5.16	
Materials fraction of blade cost	72%	Ref.[15, 16]
Labor fraction of blade cost	20%	
Tooling fraction of blade cost	8%	
M_{80}, Baseline blade set materials cost	$604,800	
L, Baseline blade set labor cost	$168,000	

T, Baseline blade set tooling cost	$67,200	
Mat_{80}, Baseline rotor materials cost per kg ($/kg)	$13.44	

$S_{80}=1{,}200*5{,}500$ Eq.(5.5)
$B_{80}=0.14*S_{80}$ Eq.(5.6)
$M_{80}=0.72*B_{80}$ Eq.(5.7)
$Mat_{80}=M_{80}/(15{,}000*3)$ Eq.(5.8)
$S_{100}=Mat_{80}*Mass_{100}+L+T+BOS$ Eq.(5.9)

Blade Tip Deflection

Computation of the appropriate blade tip deflection target, δ_{target}, was clumsy in the current implementation of these tools. HARP_Opt used WT_Perf, based on BEMT, to compute steady aerodynamic loads on the rotor at an array of wind speeds across the entire operating range of the rotor. Previous experience predicted the design driving tip deflection to occur during a dynamic aeroelastic load case involving a strong wind gust and simultaneous change in wind direction. A time marching aeroelastic simulation including blade inertial and stiffness properties was used to compute the blade deflection during the load case. The time marching aeroelastic simulation (via FAST/AeroDyn) requires orders of magnitude more computational time than the simpler BEM computation of steady loads (WT_Perf). The computational constraint drives the framework towards a process that uses aeroelastic simulation on promising designs (up to 75 simulations in a final Pareto front) and uses BEMT for evaluation of designs during the optimization (35,000 simulations).

A tip deflection ratio was used to set the value of δ_{target} such that the Pareto optimal blade designs would exhibit tip deflections which were close to targets during follow-up aeroelastic simulations. Figure 7 shows examples of the relevant data used to set the deflection ratio for Design 80. Figure 8 shows examples of the relevant data used to set the deflection ratio for Design 100 high TSR. The trends are the same in a plot corresponding to Design 100 low TSR. Deflections were computed for steady loading, "CoBlade OoP defl.," and for dynamic aeroelastic loading during the IEC ECD load case, "ECD OoP defl," for all Pareto optimal designs. The deflection ratio was computed and is plotted on the right. Deflection ratios are variable because of blade inertia and loading of Pareto optimal designs. It is up to the user to choose the appropriate deflection ratio within the range. Once a ratio is chosen, it is used to compute δ_{target}, an input for HARP_Opt. For example, if desired maximum out-of-plane tip deflection is 7 meters and the deflection ratio is 2, then δ_{target} is set as 7 / 2 = 3.5 m.

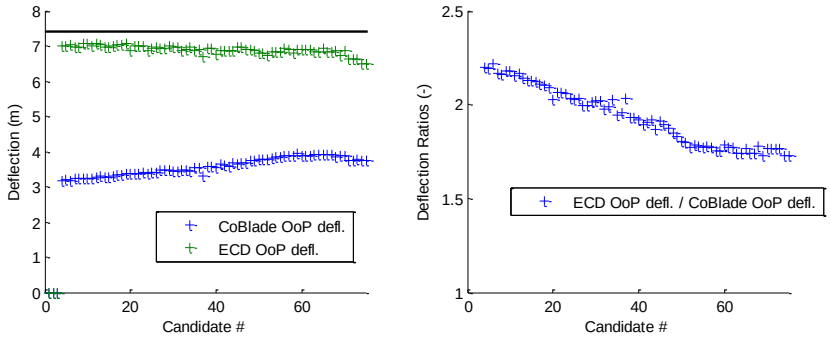

Figure 7: Steady and dynamic blade deflections for Pareto optimal Designs 80

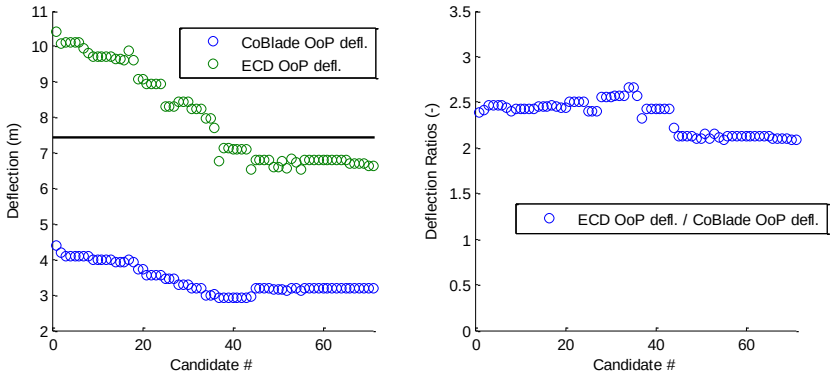

Figure 8: Steady and dynamic blade deflections for Pareto optimal Designs 100 low TSR

This approach was used to do the current work, but the topic of accurate determination of structural response during aero-structural optimization was clearly identified as an area for improvement. Blade masses of candidates in the Designs 100 Pareto fronts were sensitive to the specified value of δ_{target}. Setting δ_{target} too low led to heavy blade designs while setting it too high led to a large fraction of designs which were irrelevant because they exceeded deflection requirements when dynamic aeroelastic simulations were performed.

6. AERO-STRUCTURAL OPTIMIZATION RESULTS

Chord and Twist Distributions

Figure 9 shows the Pareto optimal chord and twist distributions for all designs. All designs tended toward a lower solidity than the original 5 MW reference turbine. The original NREL 5 MW reference blade is a clipped-tip version of a 63 meter blade. The solidity of the original reference 5 MW rotor is probably higher than what is optimal, so generally lower solidity for all designs was not surprising.

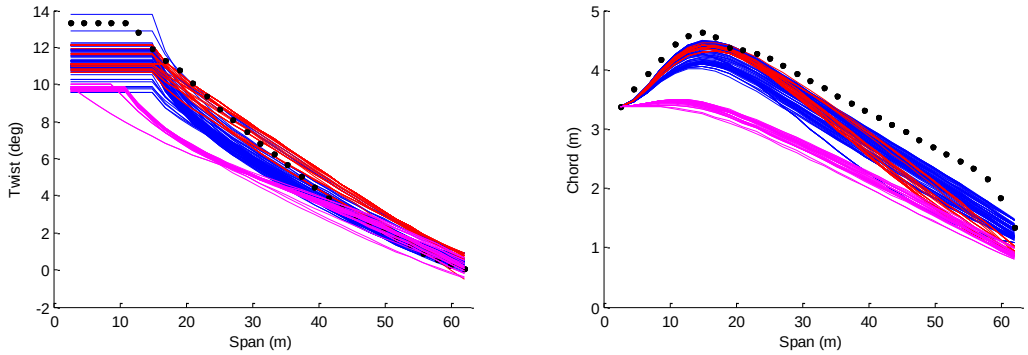

Figure 9: Pareto optimal chord and twist distributions: NREL 5MW baseline (black dots), Design 80 (blue), Design 100 low TSR (red), Design 100 high TSR (magenta)

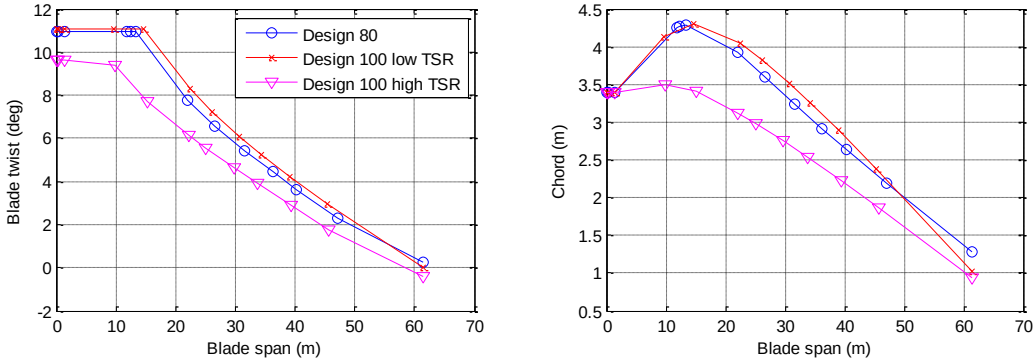

Figure 10: Chord and twist distributions of selected blade designs

Figure 10 shows chord and twist distributions of single blade designs selected from the Pareto fronts based on potential for lowest system cost per energy capture as seen in Figure 6. The similarity between Design 80 and Design 100 low TSR is evident. The data in the distributions shown here are representative of the points which define the blade geometry in NuMAD.

Thickness Distribution

Figure 11 and Figure 12 show the airfoil thickness-to-chord (t/c) ratio and the blade thickness of selected designs. With the exception of 30 and 35% thick airfoils, all airfoils were placed in more inboard locations for the higher velocity rotor. The 30 and 35% thick airfoils were located more outboard for the higher velocity rotor. The rotor is stiffness driven and the higher rotor velocity demands lower rotor solidity, thus lower chord and absolute thickness, so one might expect thicker airfoils to be used further outboard for higher velocity rotor designs. However, the thinner airfoils exhibit higher L/D ratios. The optimization approach determined the lower L/D of thinner airfoils to be more advantageous than the higher blade thickness of thicker

airfoils. The exception was in the placement of the 35% thick airfoil which was located more inboard for high velocity designs and more outboard for low velocity designs.

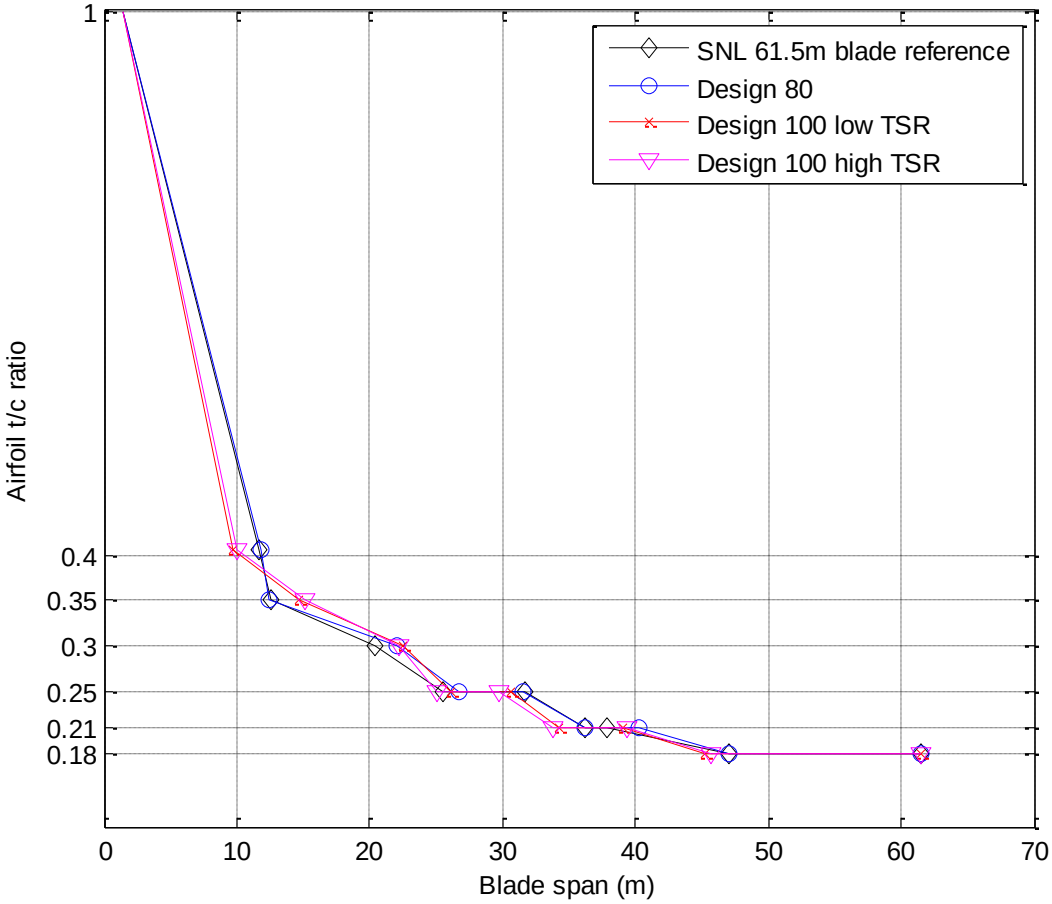

Figure 11: Airfoil t/c versus blade span

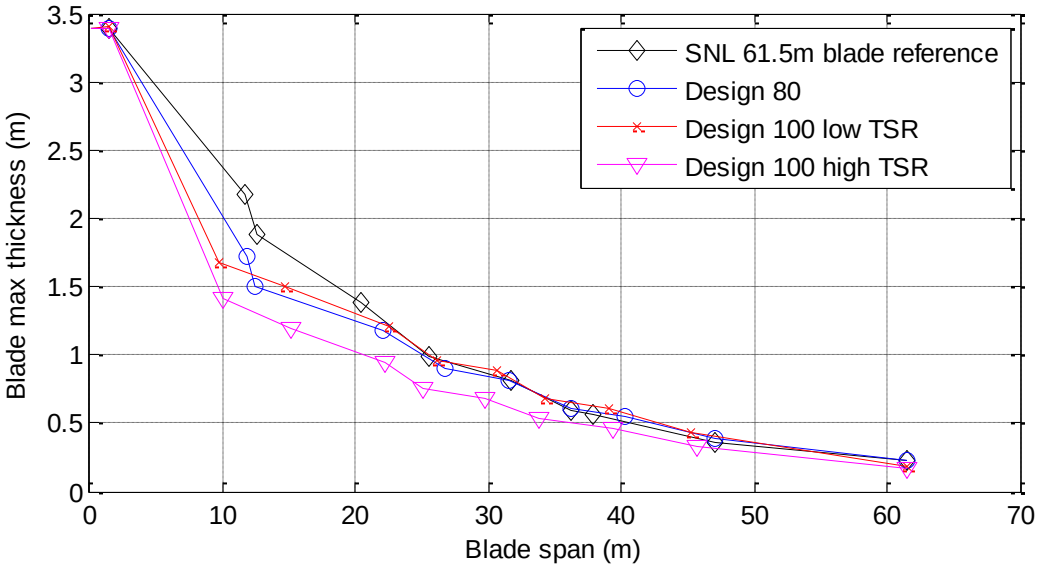

Figure 12: Blade thickness versus blade span

Rotor Aerodynamic Performance

Figure 13 shows distribution of lift coefficients for the rotor operating at its design point, i.e. Region 2 operation. BEM theory was used to compute the data, i.e. WT_Perf.

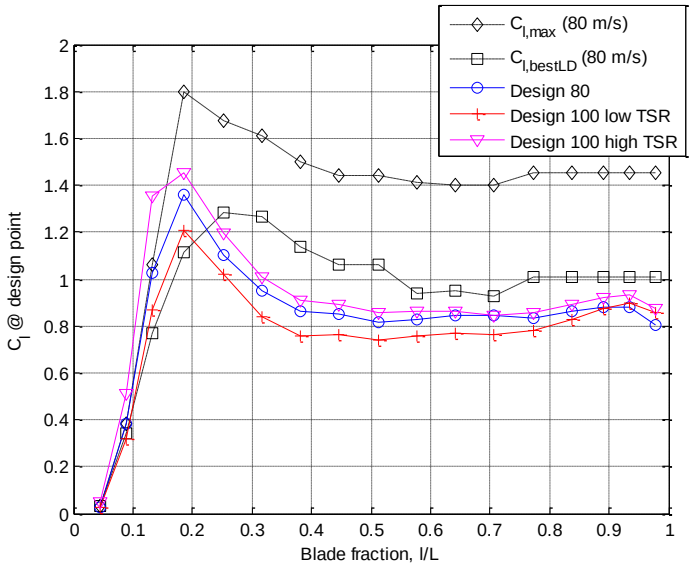

Figure 13: Lift coefficients for selected designs

Classical rotor design is done in a manner promoting operation of each airfoil at, or near, its efficient operating point. The efficient operating point is the angle of attack where the airfoil exhibits its best ratio of lift to drag. A simple blade design process follows:

1) Choose a target tip speed ratio. The choice is based on several factors, including optimization of the eventual power curve as well as the turbine wind speed class.
2) Choose an airfoil family.
3) Determine the lift coefficients and angles of attack for the family of airfoils. Lift coefficients should be chosen such that best lift-to-drag ratio is achieved.
4) Determine the thickness distribution of the blade. The distribution determines the placement of airfoils, and therefore, the distribution of lift coefficients along the blade.
5) Tip speed ratio and design lift coefficients are used to compute the rotor chord distribution.
6) Rotor geometry is used compute distribution of inflow angles.
7) Inflow angles and design angles of attack are used to compute blade twist distribution.
8) Iterate until aerodynamic design is sufficiently converged (steps 2-6).
9) The aerodynamic geometry is used for structural design.

If computation of chord and twist are done in a manner such that desired lift coefficients are achieved, the process produces a blade design which operates at best L/D for each airfoil along the blade.

However, the aero-structural optimization process used for the current work produced blade designs demonstrating lift coefficient less than that for best-L/D. An explanation and further development is needed. Ideal distributions of chord and blade twist were non-smooth along the span. For manufacturability, realistic chord and twist distributions must be smooth. The

mismatch between ideal distributions and smoothed distributions caused problems during the automated approach. Chord, lift coefficient and angle of attack for best L/D, blade pitch and inflow angle were all coupled. However, the automated approach had more unknowns than available information could uniquely define. More design guidance was needed to force the design toward specific objectives.

Results showed that designs were unloaded in an effort to pursue lighter weight blades (Figure 14). The result was a small decrease in AEP. However, the approach for unloading the designs was not intelligent. However, the outcome hints at the concept of the low load modern rotor, which is an area for further investigation. Rotor designs can be more effective, in terms of turbine capital cost per energy capture, by unloading the rotor in spite of decreased AEP. In these cases, rotor loads decrease and therefore blade weight and cost decrease. It is an effect seen in modern blade designs and is well documented in Reference [17].

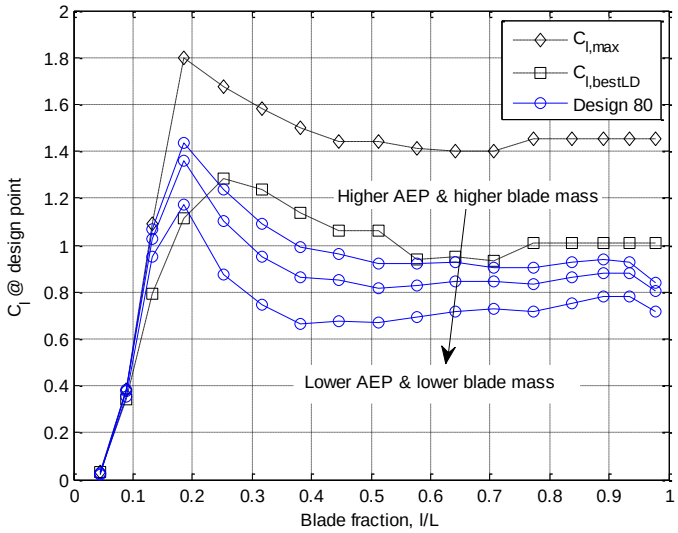

Figure 14: Lift coefficients for Pareto optimal Design 80 designs

Figure 15 illustrates blade induction values generally around 1/3. Prandtl tip loss causes induction to increase near the tip. Table 5 provides a summary of rotor aerodynamic characteristics for each design. Figure 17 shows a three dimensional rendering of the high TSR design.

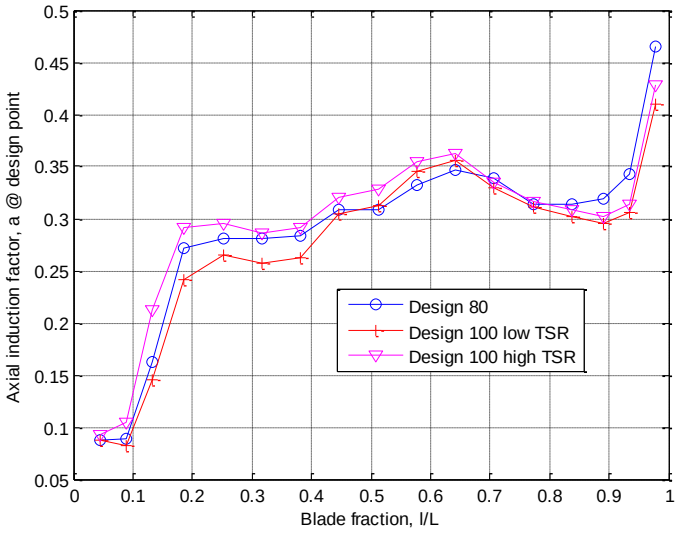

Figure 15: Axial induction factors

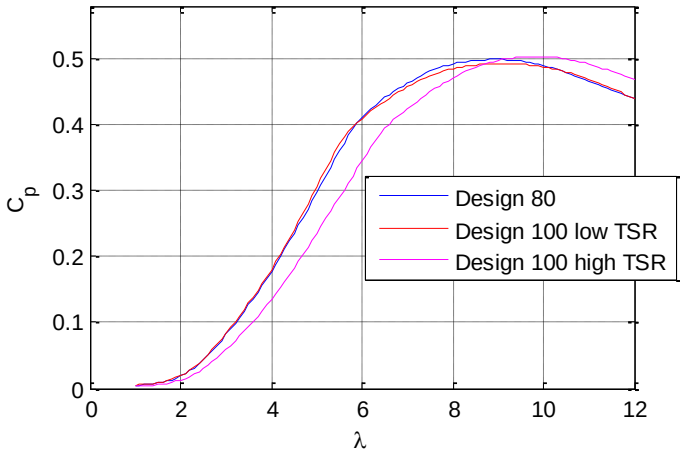

Figure 16: Cp-Lambda curves

Table 5: Summary of rotor performance parameters

	TSR	C_p,max	Rotor C_T	Solidity (%)
NREL 5MW Reference[b]	7.55	0.482	Unk.	5.16
Design 80	8.9	0.499	0.743	4.53
Design 100 low TSR	9.1	0.493	0.720	4.60
Design 100 high TSR	9.9	0.503	0.761	3.76

[b] TSR and $C_{p,max}$ as computed by FAST. See page 19 of Jonkman (2009).

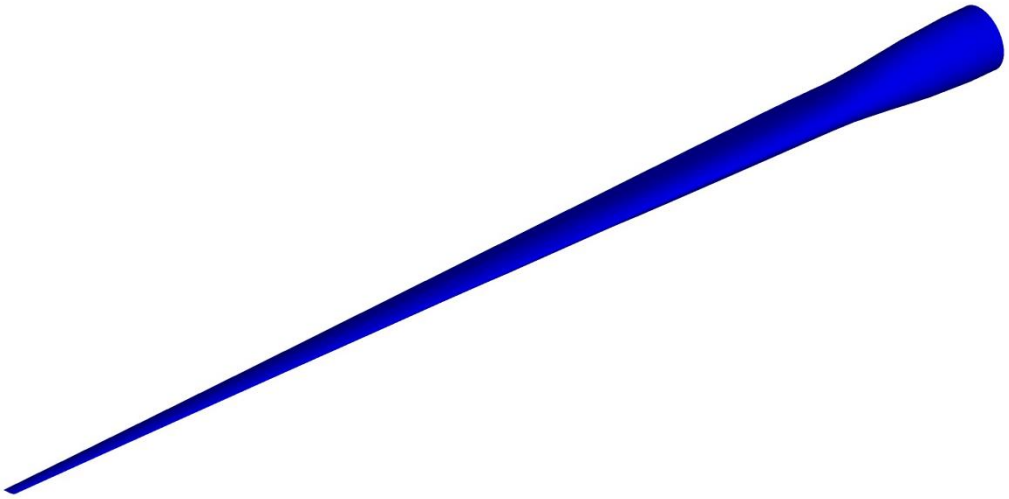

Figure 17: Solid model rendering of Design 100 high TSR

7. STRUCTURES OPTIMIZATION

The aero-structural optimization utilized a detailed representation of the blade layup. However, the blade layup was preliminary; foam thicknesses and thicknesses of reinforcements were estimates and the spar cap was crudely defined. The selected designs moved forward into a more detailed structural optimization. The goals of the structural optimization include

- **Panel sizing.** Determine the thickness of aft panels, especially near maximum chord where panel span is greatest. The thickness of these panels determines their resistance to buckling.
- **Spar cap sizing.** Determine the width (constant width) and spanwise layer schedule for the spar caps. The spar caps design affects the overall blade flapwise stiffness and flapwise frequency.
- **Trailing edge reinforcement sizing.** The amount of trailing edge reinforcing material affects the edge stiffness and edge frequency of the blade.

The layer schedule for the root buildup remained constant throughout the study. Optimization of the layer schedule is worthwhile but was reserved for future work because these designs all interface to the same hub hardware.

A single objective genetic algorithm was used to manage the structural optimization process. The goal of the optimization was to minimize the penalized blade mass, F_{struc}.

$$F_{struc}(x) = M(x) * P_{\delta} * P_{buckle} * P_{fatigue} * P_{flap} * P_{edge/flap} \quad \text{Eq.(7.1)}$$

Penalties P were applied to the blade mass M for exceeding:

- tip deflection criteria
- buckling criteria
- 20 year fatigue damage
- flap frequency criteria
- edge-flap frequency spacing criteria

$$P_{\delta} = \begin{cases} \frac{\delta(x)}{\delta_{target}}, & if\ \delta(x) > \delta_{target} \\ 1, & otherwise \end{cases} \quad \text{Eq.(7.2)}$$

$$P_{buckle} = \begin{cases} \frac{F_{cr,target}}{F_{cr(x)}}, & if\ F_{cr(x)} < F_{cr,target} \\ 1, & otherwise \end{cases} \quad \text{Eq.(7.3)}$$

$$P_{fatigue} = \begin{cases} D_{20}(x), & if\ D_{20}(x) > 1 \\ 1, & otherwise \end{cases} \quad \text{Eq.(7.4)}$$

$$P_{flap} = \begin{cases} \frac{f_{flap,target}}{f_{flap}(x)}, & if\ f_{flap}(x) < f_{flap,target} \\ 1, & otherwise \end{cases} \quad \text{Eq.(7.5)}$$

$$P_{edge/flap} = \begin{cases} \frac{r_{edge/flap,target}}{r_{edge/flap}(x)}, & if\ r_{edge/flap}(x) < r_{edge/flap,target} \\ 1, & otherwise \end{cases} \quad \text{Eq.(7.6)}$$

where F_{cr} is the computed critical buckling load, D_{20} is the computed 20 year fatigue damage, f_{flap} is the blade flapwise first natural frequency, $r_{edge/flap}$ is the ratio of blade edgewise first natural frequency to flapwise first natural frequency.

δ_{target} is the minimum allowable blade tip deflection to meet tower clearance requirements, including safety factors. $F_{cr,target}$ is the minimum allowable buckling load, including safety factors. $f_{flap,target}$ is set 10% above the rotor 3P frequency. $r_{edge/flap,target}$is set at 1.30. Criteria for $f_{flap,target}$ and $r_{edge/flap,target}$ are not called out in the IEC standards, but are often common practice in blade design. However, these criteria are often relaxed in modern blade design as blades become light and flexible if designers have confidence in their understanding of the aero-structural dynamic interactions of the system.

Following are design variables x included in the optimization:

- (2 variables) panel foam thickness, A & B, in the aft panels (see Figure 18 and aft orange region in Figure 20)
- (2 variables) spar cap thicknesses, C & D, at 20% & 50% span (see Figure 19)
- (1 variable) spar cap width, E (see green region in Figure 20)
- (1 variable) thickness of trailing edge reinforcement

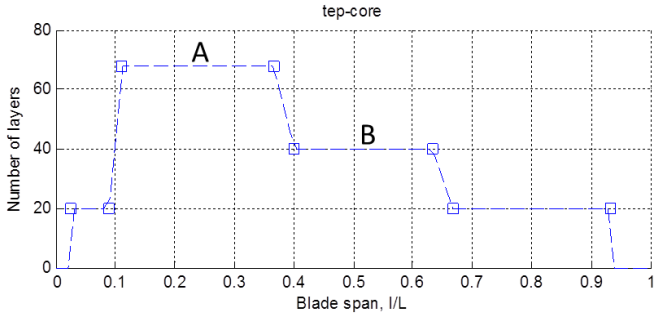

Figure 18: Illustration of schedule for foam thickness in the blade aft panels

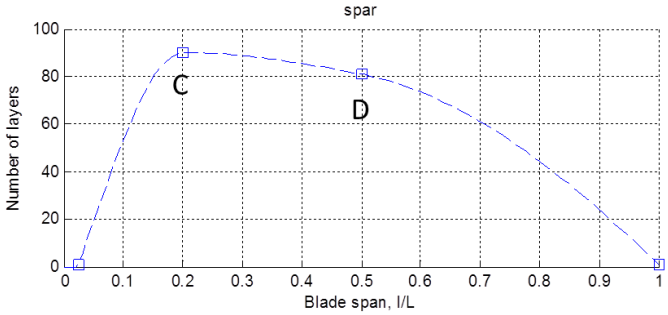

Figure 19: Illustration of layer schedule for spar caps

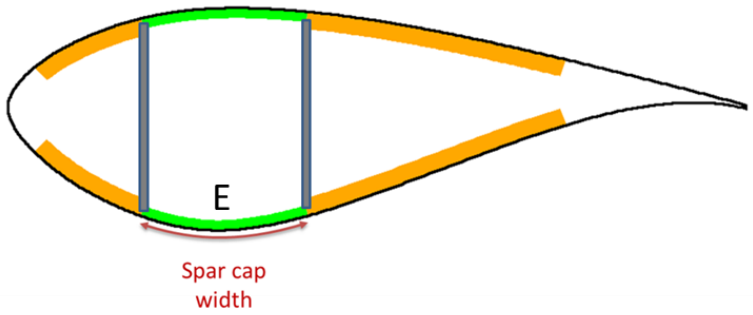

Figure 20: Illustration of blade cross section

Design criteria were evaluated during the optimization process as shown in Table 6.

Table 6: Approaches used during structural optimization

Tip deflection criteria	PreComp [18] was used to convert the NuMAD blade into a FAST blade input file. FAST/AeroDyn were used to simulate the IEC DLC and determine blade tip deflection.
Buckling criteria	NuMAD was used to create a FE shell element model in ANSYS. Aerodynamic loads from the driving IEC DLC simulation by FAST/AeroDyn were mapped onto the ANSYS model. ANSYS performed a linear buckling analysis.
20 year fatigue damage	PreComp was used to convert the NuMAD blade into a FAST blade input file. FAST/AeroDyn were used to simulate IEC DLC 1.2 (normal turbulence). Crunch [19] was used to count cycles in the dynamic data. Matlab postprocessing computed fatigue damage for various material properties.
Flap frequency criteria and edge-flap frequency spacing criteria	PreComp was used to convert the NuMAD blade into a FAST blade input file. Structural properties were used by BModes [12] to compute blade frequencies.
Blade mass	NuMAD was used to create a FE shell element model in ANSYS. The mass of the ANSYS model was computed. (Mass can also be taken from FAST outputs. The ANSYS representation is a higher fidelity representation of all the materials in the blade.)

A detailed discussion of the supporting aeroelastic system simulations in FAST/AeroDyn are the Appendices.

Flexible Designs

Additional structural designs quantified effects of removing the tip deflection constraint from the design process on the 100 m/s tip velocity blade. These blades were referred to as "flexible" blades. They crudely represented the design of an upwind rotor designed for unconventionally high upwind prebend or a downwind rotor.

Tip deflection is the driver for sizing of spar caps in typical blade designs. When the tip deflection constraint is removed, the flexible blade layup design was driven by a combination of fatigue, frequency and panel buckling criteria. The lighter spar cap promoted a lighter and cheaper blade overall.

Optimization Results

Figure 21 provides a summary of the layup design results for all Designs. More detailed information is found in Appendix D. Following are some observations regarding the layup designs:

- The root buildup material was massively heavy. The weight of the root and skin material was represented by green bars; the vast majority of each green bar was comprised of root material. Optimization of root buildup material was not a task in the investigation.
- The weight of gelcoat was small, almost negligible, and is not even visible on the chart next to the other components.
- The spar cap weight for Design 100 high TSR was nearly twice that of any other blade design.
- The amount of core material needed in the high TSR designs was less than low TSR designs and was attributable to the difference in solidity. Less material was required to meet buckling criteria as unsupported panel length decreases.
- The amount of shear web material needed in the high TSR designs was less than low TSR designs. The difference in solidity translated to thinner airfoils and shorter shear webs.
- The amount of trailing edge reinforcement material used in Design 100 low TSR appeared high in relation to the amount of spar cap material used in the same design. Results showed that the spacing of flap and edge frequencies for the design was high and implied use of excessive trailing edge reinforcement. The trailing edge reinforcement material contributed to the aft panel stiffness and therefore contributed to buckling requirements.

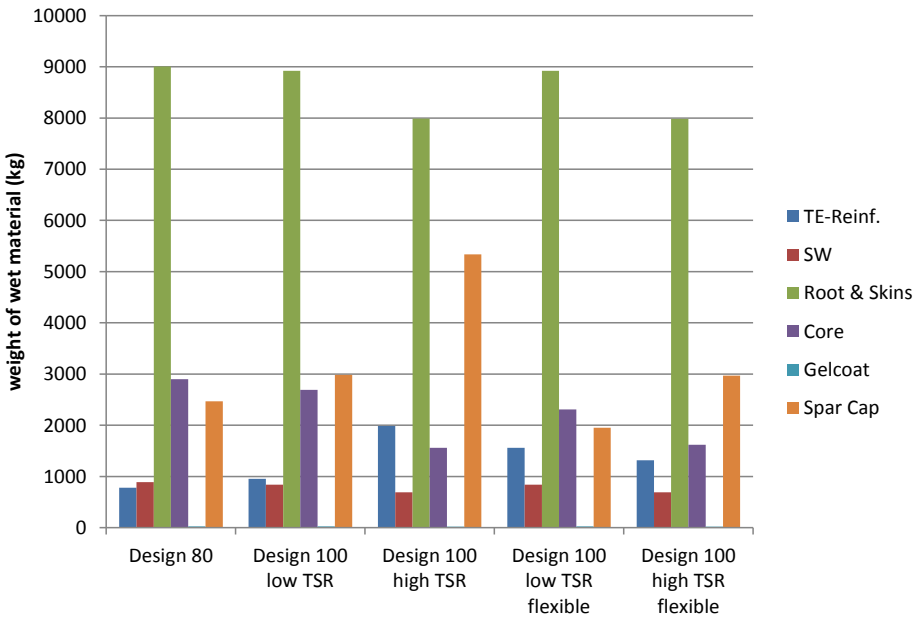

Figure 21: Weight of material per layup component

8. SUMMARY AND DISCUSSION

The initial hypothesis stated that if the acoustic (tip velocity) constraint may be removed (as is often assumed in offshore applications) the opportunity to reduce drivetrain costs is realized via a proportionate reduction in drivetrain torque capacity. The subsequent assumption was that overall system costs can go down and that the overall cost of electricity produced by the high speed rotor can decrease. The hypothesis was that innovative technologies to enable quiet rotors can enable faster rotors; therefore, cheaper turbine systems producing highly cost-competitive energy from wind power.

This section discusses outcomes of baseline rotor optimization, placement of airfoils to balance structural and aerodynamic efficiency, ideal rotor design for high speed rotors, and structural limitations which prevent the achievement of aerodynamically optimal high speed rotors.

Table 7 provides a full summary of rotor design outcomes.

80 m/s Optimized Design Results

The optimized 61.5 m blades for the 5MW rotor were different in several ways from the original 5MW reference model baseline: the solidity was lower, the design TSR for optimal C_p was higher, and the blade mass was lower. The optimized design was stiffness driven in that the requirement for maximum out-of-plane blade deflection was active, while the requirements for fatigue and blade flap frequency were not active. The blade weight was affected by the sizing of sandwich structures in the aft panels to meet buckling requirements.

Airfoil Placement

The optimization allowed modification of the blade thickness distribution to explore the design space. Utilization of the thickest airfoils outboard on the blade is advantageous in that it maximizes structural efficiency. Initial expectations were that the low solidity rotor design would take advantage of the structural efficiency by locating thick airfoils further outboard. However, use of thicker airfoils outboard incurred the cost of increased blade drag, decreased blade lift-to-drag ratio, and decreased rotor AEP. Additionally, results for all designs showed that use of the chosen family of thick airfoils outboard was not a viable strategy for high speed rotors. If higher performing, thicker airfoils were developed they would improve the structural efficiency of high speed rotors as well as lower speed rotors. High performing thick airfoils would enable more effective rotor systems across the entire design space.

Ideal High Speed Rotor Design

Explanation of an ideal scenario for aerodynamic design of a high tip speed rotor is needed to frame the results of the investigation. From a purely aerodynamic perspective, an increase in tip velocity from the baseline 80 m/s to 100 m/s would translate to an increase in rotor design tip speed ratio of 100/80, or 25%. Using the straightforward approach, the aerodynamic rotor loads on the rest of the turbine system remain unchanged. The exception is the 20% decrease in rotor torque. In this scenario, the design TSR increases; it increases from a value of 8.9 for baseline Design 80 to 8.9*1.25 = 11.125. The airfoil design lift coefficients remain unchanged; their optimal values are unchanged. Therefore, the rotor solidity decreases; it decreases from 4.53 for baseline Design 80 to 4.53/1.25 = 3.624.

The rotor performance, in terms of Regions 2, 2.5, and 3, for the nominal rotor and ideal high speed rotor are shown in Figure 22 as solid and dotted lines, respectively. Region 2 is blue; Region 2.5 is green; Region 3 is red. The curves for these two designs are identical; the exceptions are TSR, tip velocity, and rotor torque. Curves in Figure 22 are generated using simple relationships and are meant to illustrate the magnitude of quasistatic loads and performance characteristics; the curves are not representative of dynamic aero-servo-elastic events.

A third set of curves, dashed, are shown in Figure 22. The dashed curves represent the characteristics of a rotor exhibiting TSR equal to the baseline and higher speed operation. The rotor power plot shows that the rotor exhibits a higher AEP at the cost of increased thrust load. The rotor achieves rated torque and maximum rotor speed almost simultaneously because it operates at the lower TSR. Energy capture is maximized because the extent of Region 2.5 is minimized. However, Region 2.5 offers important thrust load limiting capabilities. Thus, an increase in thrust loads is shown by the dashed curves.

The optimal high speed designs did not represent ideals of the high speed rotor because the design problem is multidisciplinary, involving aerodynamics and structures. Structures are adversely affected by the low solidity of the ideal high speed rotor design. Ideal rotor solidity and blade thickness decrease as rotor speed increases. The blades' spar caps become disproportionately heavy because they are stiffness driven. Even though the decrease in solidity leads to lighter weight blade skins, the overall blade weight increases because of the larger spar caps.

Blade thickness decreases as the rotor solidity decreases for a given number of blades. One solution path is to pursue a rotor containing fewer blades, thus increasing the thickness and structural efficiency of the individual blades. However, the number of blades was held constant. Another solution path is to increase structural efficiency by utilizing thick airfoils at outboard locations. However, thick airfoils were not seen as the best option, as described above in "Airfoil Placement". A third, surprising, solution is to utilize an airfoil family which exhibits lower design lift coefficients. However, airfoil lift-to-drag ratios and rotor performance coefficient typically suffer as lift coefficients decrease. Still, an approximation of the third approach was a path taken by the aero-structural optimization as discussed in "Rotor Aerodynamic Performance."

100 m/s Design Results

The two optimal high speed designs represent two approaches from the discussion above. One maps directly to the dashed curves of Figure 22. One maps to an intermediate between dashed curves and dotted curves in Figure 22.

Design 100 low TSR was a design roughly equivalent to the dashed curves in Figure 22. Its solidity was roughly equivalent to the solidity of Design 80. However, its thrust loads were highest. Still, it was the lightest weight of the high speed designs because its high solidity allowed for a thick blade and lighter weight spar caps. Finally, because its thrust loads were highest, it had the greatest adverse effect on the sizing of the rest of the system.

Design 100 high TSR was a design anticipated to match the dotted curves in Figure 22. However, it ultimately lies in the intermediate space between the dashed curves and dotted curves because it is subject to the compromises and constraints imposed by the structural design. Its solidity was lowest, but not as low as was anticipated for the ideal aerodynamic design. Its thrust loads were increased above the baseline, but not as high as the high speed high solidity design. It was the heaviest of the high speed designs because its lower solidity and lower blade thickness required much heavier spar caps to meet stiffness requirements. Because its thrust loads were closer to those for Design 80, it had a much smaller adverse effect on the sizing of the rest of the system.

Benefits for the overall turbine in terms of decreased torque were experienced in both high speed designs. Full system sizing and cost analysis documented in the joint report [1] quantifies the costs and benefits of each full system design.

Flexible Design

The blade deflection requirement was removed from the layup design process for the low solidity design. The process led to a design driven by the flapwise frequency requirement, closely followed by spar cap fatigue. The blade weight was the lowest of all the designs. Blade tip deflections under operational load were quite high; simulations estimate regular deflections in excess of 8 meters at rated wind speed. In future work on highly flexible rotors, special considerations should be included in AEP computations for loss of swept area at rated wind speed.

Table 7: Summary of designs

	For more information	Design 80	Design 100 high TSR	Design 100 low TSR	Design 100 high TSR flexible	Design 100 low TSR flexible
Blade Designation		SNL61p5-02	SNL61p5 (100)-00	SNL61p5 (100)-01	SNL61p5 (100)-02	SNL61p5 (100)-03
IEC Turbine Class		I-B	I-B	I-B	I-B	I-B
Blade Length (m)		61.5	61.5	61.5	61.5	61.5
Rotor max Cp	Section 6	0.499	0.503	0.493	0.503	0.493
TSR for max Cp	Section 6	8.9	9.9	9.1	9.9	9.1
Rotor solidity (%)	Section 6	4.53	3.76	4.60	3.76	4.60
Rotor thrust coefficient, C_T	Section 6	0.743	0.761	0.720	0.761	0.720
Max rotor thrust (kN)	Appendix D	933 DLC1.3, ETM	1,059 DLC1.3, ETM	1,148 DLC1.3, ETM	1,007 DLC1.3, ETM	1,108 DLC1.3, ETM
Max root bending moment (rotor c.s.) (kNm)	Appendix D	15,470 DLC1.4, ECD	16,760 DLC1.3, ETM	18,810 DLC1.3, ETM	15,960 DLC1.4, ECD	17,860 DLC1.3, ETM
Max root bending moment (blade c.s.) (kNm)	Appendix D	15,910 DLC6.1, 50yrEWM	16,750 DLC1.3, ETM (16,320 DLC6.1, 50yrEWM)	19,310 DLC6.1, 50yrEWM	16,180 DLC6.1, 50yrEWM	19,210 DLC6.1, 50yrEWM
Spar cap width (mm)	Appendix D	575	587	496	553	456
Max TE panel thickness (mm)	Appendix D	68	30	57	26	34
Max spar cap thickness (number of layers)	Appendix D	90	196	120	124	102
Max TE-reinf thickness (number of layers)	Appendix D	47	122	58	80	95
Max OoPDefl (m), <7.07 req'd	Appendix D	7.05 DLC1.4, ECD	7.02 DLC1.4, ECD	6.99 DLC1.4, ECD	11.19 DLC1.4, ECD	9.87 DLC1.4, ECD
Min blade fatigue life (yrs), >20 req'd and location	Appendix D	17,788 Spar cap	111,682 TE reinf.	4,371 Spar cap	2141 Spar cap	994 Spar cap
Buckle, >1.62 req'd	Appendix D	1.64	1.67 50yrEWM, 2.50 ETM	1.62	1.67	1.63
Blade mass (kg, ANSYS computed)	Appendix D	16,097	17,590	16,423	14,607	15,611
Span-wise CG location (m)	Appendix D	17.762	20.088	18.712	17.404	17.605
1st flap freq. (Hz) >0.67 req'd, Design 80 >0.83 req'd, Design 100	Appendix D	0.95	0.86	0.95	0.89	0.93
1st edge freq. (Hz)	Appendix D	1.24	1.12	1.24	1.21	1.46
Edge/flap ratio, >1.30 req'd	Appendix D	1.30	1.30	1.30	1.36	1.57
Flutter speed (RPM)	Appendix D	20.5 3rd flap & torsion	20.5 3rd flap & torsion	21.9 3rd flap & torsion	17.8 3rd flap & torsion	22.1 3rd flap & torsion
Approximate blade materials cost	Appendix E	$122,170	$192,897	$135,511	$128,034	$109,501

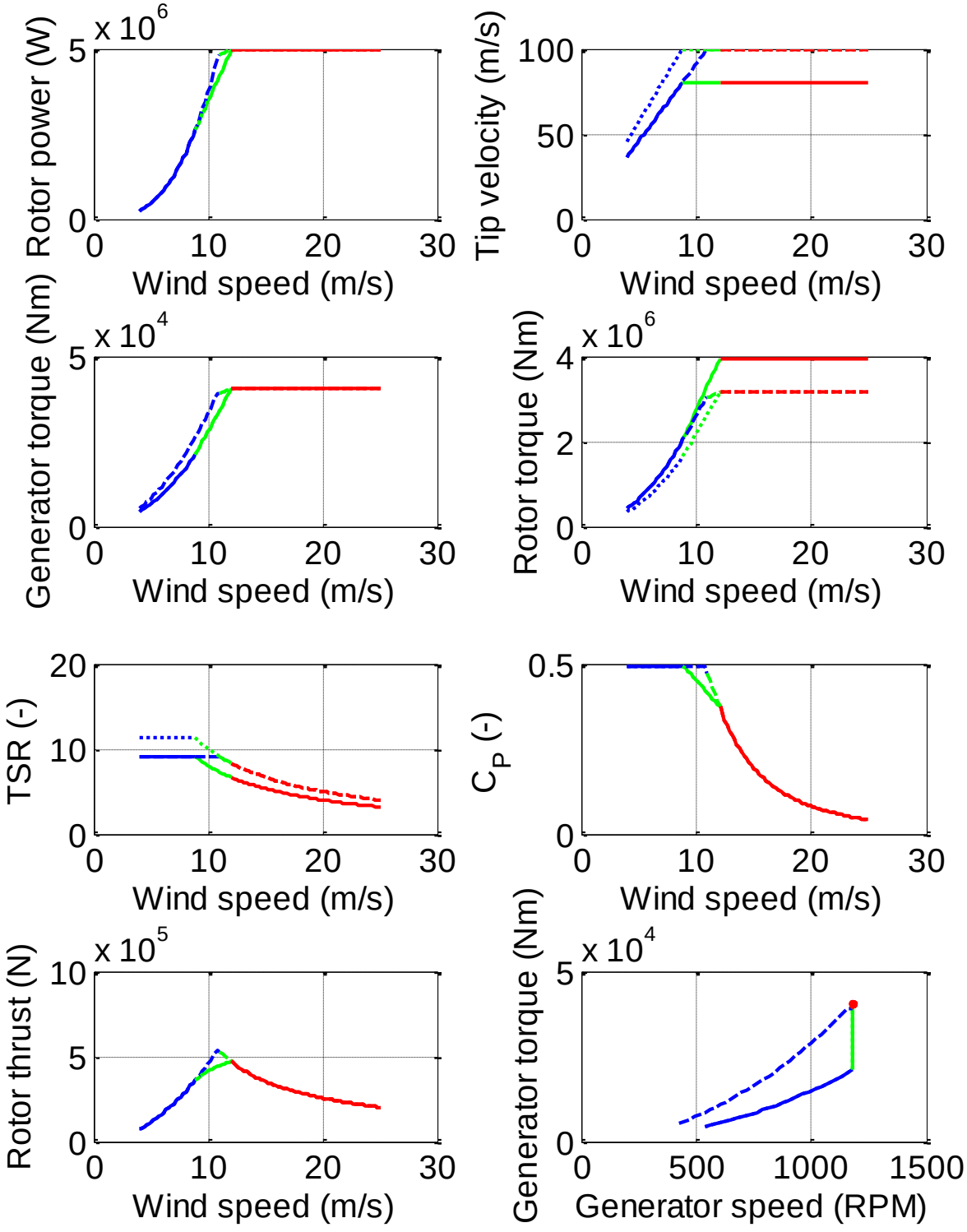

Figure 22: Illustration of turbine control regions showing three different rotor design approaches: solid-low speed, high solidity, low TSR; dotted-high speed, low solidity, high TSR; dashed-high speed, high solidity, low TSR;

Future Work

Two-Bladed Turbines

This investigation focused solely on three-bladed rotors. Jamieson [2] went beyond three bladed rotors and showed how two-bladed rotors can realize benefits through higher blade solidity and increased blade thickness. Further investigation into two-bladed rotors is worthwhile.

Investigation of Low Wind Speed Turbine Class

The current work was based on design for IEC Turbine Class I-B conditions. It would be wise to perform a similar investigation of turbine and rotor design for a lower wind speed class which is more representative of land-based deployments, such as Turbine Class III. These turbines typically exhibit high capacity factors as a result of larger rotors. Design drivers are likely to be different.

Controls

Controls were intentionally kept outside the scope of the current study because of its preliminary nature. The exceptions were adjustments to controls parameters related to variable speed control in Region 2 to enable tracking of maximum rotor C_p. It is clear now that investigation into the controls schemes used for these turbine designs is needed.

The rotor designs were largely driven by blade tip deflection. The extreme coherent gust including direction change (IEC DLC 1.4, ECD) and operation in extreme turbulence (IEC DLC 1.3, ETM) were the design load cases which produced the highest blade tip deflections. These are dynamic events in which controller design was actually quite important. Furthermore, the driving loads and responses were experienced in the vicinity of rated wind speed where speed and pitch control are active at the same time.

Additionally, more advanced aspects of setting Region 2 and 2½ controls should be examined. The rotor operates at maximum efficiency in Region 2. Depending on rated wind speed, rated generator torque, and desired tip speed ratio, the range of Region 2 wind speeds can be quite small. Changes in controller parameters which enable lower loads in exchange for decreased rotor C_p would be advantageous. For example, Jamieson [2] showed how proper adjustment of rotor fine pitch leads to greatly decreased rotor thrust loads while suffering a small amount of rotor efficiency.

Airfoils Placement

Results were surprising in that thick airfoils were not utilized further outboard in the high speed designs. Additional investigation into the optimal placement of airfoils may be warranted. Eight design variables were used to locate airfoils along the blade. Bounds were placed on those design variables to reasonably limit the time aero-structural optimization time. Utilization of a larger design space in a targeted study of optimal thickness distribution is desirable.

Materials

Additional investigations of material properties for blade design are needed. Simple assumptions regarding materials and materials properties were made. Factors such as cost and mechanical properties are critical.

Blade Cost Models

Integration of accurate blade cost models will enable rotor design work to be directly relevant to cost of energy. When blade cost, rather than blade mass, is computed, effects of rotor innovations on the potential wind energy cost of energy are quantified. Numerous blade cost modeling approaches now exist. NREL has developed cost models for non-rotor components in the turbine. These resources should be assembled in a manner that enables research projects to quantify results in terms of anticipated COE changes.

Figure 23 shows blade mass and blade material cost for each design. The charts illustrate how small differences in blade mass can actually translate to large differences in cost of material. The difference is especially true when carbon fiber is used. A good example is seen here in that the low TSR Design 100 exhibits a greater mass but lower material cost than the high TSR Design 100.

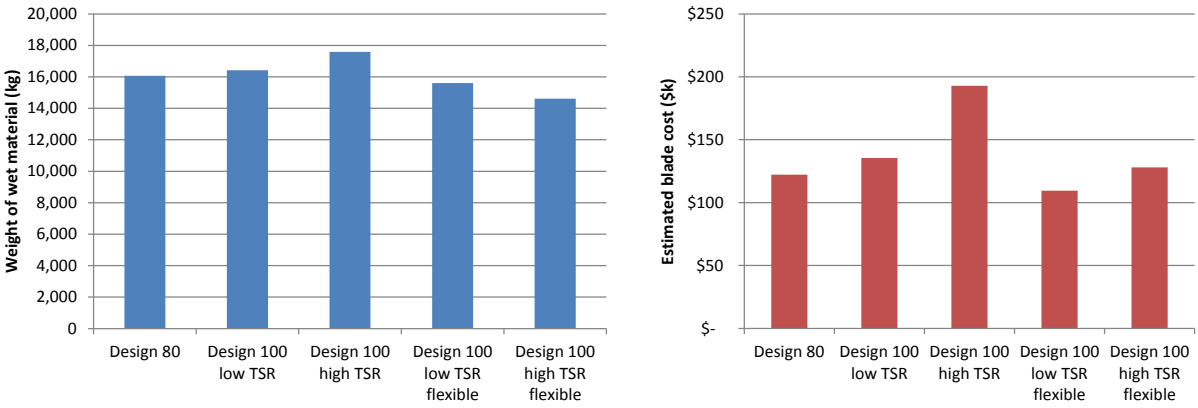

Figure 23: Blade masses and estimated blade costs

Natural Frequency Criteria

Criteria for blade flapwise natural frequency and minimum spacing of edge-flap natural frequencies were not called out in the IEC standards, but are often common practice in blade design. However, these criteria may be relaxed in modern blade design as blades become light and flexible if designers have confidence in their understanding of the aero-structural dynamic interactions of the system. The investigation showed that these criteria can drive the design of the blade, especially with respect to edgewise blade stiffness. Additional designs which exclude the natural frequency constraints will lead to lower cost blades. Research into the operation of turbines at speeds which lie near natural resonances is an important topic for further investigation.

Suggested Improvements

Many lessons were learned as the designs for these rotors were created.

Computation of the appropriate blade tip deflection target, δ_{target}, was clumsy in the current implementation of these tools. A framework which allows for better estimation of dynamic aeroelastic loads and structural responses is needed directly in the aerodynamic optimization loop.

Immediate translation of blade materials into blade materials cost through the use of an appropriate cost model is needed. The optimization should seek Pareto optimal designs in terms of cost and AEP (Figure 6) instead of seeking Pareto optimal designs in terms of mass and AEP (Figure 5). It is possible for a lighter weight blade to be the more expensive blade as shown in Figure 23. The discrepancy is especially possible when high price materials are present, such as carbon fiber.

A slightly higher fidelity structural model should be utilized during the aero-structural optimization. However, implementation of additional design variables and additional analysis checks during the optimization loop will increase optimization time. Large discrepancies in estimated blade mass become apparent upon close examination of data in Table 7 and in Figure 5. The largest contributor to the discrepancy was the failure to adequately include the edge-stiffening material in the aero-structural optimization stage of the work. Requirements governing edge stiffness, either frequency or fatigue, must be included from the beginning when changes in blade solidity are an important element in designs.

Sizing of core material in the blade panels has a secondary effect on blade mass. Computationally fast and accurate buckling models must be implemented to include these effects in the aero-structural optimization loop. Additionally, the optimization loop does not include analysis of parked loads on the blade plan form during extreme winds. Parked loads typically drive sizing of core material in blade panels. Inclusion of parked storm loads may encourage lower solidity blades.

Close control of aerodynamic design. The approach of HARP_Opt produced rotor designs that operated sub optimally in several respects. These designs demonstrated how low load rotors can be effective in terms of overall cost of energy (see Figure 14). However, the approach can be improved; its design outcomes deviated from what is typically expected for aerodynamic rotor designs. The primary clue was that design lift coefficients for Pareto optimal designs were non-optimal. The results did, however, hint at the concept of the modern low load rotor as described in Reference [17].

Better definition of structural and aerodynamic design variables is needed in future approaches. For example, the rotor TSR was not a design variable. The rotor TSR was an outcome of the various combinations of chord and twist, which are defined by design variables described above in the section on *Aero-Structural Optimization*. Instead, it is better to define the fundamental aerodynamic design parameters directly. Future design approaches for optimal aero-structural rotor design will be based on fundamental performance characteristics, such as rotor inflow distribution. Follow up discussion on the topic is found in the Sandia memo by Resor, et.al. [20]

REFERENCES

1. Dykes, K., Resor, B. R., Platt, A., Guo, Y., Ning, A., King, R., and Petch, D. "Effect of Tip Speed Constraints on Optimized Design of a Wind Turbine," National Renewable Energy Laboratory: NREL-XXXX, 2014 [draft].
2. Jamieson, P. "Light-Weight, High-Speed Rotors for Offshore," *European Offshore Wind Conference*. 2009.
3. Keegan, M. H., Nash, D. H., and Stack, M. M. "On erosion issues associated with the leading edge of wind turbine blades," *Journal of Physics D: Applied Physics* Vol. 46, 2013.doi: 10.1088/0022-3727/46/38/383001
4. Resor, B. R. "Definition of a 5MW/61.5m Wind Turbine Blade Reference Model," Sandia National Laboratories: SAND2013-2569, 2013.
5. Hansen, C. National Wind Technology Center. *NWTC Design Codes AirfoilPrep*. (v2.2) http://wind.nrel.gov/designcodes/preprocessors/airfoilprep/. June 28, 2012.
6. Moriarty, P., and Migliore, P. "Semi-Empirical Aeroacoustic Noise Prediction Code for Wind Turbines," National Renewable Energy Laboratory: NREL/TP-500-34478, 2003.
7. Griffith, D. T., and Ashwill, T. D. "The Sandia 100-meter All-glass Baseline Wind Turbine Blade: SNL100-00," Sandia National Laboratories: SAND2011-3779, 2011.
8. Sale, D. C. *NWTC Design Codes HARP_Opt*. (v2.00.00) http://wind.nrel.gov/designcodes/simulators/HARP_Opt/. October 10, 2013.
9. Sale, D. *Co-Blade v1.20.00*. https://code.google.com/p/co-blade/. 2012.
10. Berg, J., Resor, B. R., Owens, B. C., and Laird, D. *Numerical Manufacturing and Design Tool (NuMAD) for Wind Turbine Blades*. (v2.0) http://energy.sandia.gov/?page_id=2238. 2012.
11. Platt, A. *NWTC Design Codes WT_Perf*. (3.0.00a-adp) http://wind.nrel.gov/designcodes/simulators/wtperf/. November 26, 2012.
12. Bir, G. *NWTC Design Codes BModes*. (v3.00.00) http://wind.nrel.gov/designcodes/preprocessors/bmodes/. June 28, 2008.
13. Wiser, R., and Bolinger, M. "2012 Wind Technologies Market Report," Energy Efficiency and Renewable Energy Report: 2013.
14. Tegen, S., Lantz, E., Hand, M., Maples, B., Smith, A., and Schwabe, P. "2011 Cost of Wind Energy Review," National Renewable Energy Laboratory: NREL/TP-5000-56266, 2013.
15. Johanns, W., and Griffith, D. T. "User Manual for Sandia Blade Manufacturing Cost Tool: Version 1.0," Sandia National Laboratories: SAND2013-2733, 2013.
16. Griffith, D. T., and Johanns, W. "Large Blade Manufacturing Cost Studies Using the Sandia Blade Manufacturing Cost Tool and Sandia 100-meter Blades," Sandia National Laboratories: SAND2013-2734, 2013.
17. Chaviaropoulos, P. K., and Sieros, G. "Design of Low Induction Rotors for Use in Large Offshore Wind Farms," *Proceedings of the 2014 European Wind Energy Association Conference*. Barcelona, Spain, 2014.
18. Damiani, R., and Bir, G. S. *NWTC Design Codes PreComp*. (v1.00.03) http://wind.nrel.gov/designcodes/preprocessors/precomp. July 2012.
19. Buhl, M. *NWTC Design Codes Crunch*. (v3.00.00) http://wind.nrel.gov/designcodes/postprocessors/crunch/. April 6, 2007.

20. Resor, B. R., Kelley, C., Maniaci, D. C., and Berg, J. "Background and Recommendations for a Future Sandia Rotor Design Capability (Memo to Michael Derby and Shreyas Ananthan)." 2014.
21. Jonkman, J. *NWTC Design Codes FAST*. (v7.01a) http://wind.nrel.gov/designcodes/simulators/fast/. December 3, 2012.
22. Laino, D. J., Jonkman, B., and Nguyen, K. *NWTC Design Codes AeroDyn*. (v13.00.01a) http://wind.nrel.gov/designcodes/simulators/aerodyn/. February 21, 2012.
23. Kelley, N., and Jonkman, B. *NWTC Design Codes TurbSim*. (v1.06.00) http://wind.nrel.gov/designcodes/preprocessors/turbsim/. September 25, 2012.
24. Buhl, M. *NWTC Design Codes IECWind*. (v5.01.02) http://wind.nrel.gov/designcodes/preprocessors/iecwind. October 8, 2012.
25. *IEC 61400-1 Ed.3: Wind turbines - Part 1: Design requirements*, International Electrotechnical Committee, 2005.
26. *Guideline for the certification of wind turbines*, Germanischer Lloyd, 2010.
27. Fingersh, L. J., Hand, M., and Laxson, A. "Wind Turbine Design Cost and Scaling Model," National Renewable Energy Laboratory: NREL/TP-500-40566, 2006.

APPENDIX A – SUMMARY OF AERO-STRUCTURAL OPTIMIZATION INPUT PARAMETERS

Following is a summary of input parameters used for the modified version of HARP-Opt.

	80 m/s optimized	100 m/s optimized (low TSR)	100 m/s optimized (high TSR)
Number of blades	3	3	3
Number of spanwise aerodynamic analysis elements	30	30	30
Rated power (kW)	5000	5000	5000
Rotor radius (m)	63	63	63
Hub radius (m)	1.5	1.5	1.5
Hub height (m)	90	90	90
Minimum rotor speed (rpm)	6.9	6.9	6.9
Maximum rotor speed (rpm)	12.13	15.16	15.16
Maximum tip velocity (m/s)	80	100	100
Fluid properties			
Mean wind speed (m/s)	10	10	10
Air density (kg/m^3)	1.225	1.225	1.225
Kinetic viscosity (m^2/s)	0	0	0
Lowest wind speed analysis (m/s)	2	2	2
Highest wind speed analysis (m/s)	26	26	26
Aero-structural properties			
Target maximum allowable OoP tip deflection (m)	3.05	2.72	3.25
Baseline blade structural file	SNL61p5m.xlsx	SNL61p5m.xlsx	SNL61p5m.xlsx
Allowable root chord min (m)	3.386	3.386	3.386
Allowable root chord max (m)	3.386	3.386	3.386
Root transition start (m)	0.045	0.045	0.045
Root transition end (m)	0.252	0.252	0.252
Rotor radii of chord and twist control points (m)	15.85| 19.44| 29.66| 44.96| 44.96	15.85| 19.44| 29.66| 44.96| 44.96	15.85| 19.44| 29.66| 44.96| 44.96
Twist LBs (deg)	9.0| 5.0| 5.0| 1.0| 1.0	9.0| 5.0| 5.0| 1.0| 1.0	9.0| 5.0| 5.0| 1.0| 1.0
Twist UBs (deg)	14.5| 13.0| 11.0| 4.0| 4.0	14.5| 13.0| 11.0| 4.0| 4.0	14.5| 13.0| 11.0| 4.0| 4.0
Chord LBs (m)	3.0| 2.0| 1.0| 1.0| 1.0	3.0| 2.0| 1.0| 0.8| 0.8	2.4| 1.6| 0.8| 0.6| 0.6
Chord UBs (m)	5.0| 5.0| 5.0| 4.0| 4.0	5.0| 5.0| 5.0| 4.0| 4.0	4.0| 4.0| 4.0| 3.2| 3.2
Airfoil family	DU-NACA	DU-NACA	DU-NACA

Airfoil thickness values (%)	40| 35| 30| 25| 25| 21| 21| 21	40| 35| 30| 25| 25| 21| 21| 21	40| 35| 30| 25| 25| 21| 21| 21
Airfoil locations LBs (m)	0.1679| 0.2264| 0.3436| 0.4101| 0.4751| 0.5401| 0.6051| 0.6051	0.1679| 0.2264| 0.3436| 0.4101| 0.4751| 0.5401| 0.6051| 0.6051	0.1679| 0.2264| 0.3436| 0.4101| 0.4751| 0.5401| 0.6051| 0.6051
Airfoil locations UBs (m)	0.2052| 0.2767| 0.4100| 0.4750| 0.5400| 0.6050| 0.6800| 0.6800	0.2052| 0.2767| 0.4100| 0.4750| 0.5400| 0.6050| 0.6800| 0.6800	0.2052| 0.2767| 0.4100| 0.4750| 0.5400| 0.6050| 0.6800| 0.6800
Spar cap thickness min (#-layers)	50| 50	50| 50	50| 50
Spar cap thickness max (#-layers)	200| 200	300| 300	300| 300
Genetic algorithm settings			
Elite count	1	1	1
Pareto fraction	0.5	0.5	0.5
Crossover fraction	0.25	0.25	0.25

LB = lower bound
UB = upper bound
DV = design variable

APPENDIX B - REGION 2 CONTROLLER

This investigation assumed no change in the generator specifications for the two rotor velocities. A lower gearbox ratio results when increasing the maximum allowable rotor speed while keeping the generator speed and torque limits the same. The Region 2 torque constant in the FAST/AeroDyn controller was updated based on the rotor performance parameters. Table 8 summarizes these parameters. Region 2 torque constants and gearbox ratios were computed as shown in Eqs.(B.1, B.2).

GB = PC_RefSpd / rotor speed Eq.(B.1)

$$VS\_Rgn2k = \frac{1}{2}\frac{\rho\pi R^5 C_p}{\lambda^3 GB^3} \quad \text{Eq.(B.2)}$$

Table 8: Parameters used in the FAST DISCON DLL-style controller

	NREL 5MW reference	Design 80	Design 100 high TSR	Design 100 low TSR
PC_RefSpd (RPM)	1174	1174	1174	1174
Rotor speed for max tip velocity (RPM)	12.13	12.13	15.16	15.16
Rho (kg/m^3)	1.225	1.225	1.225	1.225
R (m)	63	63	63	63
$C_{p,max}$	0.482	0.499	0.503	0.493
TSR for $C_{p,max}$	7.55	8.9	9.9	9.1
Gearbox ratio	97	96.76	77.41	77.41
VS_Rgn2K, used in simulations	2.332287	1.5670	2.3400	2.9370

A slow, steady wind ramp rate of 200 seconds per 1 m/s wind speed increase was used to estimate the quasi-steady operating characteristics of the turbines in FAST/AeroDyn. Table 9 summarizes the boundaries between the major regions of turbine control. Figure 24 and Figure 25 illustrate important outputs from the aeroelastic model for the 1,000 second wind speed sweep.

Table 9: Turbine control regions boundaries as modeled in FAST

	Generator speed (rad/sec)			Wind speed (m/s)		
Region boundary	Design 80	Design 100 high TSR	Design 100 low TSR	Design 80	Design 100 high TSR	Design 100 low TSR
1 ½ to 2	91.2	91.2	91.2	8.5	7.9	8.7
2 to 2 ½	116.2	119.1	NA	8.8	10.3	NA
2 ½ to 3	121.7	121.7	121.7	11.6	11.6	11.6

Notice that the 100 m/s design transitions directly into Region 3 operation from Region 2 operation. No intermediate Region 2 ½ is present. According to equation 2.2, the gearbox ratio was sufficiently low enough that the Region 2 torque at rated speed was approximately equal to the rated torque. A rotor of higher than 100 m/s tip velocity would either require a modification to generation specifications or decrease in rotor C_p or increase in design TSR.

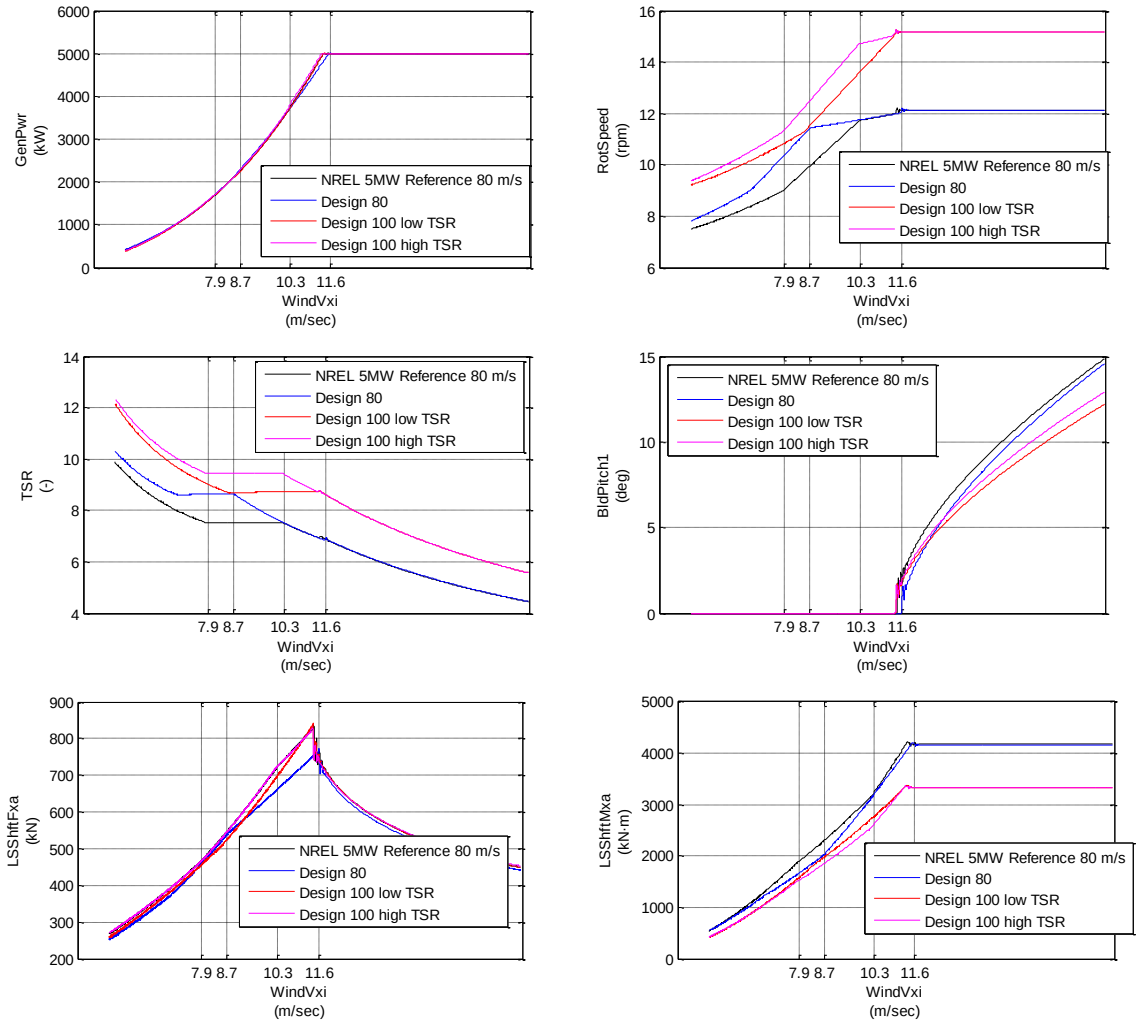

Figure 24: Turbine operational parameters versus wind speed

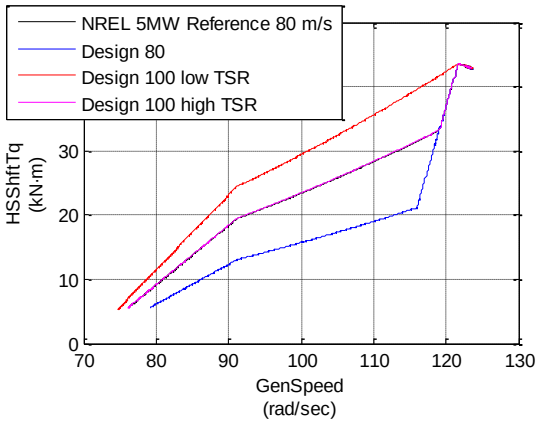

Figure 25: Generator torque-speed curves

No yaw controller was modeled. Typical utility scale turbine yaw rates are about 1.5 degrees per second. The most rapid change in wind direction in the IEC DLC's is the ECD case, which is about 6.5 degrees per second. In effect, the turbine yaw control has little effect on the turbine's ability to maintain yaw alignment in an extreme case.

APPENDIX C - SIMULATION AND ANALYSIS OF DESIGN LOAD CASES

Aeroelastic simulations were used to evaluate the loads experienced by the blades during design load cases (DLCs). The blade was analyzed under the assumption that it was for onshore use. FAST [21] and AeroDyn [22] were used to perform the aeroelastic simulations. TurbSim [23] and IECWind [24] were used to generate wind input files for the simulations. Matlab was used to process the computed responses from simulations. Crunch [19] was used to perform rainflow cycle counting of response waveforms used as input for fatigue analyses.

An automated process based in Matlab was created to manage all the IEC DLC simulations, analyses and results discussed here.

Design load cases (DLC's) as specified by the IEC Design Standard for wind turbines [25] were used. The goal in each case was to evaluate the turbine response with respect to the following failure modes:

- analysis of ultimate strength;
- analysis of fatigue failure;
- stability analysis (buckling, etc.);
- critical deflection analysis (mechanical interference between blade and tower, etc.).

The full set of required design load cases includes power production (with and without faults), startup, shutdown (emergency and normal), parked configuration (with and without faults), transport and erection. The subset of DLC's, listed in Table 10, was examined. These load cases were likely the influential design drivers for the majority of turbine blades. Table 11 summarizes the important input parameters for the IEC aeroelastic simulations. Table 12 summarizes the spanwise location of simulation blade gages during the aeroelastic simulations.

A yaw controller was not modeled. Typical utility scale turbine yaw rates are about 1.5 degrees per second. The most rapid change in wind direction in the IEC DLC's is the ECD case, which is about 6.5 degrees per second. In effect, the turbine yaw control has little effect on the turbine's ability to maintain yaw alignment in an extreme case.

Table 10: IEC DLC's used in design of blades

DLC 1.2 (NTM)	Fatigue damage evaluation during normal power production in normal turbulence
DLC 1.3 (ETM)	Ultimate loads evaluation during normal power production in extreme turbulence
DLC 1.4 (ECD)	Ultimate loads evaluation during normal power production; an extreme coherence gust and change in wind direction
DLC 1.5 (EWS)	Ultimate loads evaluation during normal power production in the presence of extreme wind shear
DLC 6.1 (EWM50)	Ultimate loads evaluation while in a parked configuration during a 50-year extreme steady wind event
DLC 6.3 (EWM01)	Ultimate loads evaluation while in a parked configuration during a 1-year extreme steady wind event including extreme yaw misalignment

Table 11: Important input parameters for IEC analyses

V_{in}	3 m/s
V_{out}	25 m/s
V_{rated}	11.4 m/s
IEC Class	I
Turbulence Class	B
Vref	50 m/s [IEC 6.2, Table 1]
Specified structural damping ratio for blades in FAST (All Modes)	1.5%[c]
Component Class	2[d]
Average wind speed	0.2*Vref=10m/s [IEC 6.3.1.1]
V_{50}	1.4*Vref=70 m/s
V_1	0.8*V_{50}=56 m/s
Mean wind speeds for turbulent wind simulations	5, 7, 9, 11, 13, 15, 17, 19, 21, 23m/s
Turbulence model	Kaimal
Aeroelastic simulation usable record length	600 seconds (turbulent) 100 seconds (steady)
Number of turbulent aeroelastic simulations at each	6

[c] The NREL reference turbine document calls for structural damping of 0.477465% for all blade modes. However, using this value in the simulations for extreme wind in a parked configuration resulted in structural instability. Determination of the correct approach for modeling such behavior should be investigated as part of future work. For the current work, damping values were increased to 1.5% for all modes.

[d] Component Class 2 is used to refer to "non fail-safe" structural components whose failures may lead to the failure of a major part of a wind turbine.

wind speed	
Turbine design life	20 years

Table 12: Spanwise location of simulated blade gages

Blade Gage Name	Span Location (m)
RootM	0
Spn1ML	1.3667
Spn2ML	4.1
Spn3ML	6.8333
Spn4ML	10.25
Spn5ML	14.35
Spn6ML	22.55
Spn7ML	30.75
Spn8ML	38.95
Spn9ML	47.15

Simulation of IEC DLC 1.0 Power Production

DLC 1.2 NTM Fatigue During Normal Operation (NTM)
FAST and AeroDyn were used to perform these simulations. TurbSim was used to provide three-dimensional full-field wind data representative of normal turbulence.

All normal settings were used in the aeroelastic simulation (i.e. NREL 5MW reference turbine inputs files used as-is). One hour of power generation was simulated at each wind speed in the operational range of the turbine, evenly spaced every 2 m/s.

DLC 1.3 NTM Ultimate Strength During Extreme Turbulence (ETM)
FAST and AeroDyn were used to perform these simulations. TurbSim was used to provide three-dimensional full-field wind data representative of normal turbulence.

All normal settings were used in the aeroelastic simulation (i.e. NREL 5MW reference turbine inputs files used as-is). One hour of power generation was simulated at each wind speed in the operational range of the turbine, evenly spaced every 2 m/s.

DLC 1.4 NTM Ultimate Strength During Coherent Gust Including Direction Change (ECD)
FAST and AeroDyn were used to perform these simulations. IECWind was used to provide hub-height wind data for a Class IB turbine.

All normal settings were used in the aeroelastic simulation (i.e. NREL 5MW reference turbine inputs files used as-is). Wind speeds of rated, 2m/s above rated and 2m/s below rated, including wind changes in both directions, were analyzed.

DLC 1.5 NTM Ultimate Strength in Extreme Wind Shear (EWS)
FAST and AeroDyn were used to perform these simulations. IECWind was used to provide hub-height wind data for a Class IB turbine.

All normal settings were used in the aeroelastic simulation (i.e. NREL 5MW reference turbine inputs files used as-is). Steady wind including positive and negative vertical shear were analyzed every 2 m/s throughout the operational range of the turbine.

Simulation of IEC DLC 6.0 Parked Turbine

One of the standard IEC test cases is to model the turbine in high winds when the turbine is parked. Various approaches can be used to model a parked rotor, depending on the design of the turbine system. The steady extreme wind model was used for design of the rotors.[e]

This work uses the following assumptions regarding the parked configuration:

- This turbine used full-span pitch so blades were feathered (pitch angle 90-degrees).

[e] The IEC standard explains the criteria for use of extreme turbulent wind versus steady wind in aeroelastic simulation of the parked scenarios. If the steady extreme wind model is used, the effects of resonant response shall be estimated from the quasi-steady analysis (ETM). If the ratio of resonant to background response (R/B) is less than 5 %, a static analysis using the steady extreme wind model may be used.

- The turbine's HSS brake was engaged for a parked configuration so rotor rotation was fixed at zero.
- The turbine drivetrain model was active so that basic drivetrain dynamics were included in the model response.
- Computation of inflow factors was turned off in AeroDyn because the rotor was stationary.

DLC 6.1 Ultimate Strength in Fifty Year Wind

FAST and AeroDyn were used to perform these simulations. IECWind was used to provide hub-height wind data for a Class IB turbine.

Normal settings were used in the aeroelastic simulation (i.e. NREL 5MW reference turbine inputs files used as-is). Modifications for the parked configuration are described above. Yaw misalignment angles of -15 through 15 degrees, in 5 degree increments were simulated.

DLC 6.3 Ultimate Strength in One Year Wind Including Extreme Yaw Misalignment

FAST and AeroDyn were used to perform these simulations. IECWind was used to provide the hub-height wind data for a Class IB turbine.

Normal settings were used in the aeroelastic simulation (i.e. NREL 5MW reference turbine inputs files used as-is). Modifications for the parked configuration are described above. Yaw misalignment angles of -30 through 30 degrees, in 5 degree increments, were simulated.

APPENDIX D - STRUCTURES OPTIMIZATION COMPLETE RESULTS

Mesh Convergence

An element size study was performed to set an adequate global element size for the model. The output metric of interest is the computed buckling load when a distributed force is applied to the model. ANSYS Shell181 (4-node) elements were used in the model. Figure 26 shows results of the element size study.

It is good practice to use a mesh size that yields little change in computed buckling load factors. A sufficiently accurate mesh for linear FE buckling computations can be assumed when the buckling eigenvalue does not change by more than 5% if the number of elements is doubled. [26]

A global element size of 0.1m meets the criteria and was used for the blade design buckling analyses as described in the Appendix section titled, "Structural Stability (Buckling)." Figure 27, Figure 28 and Figure 29 illustrate the finite element model for each blade.

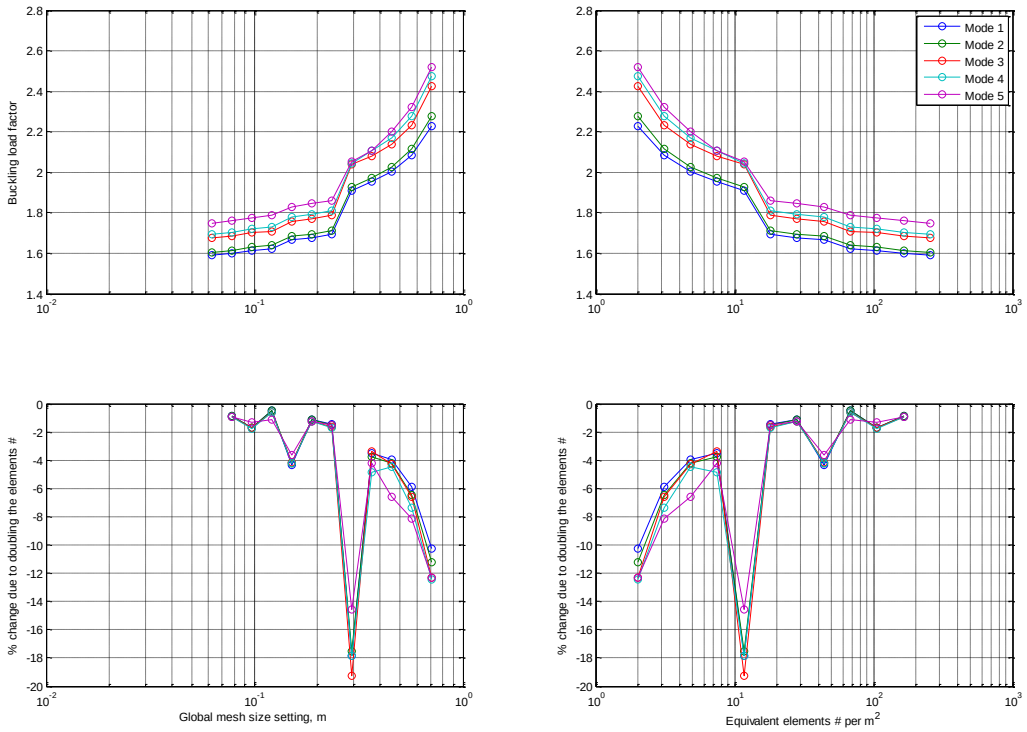

Figure 26: Variation in computed buckling load factors during mesh convergence study

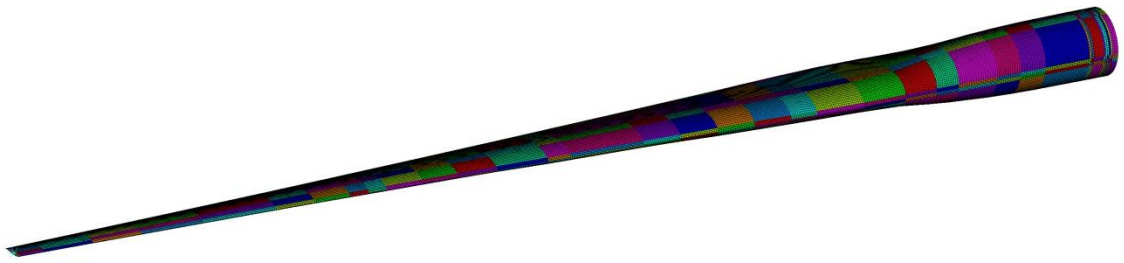

Figure 27: ANSYS FE model of Design 80; global mesh size of 0.10m

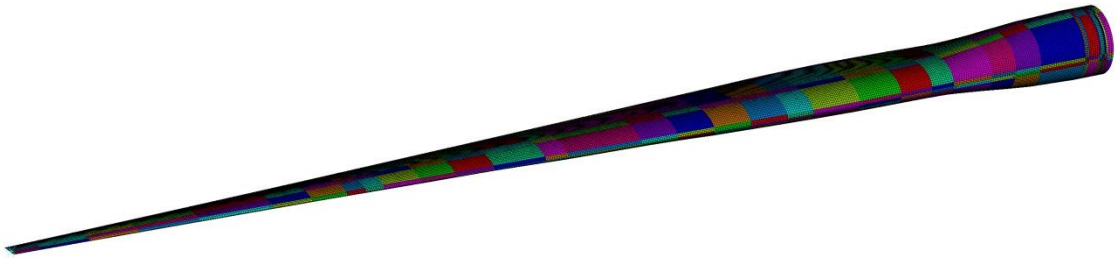

Figure 28: ANSYS FE model of Design 100 low TSR; global mesh size of 0.10m

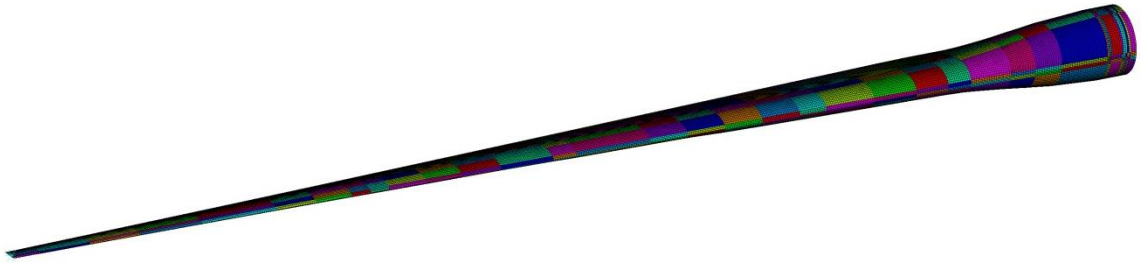

Figure 29: ANSYS FE model of Design 100 high TSR; global mesh size of 0.10m

Material Layup and Structural Design Variables

Figure 30 shows the layer schedule for each layup component in the blade designs. Note that the root buildup was left unchanged for all three designs. Significant changes occurred in layer schedules for the spar cap, trailing edge panel foam thicknesses and trailing edge reinforcement thicknesses. The figures do not capture the changing spar cap width between each design. Table 7 summarizes design variables for all designs and contains spar cap dimensions.

One anomaly is worth noting. The thickness of trailing edge reinforcement in the flexible 100 m/s design is quite high. The edge-flap frequency spacing criteria is much higher than necessary. An extensive run of the global optimization was used to determine the combination of design variables that comprise the structural design. The optimization found a scenario where the in-plane bending stiffness of the trailing edge reinforcement contributed to the buckling

resistance of the aft panel. If the trailing edge reinforcement thickness was reduced any further, the buckling criterion for the blade was violated.

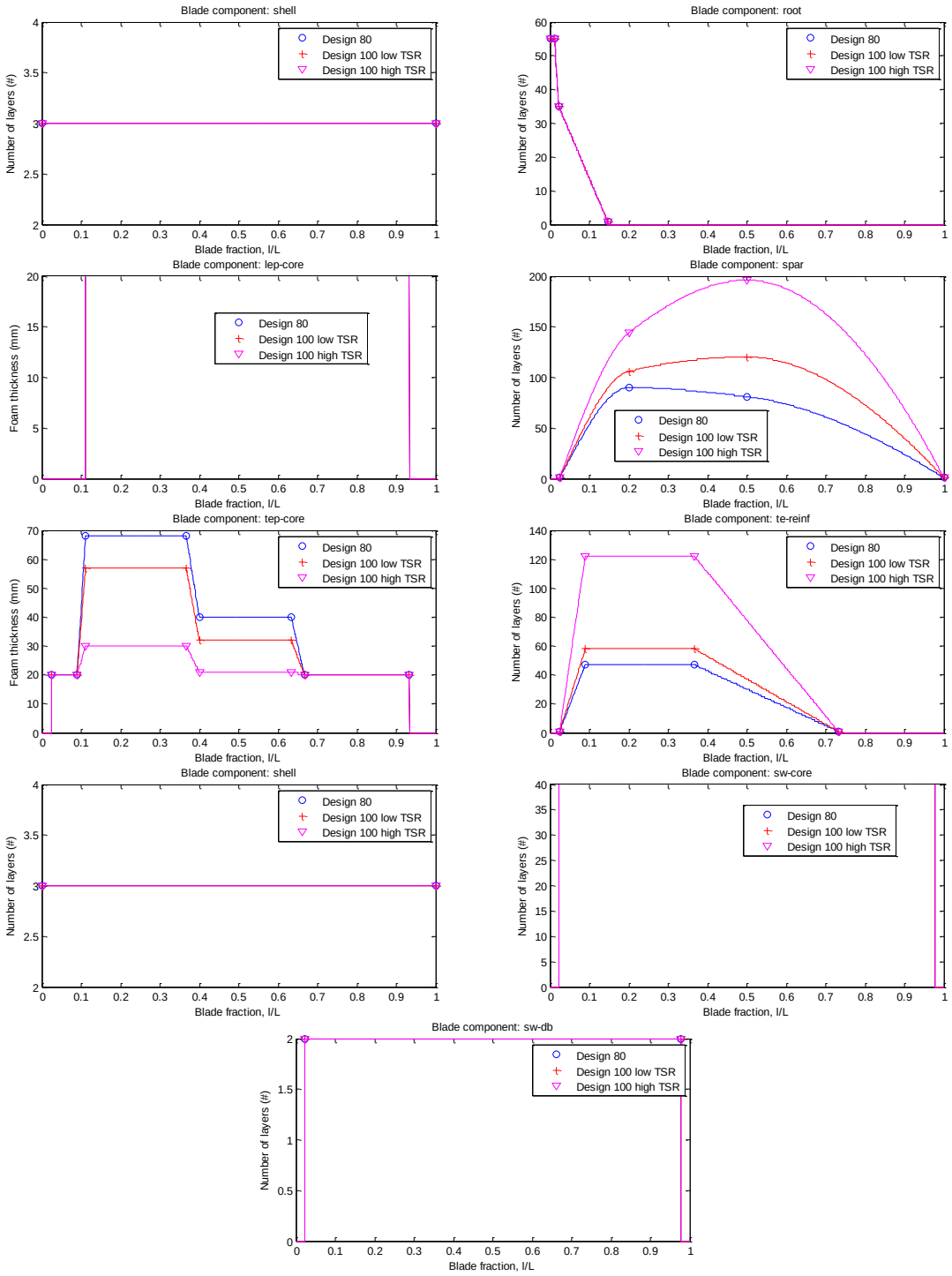

Figure 30: Layer schedules for each major layup component in the blade design concepts

Finite Element Model Cross Sections

Cross sections of the finite element models for Design 80 and Design 100 low TSR are shown in Figures immediately below.

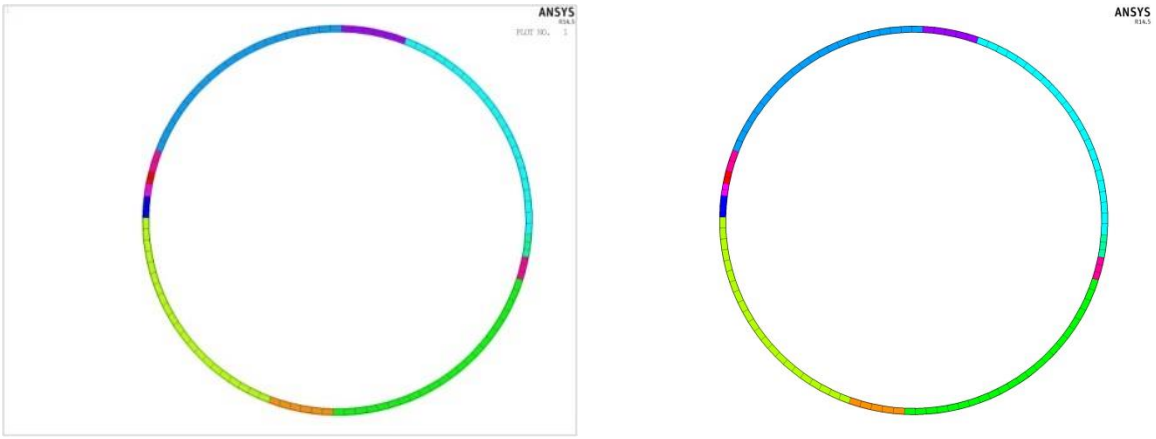

Figure 31: 0.65 m span: Design 80 and Design 100 low TSR

Figure 32: 7 m span: Design 80 and Design 100 low TSR

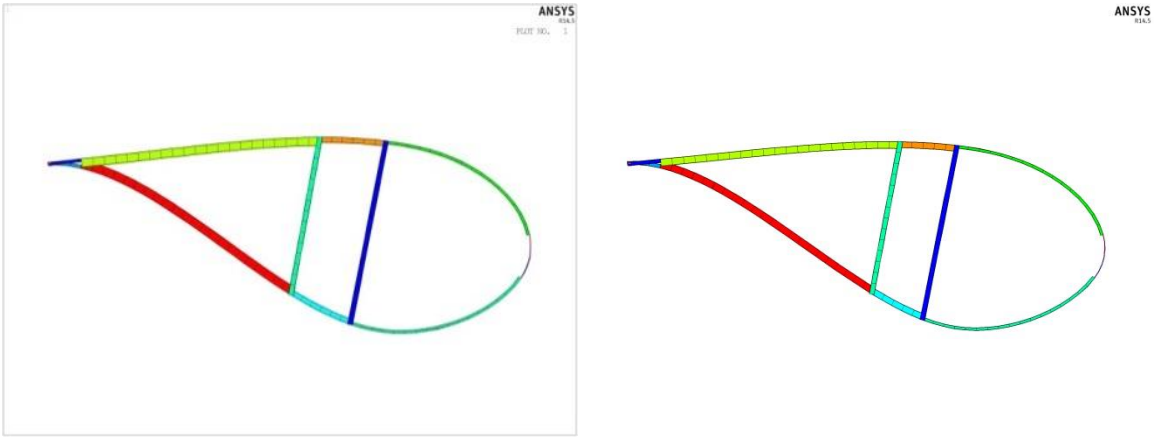

Figure 33: 12 m span: Design 80 and Design 100 low TSR

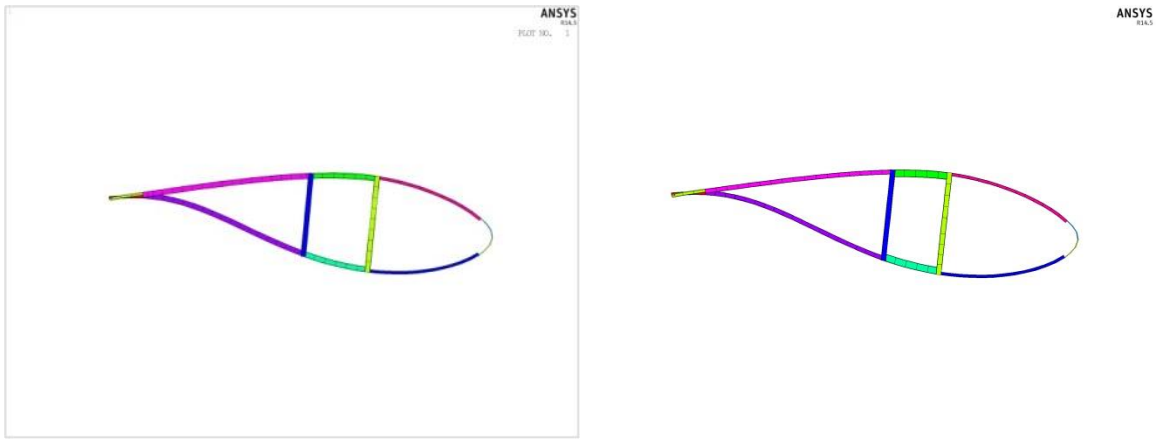

Figure 34: 30 m span: Design 80 and Design 100 low TSR

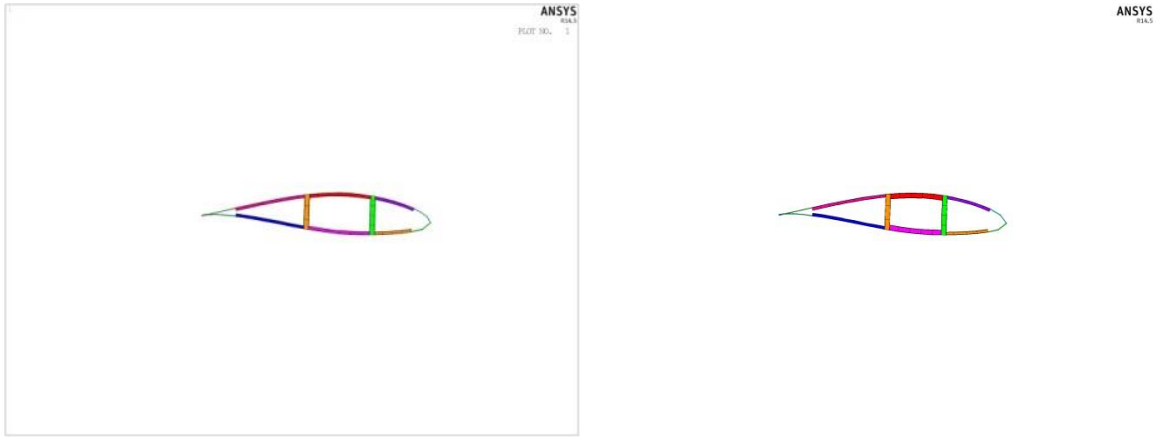

Figure 35: 50 m span: Design 80 and Design 100 low TSR

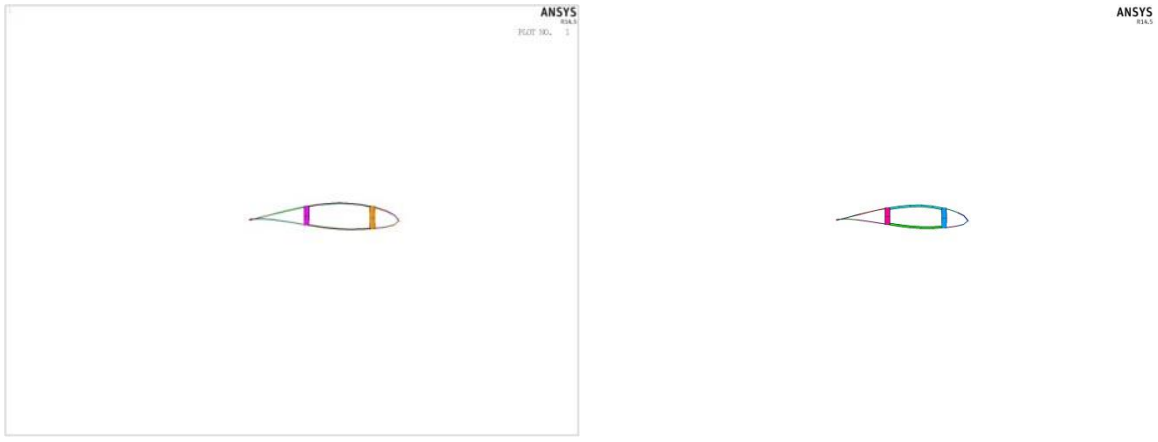

Figure 36: 61 m span: Design 80 and Design 100 low TSR

Distributed Blade Properties

NuMAD was used to convert these blade models into the input files required for PreComp [18] sectional analysis. The computed blade properties are shown in plots of Figure 37.

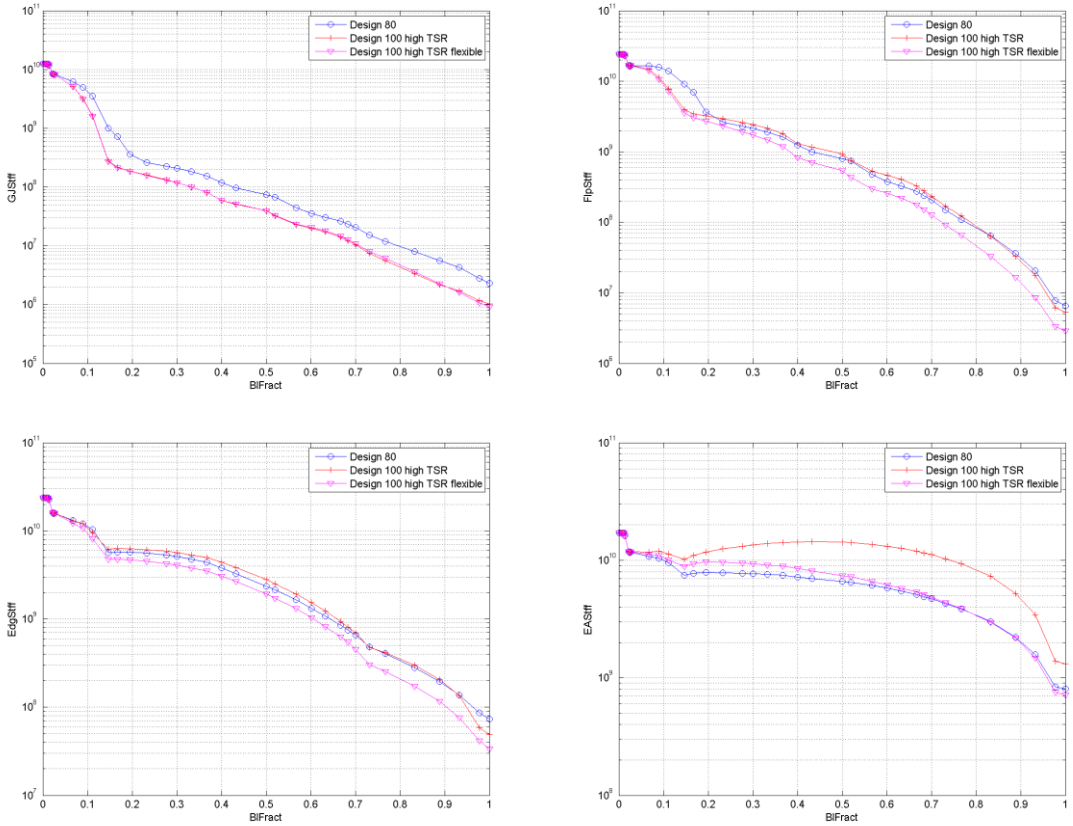

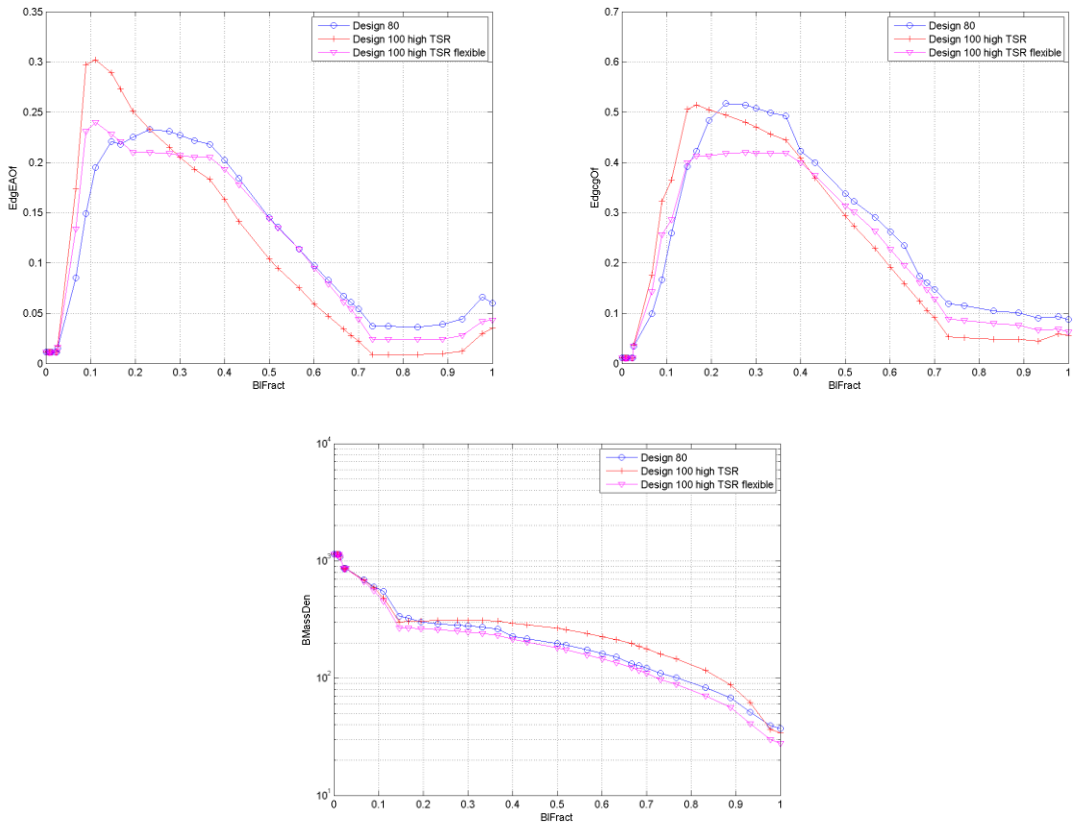

Figure 37: Distributed blade properties as computed by PreComp. All ordinates are defined as FAST blade input parameters.

Critical Deflection

FAST computes the out-of-plane deflection of the blade tip for all simulations. A summary of maximum deflections is found earlier in Table 7. Table 14 summarizes other important information regarding computation of tower clearance. The tower radius information used here is taken from the ADAMS-specific input for the NREL 5MW reference turbine.

Table 13: Safety factors used in evaluation of tower clearance (IEC 7.6.5)

Partial safety factor for loads, γ_f	1.35	Do not use for DLC 1.1
Partial safety factor for materials, γ_m	1.1	
Partial safety factors for consequences of failure, γ_n	1.0	Component class 2
Total safety factor	1.485	

Table 14: Allowable OoP tip deflection parameters

Tower height (m)	87.6	FAST model input
Tower-to-shaft (m)	1.96256	FAST model input
Shaft tilt (deg)	5	FAST model input
Shaft horizontal length (m)	5.0191	FAST model input

Precone (deg)	2.5	FAST model input
Rotor radius (m)	62.5	FAST model input
Tower base radius (m)	3.000	ADAMS-specific input
Tower top radius (m)	1.935	ADAMS-specific input
Tower radius @ blade tip (m)	2.660	Computed
Nominal tower clearance (m)	13.16	Computed
Available clearance (m)	10.50	Computed

Allowable tower clearance, including safety factor, is computed as $\frac{10.50m}{1.485} = 7.07m$.

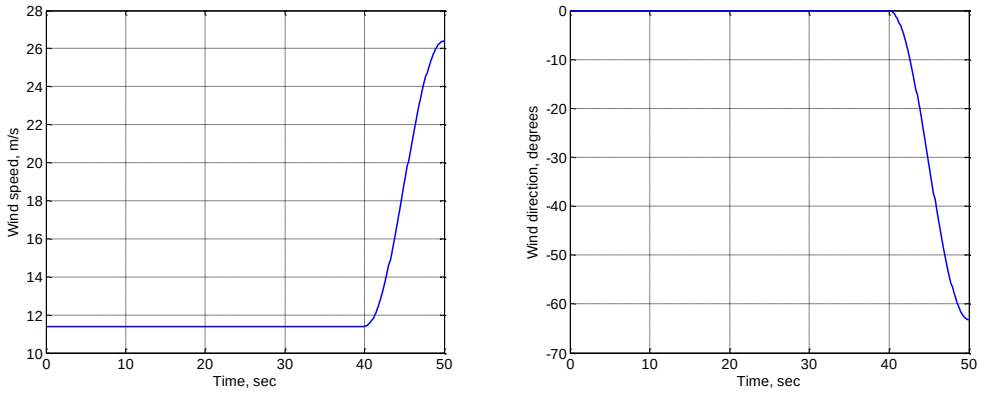

Figure 38. Wind speed and direction for the ECD-R analysis

Fatigue Damage

Fatigue analysis was performed in the same manner as is documented in Appendix A of the Sandia 100m blade report, Reference [7]. A simple two-parameter fatigue model was used. Rain flow cycle accumulation rates from the collection of aeroelastic simulations were scaled according to a Rayleigh wind distribution. Average wind speed is found in Table 11. Twenty years of operation at 100% availability was assumed. Important material properties for the fatigue damage analysis are summarized in Table 15. Stresses used in the fatigue analysis include the total safety factor from Table 16. The end result of the analysis was a series of Miner's rule fatigue damage ratios shown in Appendix Sections titled, "Computed Fatigue Damage …." Ratios of greater than 1.0 indicate fatigue failure.

Table 15: Material properties for fatigue analysis

	b[f]	C (MPa)	E
E-LT-5500(UD)	10	1000	See Table 2
Carbon(UD)	14	1546	See Table 2
SNLTriax	10	700	See Table 2

The quality of fatigue test data has a large effect on the safety factors which are used in the fatigue damage analysis. Regarding material safety factors for fatigue,

[f] To promote simplicity, the fatigue slope parameter, b, is set to 10 (GRP) or 14 (CRP) for all materials for these analyses. The choice is consistent with GL standards for computation of fatigue damage in epoxy-laminate [GL 5.5.4.(13)] or carbon/epoxy laminate [GL 5.5.5.(6)]

"The partial safety factor for materials shall be at least 1.5 provided that the SN curve is based on 50 % survival probability and coefficient of variation < 15 %. For components with large coefficient of variation for fatigue strength, i.e. 15 % to 20 % (such as for many components made of composites, for example reinforced concrete or fiber composites), the partial safety factor γ_m must be increased accordingly and at least to 1.7. For fiber composites, the strength distribution shall be established from test data for the actual material. The 95 % survival probability with a confidence level of 95% shall be used as a basis for the SN-curve. In that case γ_m may be taken as 1.2. The same approach may be used for other materials." From Reference [25].

Table 16: Safety factors used in evaluation of fatigue damage (IEC 7.6.3)

Partial safety factor for loads, γ_f	1.0	
Partial safety factor for materials, γ_m	1.7	Assuming large COV for fatigue strength
Partial safety factor for materials, γ_m	1.2	Assuming 95% survival probability; 95% confidence for fatigue data
Partial safety factors for consequences of failure, γ_n	1.15	Component class 2
Total safety factor	1.38	Assuming great SN curve data

Driving fatigue lifetimes are shown in Summary Table 7.

Structural Stability (Buckling)

Table 17: Safety factors used in evaluation of buckling loads (IEC 7.6.4)

Partial safety factor for loads, γ_f	1.35	Do not use for DLC 1.1
Partial safety factor for materials, γ_m	1.2	Global buckling of curved shells, such as blades
Partial safety factors for consequences of failure, γ_n	1.0	Component class 2
Total safety factor	1.62	

Table 18: Buckling modes for load cases exhibiting highest root moments for Design 80

Load case		Load factor	Buckled mode shape
IECDLC6p1EWM50	+15 degree yaw misalignment	1.6388	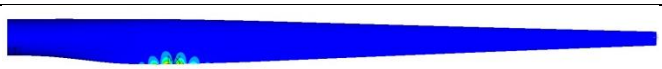
		1.6404	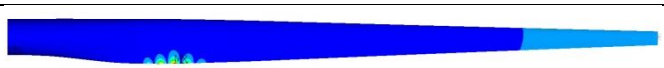
		1.7476	
IECDLC1p4ECD	Negative gust at rated speed	1.9164	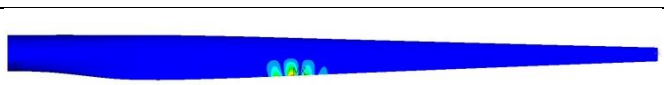

Mass Properties

The ANSYS FE model of each blade was used to compute blade mass properties. Note that the mass computed determined by ANSYS model and mass determined by FAST are different. FAST computes blade mass based on the mass distribution computed by PreComp and listed in the FAST blade input file. The distribution can be seen as the plot *BMassDen* in Figure 37. The distribution does not capture spanwise variation in layups as well as the detailed ANSYS model.

Table 19: Blade model mass properties

	Original 61.5m blade (SAND2013-2569)	Design 80	Design 100 high TSR	Design 100 high TSR flexible	Design 100 low TSR	Design 100 low TSR flexible
Blade mass (kg, ANSYS computed)	17,770	16,097	17,590	14,607	16,423	15,611
Span-wise CG location (m, ANSYS computed)	19.102	17.762	20.088	17.404	18.712	17.605
Blade mass (kg, FAST computed)	16,878	15,241	17,042	13,776	15,598	14,759

Ultimate Strength

The following relationship was used to estimate strain in the skin of the blade:

$$\varepsilon = \frac{Mc}{EI} \qquad \text{Eq.(D.1)}$$

The section stiffness, EI, includes effects of multiple materials and the blade cross section shape. It is defined as follows

$$Flapwise, EI = \iint E(x,y)x^2 dxdy$$
$$Edgewise, EI = \iint E(x,y)y^2 dxdy \qquad \text{Eq.(D.2)}$$

Where x and y are the flap and edgewise coordinates of the differential area elements, respectively, with respect to the section elastic center. PreComp was used to compute flapwise and edgewise stiffness of the blades. Those results are plotted in Figure 37.

The distance, c, is assumed here to be the half height of the airfoil (flapwise c) or the distance from the blade reference axis (i.e. pitch axis; defined by NuMAD x-offset) to the blade trailing edge (edgewise c). The definition of edgewise c assumes colocation of the blade reference axis and the elastic axis of the section. Flap and edge c values are plotted in Figure 39.

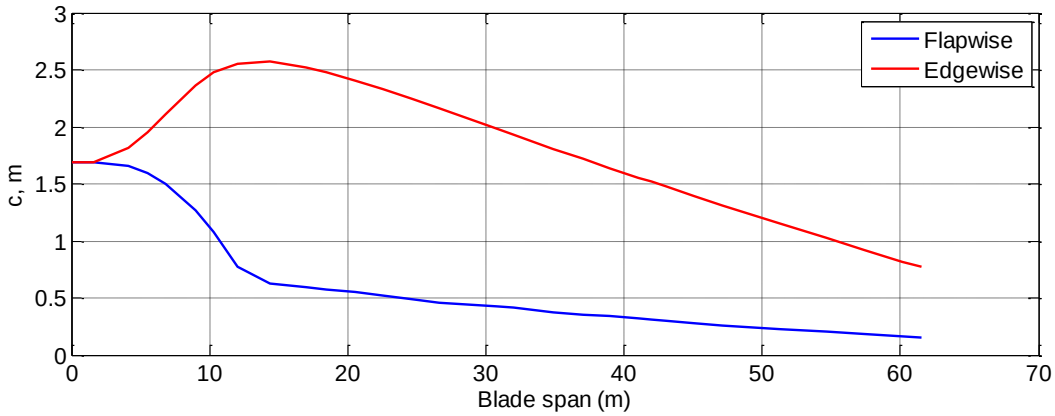

Figure 39: Distributions of skin distance from neutral axes for Design 80

It is important to note that edge and flap loadings were analyzed separately in the blade design. A more thorough approach would involve computing the combined loading effects of flap and edge moments, and axial forces at each blade gage location. The combined load states could then be used to compute strains.

Finally, stress is proportional to strain,

$$S = E\varepsilon \qquad \text{(D.3)}$$

Table 20: Safety factors used in evaluation of ultimate strength (IEC 7.6.2)

Partial safety factor for loads, γ_f	1.35	Do not use for DLC 1.1
Partial safety factor for materials, γ_m	1.3	Rupture from exceeding tensile or compression strength
Partial safety factors for consequences of failure, γ_n	1.0	Component class 2
Total safety factor	1.755	

Maximum stresses in are estimated by multiplication of maximum strains by the elastic moduli in Table 2 and by the total safety factor from Table 20.

None of the materials exceed their maximum allowable stress.

Table 21: Computed ultimate stresses for Design 80

	Max Flapwise Stress (including s.f.) (MPa)	Max Edgewise Stress (including s.f.) (MPa)
E-LT-5500(UD)	179	83
SNL(Triax)		55
Carbon(UD)	490	

Table 22: Computed ultimate stresses for Design 100 low TSR

	Max Flapwise Stress	Max Edgewise Stress

	(including s.f.) (MPa)	(including s.f.) (MPa)
E-LT-5500(UD)	227	100
SNL(Triax)		66
Carbon(UD)	622	

Natural Frequency Criteria

Blade frequency criteria help ensure that the rotor does not operate in the range of any major structural resonances. The goals of these criteria are to avoid the 1P and 3P rotor frequencies as well as to ensure adequate spacing between the blade flap and edge resonances. The criteria do not originate from the IEC standard; it comes from anecdotal feedback from blade manufacturers. It is feasible that these frequency criteria are relaxed during design of modern rotors on a case by cases bases to enable lighter, more flexible blades. Still, the criteria are useful in the investigation because they provide rigorous criteria for definition of blade flapwise and edgewise stiffness.

Table 23: Requirements for blade modal frequencies

Exclusion zones for the natural frequencies of the Dynamic Modes, while rotating at rated shaft speed.	$f > 2P + 10\%$, $3P - 10\% < f < 3P + 10\%$, $6P - 5\% < f < 6P + 5\%$
Minimum Margin of separation between the natural frequencies of the first flap and first edge dynamic modes	$f_{edge} \geq 1.30\ f_{flap}$

Table 24: Single blade frequencies and frequency criteria

	Design 80	Design 100 high TSR	Design 100 high TSR flexible	Design 100 low TSR	Design 100 low TSR flexible
BModes computed frequencies					
Blade 1st flap (Hz)	0.95	0.86	0.89	0.95	0.93
Blade 1st edge (Hz)	1.24	1.12	1.21	1.24	1.46
Blade 2nd flap (Hz)	2.63	2.37	2.29	2.69	2.40
Frequency criteria					
Rotor rated speed (RPM)	12.13	15.16	15.16	15.16	15.16
Rotor rated speed (Hz)	0.20	0.25	0.25	0.25	0.25
3P + 10% (Hz)	0.67	0.83	0.83	0.83	0.83
1st flap + 30% (Hz)	1.24	1.12	1.16	1.24	1.21
1st edge / 1st flap ratio	1.30	1.30	1.36	1.30	1.57

Classical Flutter

NuMAD was used to estimate onset of classical flutter for each blade design. Detailed discussion and additional references for the aeroelastic stability analysis used to perform the estimate can be found in the NuMAD v2.0 user's manual [10].

Table 25: Summary of classical flutter predictions

	Design 80	Design 100 high TSR	Design 100 high TSR flexible	Design 100 low TSR	Design 100 low TSR flexible
Flutter speed (RPM)	20.5 3rd flap/ torsion	20.5 3rd flap/ torsion	17.75 3rd flap/ torsion	21.9 3rd flap/ torsion	22.1 3rd flap/ torsion

Aeroelastic Simulation Outputs – Design 80

All values reported here are characteristic values. No safety factors are included in the following table.

DLC Name	MaxFlapBendingMoment	Occurring at time (sec)	on Channel	in File
IECSweep	9765	413.513	RootMyb1	out/IECSweep_ramp.out
IECDLC1p2NTM	13120	355.212	RootMyb3	out/IECDLC1p2NTM_13mps_seed4.out
IECDLC1p3ETM	14670	528.713	RootMyb2	out/IECDLC1p3ETM_15mps_seed5.out
IECDLC1p4ECD	15470	57.538	RootMyb1	out/IECDLC1p4ECD_ECD-R.out
IECDLC1p5EWS	11160	45.325	RootMyb2	out/IECDLC1p5EWS_EWSV+11.0.out
IECDLC6p1EWM50	15910	251.213	RootMyb1	out/IECDLC6p1EWM50_EWM50+15.out
IECDLC6p3EWM01	11020	281.263	RootMyb3	out/IECDLC6p3EWM01_EWM01-25.out
DLC Name	MaxRotorFlapBendingMoment	Occurring at time (sec)	on Channel	in File
IECSweep	9758	413.5	RootMyc1	out/IECSweep_ramp.out
IECDLC1p2NTM	13120	355.212	RootMyc3	out/IECDLC1p2NTM_13mps_seed4.out
IECDLC1p3ETM	14670	528.713	RootMyc2	out/IECDLC1p3ETM_15mps_seed5.out
IECDLC1p4ECD	15470	57.538	RootMyc1	out/IECDLC1p4ECD_ECD-R.out
IECDLC1p5EWS	11160	45.325	RootMyc2	out/IECDLC1p5EWS_EWSV+11.0.out
IECDLC6p1EWM50	755	250.175	RootMyc3	out/IECDLC6p1EWM50_EWM50+15.out
IECDLC6p3EWM01	794	251.375	RootMyc3	out/IECDLC6p3EWM01_EWM01+30.out
DLC Name	MaxFlapStrain	Occurring at time (sec)	on Channel	in File
IECSweep	1492	413.225	Spn5MLyb1	out/IECSweep_ramp.out
IECDLC1p2NTM	1975	353.85	Spn5MLyb1	out/IECDLC1p2NTM_13mps_seed4.out
IECDLC1p3ETM	2165	349.413	Spn5MLyb1	out/IECDLC1p3ETM_13mps_seed4.out
IECDLC1p4ECD	2437	57.55	Spn5MLyb1	out/IECDLC1p4ECD_ECD-R.out
IECDLC1p5EWS	1701	47.038	Spn5MLyb1	out/IECDLC1p5EWS_EWSV+11.0.out
IECDLC6p1EWM50	2353	251.913	Spn5MLyb1	out/IECDLC6p1EWM50_EWM50+15.out
IECDLC6p3EWM01	1408	251.7	Spn5MLyb1	out/IECDLC6p3EWM01_EWM01+15.out
DLC Name	MaxEdgeStrain	Occurring at	on Channel	in File

		time (sec)		
IECSweep	582	50.55	Spn4MLxb1	out/IECSweep_ramp.out
IECDLC1p2NTM	930	168.875	Spn4MLxb1	out/IECDLC1p2NTM_23mps_seed2.out
IECDLC1p3ETM	1132	234.725	Spn4MLxb1	out/IECDLC1p3ETM_23mps_seed1.out
IECDLC1p4ECD	760	47.225	Spn4MLxb1	out/IECDLC1p4ECD_ECD-R.out
IECDLC1p5EWS	604	34.913	Spn4MLxb1	out/IECDLC1p5EWS_EWSV+3.0.out
IECDLC6p1EWM50	487	250.05	Spn4MLxb1	out/IECDLC6p1EWM50_EWM50-15.out
IECDLC6p3EWM01	712	250.6	Spn4MLxb1	out/IECDLC6p3EWM01_EWM01-30.out
DLC Name	MaxOoPDefl	Occurring at time (sec)	on Channel	in File
IECSweep	4.10	413.375	OoPDefl1	out/IECSweep_ramp.out
IECDLC1p2NTM	5.70	350.438	OoPDefl3	out/IECDLC1p2NTM_13mps_seed4.out
IECDLC1p3ETM	6.24	528.8	OoPDefl2	out/IECDLC1p3ETM_15mps_seed5.out
IECDLC1p4ECD	7.05	57.575	OoPDefl1	out/IECDLC1p4ECD_ECD-R.out
IECDLC1p5EWS	4.85	45.438	OoPDefl2	out/IECDLC1p5EWS_EWSV+11.0.out
IECDLC6p1EWM50	0.18	250.175	OoPDefl3	out/IECDLC6p1EWM50_EWM50+15.out
IECDLC6p3EWM01	0.16	251.275	OoPDefl3	out/IECDLC6p3EWM01_EWM01+30.out
DLC Name	MaxRotorTh	Occurring at time (sec)	on Channel	in File
IECSweep	785.0	413.288	LSShftFxa	out/IECSweep_ramp.out
IECDLC1p2NTM	886.9	183.95	LSShftFxa	out/IECDLC1p2NTM_19mps_seed4.out
IECDLC1p3ETM	932.5	485.25	LSShftFxa	out/IECDLC1p3ETM_15mps_seed4.out
IECDLC1p4ECD	918.1	42.9	LSShftFxa	out/IECDLC1p4ECD_ECD-R.out
IECDLC1p5EWS	759.6	55.688	LSShftFxa	out/IECDLC1p5EWS_EWSV+12.0.out
IECDLC6p1EWM50	216.5	251.688	LSShftFxa	out/IECDLC6p1EWM50_EWM50+00.out
IECDLC6p3EWM01	173.8	251.588	LSShftFxa	out/IECDLC6p3EWM01_EWM01+00.out
DLC Name	MinFlapBendingMoment	Occurring at time (sec)	on Channel	in File
IECSweep	1139	31.85	RootMyb1	out/IECSweep_ramp.out
IECDLC1p2NTM	-4043	301.363	RootMyb2	out/IECDLC1p2NTM_23mps_seed5.out
IECDLC1p3ETM	-5762	301.062	RootMyb1	out/IECDLC1p3ETM_23mps_seed5.out
IECDLC1p4ECD	-2390	48.075	RootMyb3	out/IECDLC1p4ECD_ECD-R.out
IECDLC1p5EWS	-2048	46.725	RootMyb1	out/IECDLC1p5EWS_EWSV+25.0.out
IECDLC6p1EWM50	-12100	250.738	RootMyb3	out/IECDLC6p1EWM50_EWM50+15.out
IECDLC6p3EWM01	-9670	250.637	RootMyb1	out/IECDLC6p3EWM01_EWM01-30.out
DLC Name	MinRotorFlapBendingMoment	Occurring at time (sec)	on Channel	in File
IECSweep	1139	31.85	RootMyc1	out/IECSweep_ramp.out
IECDLC1p2NTM	-4075	301.337	RootMyc2	out/IECDLC1p2NTM_23mps_seed5.out
IECDLC1p3ETM	-5820	301.05	RootMyc1	out/IECDLC1p3ETM_23mps_seed5.out
IECDLC1p4ECD	-2905	48.125	RootMyc3	out/IECDLC1p4ECD_ECD-R.out
IECDLC1p5EWS	-1706	46.562	RootMyc1	out/IECDLC1p5EWS_EWSV+25.0.out
IECDLC6p1EWM50	-4077	251.85	RootMyc1	out/IECDLC6p1EWM50_EWM50+15.out
IECDLC6p3EWM01	-2842	252.525	RootMyc1	out/IECDLC6p3EWM01_EWM01+25.out

DLC Name	MinFlapStrain	Occurring at time (sec)	on Channel	in File
IECSweep	40	997.812	Spn7MLyb1	out/IECSweep_ramp.out
IECDLC1p2NTM	-842	342.6	Spn7MLyb1	out/IECDLC1p2NTM_23mps_seed6.out
IECDLC1p3ETM	-1034	621.35	Spn7MLyb1	out/IECDLC1p3ETM_19mps_seed3.out
IECDLC1p4ECD	17	46.9	Spn7MLyb1	out/IECDLC1p4ECD_ECD-R.out
IECDLC1p5EWS	-654	46.688	Spn7MLyb1	out/IECDLC1p5EWS_EWSV+25.0.out
IECDLC6p1EWM50	-993	250.688	Spn5MLyb1	out/IECDLC6p1EWM50_EWM50-15.out
IECDLC6p3EWM01	-1175	251.425	Spn5MLyb1	out/IECDLC6p3EWM01_EWM01-30.out
DLC Name	MinEdgeStrain	Occurring at time (sec)	on Channel	in File
IECSweep	-896	484.35	Spn4MLxb1	out/IECSweep_ramp.out
IECDLC1p2NTM	-1218	207.225	Spn4MLxb1	out/IECDLC1p2NTM_17mps_seed2.out
IECDLC1p3ETM	-1266	316.363	Spn4MLxb1	out/IECDLC1p3ETM_15mps_seed3.out
IECDLC1p4ECD	-1079	55.925	Spn4MLxb1	out/IECDLC1p4ECD_ECD-R.out
IECDLC1p5EWS	-914	44.5	Spn4MLxb1	out/IECDLC1p5EWS_EWSV+13.0.out
IECDLC6p1EWM50	-209	251.738	Spn4MLxb1	out/IECDLC6p1EWM50_EWM50+00.out
IECDLC6p3EWM01	-114	251.637	Spn4MLxb1	out/IECDLC6p3EWM01_EWM01+00.out
DLC Name	MinOoPDefl	Occurring at time (sec)	on Channel	in File
IECSweep	0.18	999.8	OoPDefl1	out/IECSweep_ramp.out
IECDLC1p2NTM	-2.17	301.375	OoPDefl2	out/IECDLC1p2NTM_23mps_seed5.out
IECDLC1p3ETM	-2.82	301.1	OoPDefl1	out/IECDLC1p3ETM_23mps_seed5.out
IECDLC1p4ECD	-1.11	48.237	OoPDefl3	out/IECDLC1p4ECD_ECD-R.out
IECDLC1p5EWS	-1.65	46.638	OoPDefl1	out/IECDLC1p5EWS_EWSV+25.0.out
IECDLC6p1EWM50	-0.98	251.85	OoPDefl1	out/IECDLC6p1EWM50_EWM50+15.out
IECDLC6p3EWM01	-0.58	252.413	OoPDefl1	out/IECDLC6p3EWM01_EWM01+20.out
DLC Name	MinRotorTh	Occurring at time (sec)	on Channel	in File
IECSweep	119.9	31.837	LSShftFxa	out/IECSweep_ramp.out
IECDLC1p2NTM	117.4	619.95	LSShftFxa	out/IECDLC1p2NTM_5mps_seed2.out
IECDLC1p3ETM	16.2	618.275	LSShftFxa	out/IECDLC1p3ETM_5mps_seed2.out
IECDLC1p4ECD	93.4	48.413	LSShftFxa	out/IECDLC1p4ECD_ECD-R.out
IECDLC1p5EWS	116.8	31.837	LSShftFxa	out/IECDLC1p5EWS_EWSV+3.0.out
IECDLC6p1EWM50	47.0	250.188	LSShftFxa	out/IECDLC6p1EWM50_EWM50-15.out
IECDLC6p3EWM01	1.4	259.562	LSShftFxa	out/IECDLC6p3EWM01_EWM01-25.out

Aeroelastic Simulation Outputs – Design 100 high TSR

All values reported here are characteristic values. No safety factors are included in the following table.

DLC Name	MaxFlapBendingMoment	Occurring at time (sec)	on Channel	in File
IECSweep	10590	405.025	RootMyb1	out/IECSweep_ramp.out
IECDLC1p2NTM	14370	400.225	RootMyb1	out/IECDLC1p2NTM_15mps_seed1.out

IECDLC1p3ETM	16750	538.788	RootMyb1	out/IECDLC1p3ETM_19mps_seed2.out
IECDLC1p4ECD	16350	60.838	RootMyb3	out/IECDLC1p4ECD_ECD-R.out
IECDLC1p5EWS	12610	46.237	RootMyb2	out/IECDLC1p5EWS_EWSV+11.0.out
IECDLC6p1EWM50	16320	250	RootMyb1	out/IECDLC6p1EWM50_EWM50+15.out
IECDLC6p3EWM01	10790	250	RootMyb1	out/IECDLC6p3EWM01_EWM01+20.out
DLC Name	MaxRotorFlapBendingMoment	Occurring at time (sec)	on Channel	in File
IECSweep	10580	404.975	RootMyc1	out/IECSweep_ramp.out
IECDLC1p2NTM	14360	400.238	RootMyc1	out/IECDLC1p2NTM_15mps_seed1.out
IECDLC1p3ETM	16710	538.788	RootMyc1	out/IECDLC1p3ETM_19mps_seed2.out
IECDLC1p4ECD	16320	60.85	RootMyc3	out/IECDLC1p4ECD_ECD-R.out
IECDLC1p5EWS	12610	46.237	RootMyc2	out/IECDLC1p5EWS_EWSV+11.0.out
IECDLC6p1EWM50	595	250	RootMyc3	out/IECDLC6p1EWM50_EWM50+10.out
IECDLC6p3EWM01	514	252.713	RootMyc3	out/IECDLC6p3EWM01_EWM01+10.out
DLC Name	MaxFlapStrain	Occurring at time (sec)	on Channel	in File
IECSweep	1717	404.575	Spn4MLyb 1	out/IECSweep_ramp.out
IECDLC1p2NTM	2313	559.362	Spn4MLyb 1	out/IECDLC1p2NTM_11mps_seed6.out
IECDLC1p3ETM	2704	538.763	Spn4MLyb 1	out/IECDLC1p3ETM_19mps_seed2.out
IECDLC1p4ECD	2668	59.55	Spn4MLyb 1	out/IECDLC1p4ECD_ECD-R.out
IECDLC1p5EWS	1986	47.65	Spn4MLyb 1	out/IECDLC1p5EWS_EWSV+11.0.out
IECDLC6p1EWM50	2500	250	Spn4MLyb 1	out/IECDLC6p1EWM50_EWM50+15.out
IECDLC6p3EWM01	1613	252.262	Spn4MLyb 1	out/IECDLC6p3EWM01_EWM01+20.out
DLC Name	MaxEdgeStrain	Occurring at time (sec)	on Channel	in File
IECSweep	723	33.625	Spn4MLxb 1	out/IECSweep_ramp.out
IECDLC1p2NTM	1077	284.9	Spn4MLxb 1	out/IECDLC1p2NTM_23mps_seed5.out
IECDLC1p3ETM	1276	408.263	Spn4MLxb 1	out/IECDLC1p3ETM_23mps_seed3.out
IECDLC1p4ECD	886	59.938	Spn4MLxb 1	out/IECDLC1p4ECD_ECD-R.out
IECDLC1p5EWS	732	56.75	Spn4MLxb 1	out/IECDLC1p5EWS_EWSV+3.0.out
IECDLC6p1EWM50	863	251.738	Spn4MLxb 1	out/IECDLC6p1EWM50_EWM50-15.out
IECDLC6p3EWM01	539	251.062	Spn4MLxb 1	out/IECDLC6p3EWM01_EWM01-15.out
DLC Name	MaxOoPDefl	Occurring at time (sec)	on Channel	in File
IECSweep	4.28	404.8	OoPDefl1	out/IECSweep_ramp.out
IECDLC1p2NTM	5.83	431.837	OoPDefl1	out/IECDLC1p2NTM_15mps_seed1.out
IECDLC1p3ETM	6.86	538.725	OoPDefl1	out/IECDLC1p3ETM_19mps_seed2.out
IECDLC1p4ECD	7.02	60.862	OoPDefl3	out/IECDLC1p4ECD_ECD-R.out
IECDLC1p5EWS	5.26	46.3	OoPDefl2	out/IECDLC1p5EWS_EWSV+11.0.out
IECDLC6p1EWM50	0.09	250	OoPDefl3	out/IECDLC6p1EWM50_EWM50+15.out
IECDLC6p3EWM01	0.12	251.463	OoPDefl1	out/IECDLC6p3EWM01_EWM01-30.out

DLC Name	MaxRotorTh	Occurring at time (sec)	on Channel	in File
IECSweep	837.9	405	LSShftFxa	out/IECSweep_ramp.out
IECDLC1p2NTM	989.9	208.725	LSShftFxa	out/IECDLC1p2NTM_17mps_seed2.out
IECDLC1p3ETM	1059.0	544.425	LSShftFxa	out/IECDLC1p3ETM_11mps_seed5.out
IECDLC1p4ECD	954.2	45.375	LSShftFxa	out/IECDLC1p4ECD_ECD-R-2.0.out
IECDLC1p5EWS	784.4	42.263	LSShftFxa	out/IECDLC1p5EWS_EWSV-11.0.out
IECDLC6p1EWM50	188.0	250	LSShftFxa	out/IECDLC6p1EWM50_EWM50+00.out
IECDLC6p3EWM01	154.1	252.625	LSShftFxa	out/IECDLC6p3EWM01_EWM01+00.out
DLC Name	MinFlapBendingMoment	Occurring at time (sec)	on Channel	in File
IECSweep	1660	30	RootMyb2	out/IECSweep_ramp.out
IECDLC1p2NTM	-2958	301.513	RootMyb1	out/IECDLC1p2NTM_23mps_seed5.out
IECDLC1p3ETM	-4529	301.263	RootMyb2	out/IECDLC1p3ETM_23mps_seed5.out
IECDLC1p4ECD	-3521	49.6	RootMyb3	out/IECDLC1p4ECD_ECD+R+2.0.out
IECDLC1p5EWS	-1440	46.1	RootMyb2	out/IECDLC1p5EWS_EWSV+25.0.out
IECDLC6p1EWM50	-12050	250	RootMyb1	out/IECDLC6p1EWM50_EWM50-15.out
IECDLC6p3EWM01	-8158	299.663	RootMyb3	out/IECDLC6p3EWM01_EWM01+30.out
DLC Name	MinRotorFlapBendingMoment	Occurring at time (sec)	on Channel	in File
IECSweep	1660	30	RootMyc2	out/IECSweep_ramp.out
IECDLC1p2NTM	-3284	301.462	RootMyc1	out/IECDLC1p2NTM_23mps_seed5.out
IECDLC1p3ETM	-4773	301.238	RootMyc2	out/IECDLC1p3ETM_23mps_seed5.out
IECDLC1p4ECD	-2970	49.5	RootMyc3	out/IECDLC1p4ECD_ECD+R+2.0.out
IECDLC1p5EWS	-860.4	45.975	RootMyc2	out/IECDLC1p5EWS_EWSV+25.0.out
IECDLC6p1EWM50	-3346	251.15	RootMyc1	out/IECDLC6p1EWM50_EWM50+15.out
IECDLC6p3EWM01	-2490	275.5	RootMyc1	out/IECDLC6p3EWM01_EWM01+25.out
DLC Name	MinFlapStrain	Occurring at time (sec)	on Channel	in File
IECSweep	97	999.075	Spn7MLyb 1	out/IECSweep_ramp.out
IECDLC1p2NTM	-665	526.888	Spn7MLyb 1	out/IECDLC1p2NTM_23mps_seed4.out
IECDLC1p3ETM	-834	622.05	Spn7MLyb 1	out/IECDLC1p3ETM_19mps_seed3.out
IECDLC1p4ECD	-513	48.475	Spn4MLyb 1	out/IECDLC1p4ECD_ECD+R+2.0.out
IECDLC1p5EWS	-498	47.325	Spn7MLyb 1	out/IECDLC1p5EWS_EWSV+25.0.out
IECDLC6p1EWM50	-1723	255.988	Spn4MLyb 1	out/IECDLC6p1EWM50_EWM50-15.out
IECDLC6p3EWM01	-1140	251.163	Spn4MLyb 1	out/IECDLC6p3EWM01_EWM01-30.out
DLC Name	MinEdgeStrain	Occurring at time (sec)	on Channel	in File
IECSweep	-1082	998.888	Spn4MLxb 1	out/IECSweep_ramp.out
IECDLC1p2NTM	-1463	92.7	Spn4MLxb 1	out/IECDLC1p2NTM_23mps_seed5.out
IECDLC1p3ETM	-1630	162.438	Spn4MLxb 1	out/IECDLC1p3ETM_17mps_seed4.out
IECDLC1p4ECD	-1243	45.225	Spn4MLxb 1	out/IECDLC1p4ECD_ECD+R+2.0.out
IECDLC1p5EWS	-1081	45.5	Spn4MLxb 1	out/IECDLC1p5EWS_EWSV+13.0.out

IECDLC6p1EWM50	-228	250	Spn4MLxb1	out/IECDLC6p1EWM50_EWM50+05.out
IECDLC6p3EWM01	-158	252.838	Spn4MLxb1	out/IECDLC6p3EWM01_EWM01+05.out
DLC Name	MinOoPDefl	Occurring at time (sec)	on Channel	in File
IECSweep	0.59	1000.013	OoPDefl1	out/IECSweep_ramp.out
IECDLC1p2NTM	-1.86	526.862	OoPDefl1	out/IECDLC1p2NTM_23mps_seed4.out
IECDLC1p3ETM	-2.37	622.075	OoPDefl1	out/IECDLC1p3ETM_19mps_seed3.out
IECDLC1p4ECD	-1.46	49.65	OoPDefl3	out/IECDLC1p4ECD_ECD+R+2.0.out
IECDLC1p5EWS	-1.34	46.025	OoPDefl2	out/IECDLC1p5EWS_EWSV+25.0.out
IECDLC6p1EWM50	-0.72	251.188	OoPDefl1	out/IECDLC6p1EWM50_EWM50+15.out
IECDLC6p3EWM01	-0.49	252.35	OoPDefl1	out/IECDLC6p3EWM01_EWM01+20.out
DLC Name	MinRotorTh	Occurring at time (sec)	on Channel	in File
IECSweep	168.9	30.538	LSShftFxa	out/IECSweep_ramp.out
IECDLC1p2NTM	107.2	535.95	LSShftFxa	out/IECDLC1p2NTM_23mps_seed3.out
IECDLC1p3ETM	34.3	535.862	LSShftFxa	out/IECDLC1p3ETM_23mps_seed3.out
IECDLC1p4ECD	73.3	48.763	LSShftFxa	out/IECDLC1p4ECD_ECD+R.out
IECDLC1p5EWS	144.6	32.237	LSShftFxa	out/IECDLC1p5EWS_EWSV+3.0.out
IECDLC6p1EWM50	38.6	251.4	LSShftFxa	out/IECDLC6p1EWM50_EWM50+15.out
IECDLC6p3EWM01	-10.7	297.062	LSShftFxa	out/IECDLC6p3EWM01_EWM01+30.out

Aeroelastic Simulation Outputs – Design 100 high TSR flexible

All values reported here are characteristic values. No safety factors are included in the following table.

DLC Name	MaxFlapBendingMoment	Occurring at time (sec)	on Channel	in File
IECSweep	10070	404.8	RootMyb1	out/IECSweep_ramp.out
IECDLC1p2NTM	13280	400.163	RootMyb1	out/IECDLC1p2NTM_15mps_seed1.out
IECDLC1p3ETM	15470	538.413	RootMyb1	out/IECDLC1p3ETM_19mps_seed2.out
IECDLC1p4ECD	15960	56.963	RootMyb3	out/IECDLC1p4ECD_ECD-R.out
IECDLC1p5EWS	11920	46.038	RootMyb2	out/IECDLC1p5EWS_EWSV+11.0.out
IECDLC6p1EWM50	16180	250	RootMyb1	out/IECDLC6p1EWM50_EWM50+15.out
IECDLC6p3EWM01	11560	252.875	RootMyb1	out/IECDLC6p3EWM01_EWM01+25.out
DLC Name	MaxRotorFlapBendingMoment	Occurring at time (sec)	on Channel	in File
IECSweep	10070	404.8	RootMyc1	out/IECSweep_ramp.out
IECDLC1p2NTM	13250	400.163	RootMyc1	out/IECDLC1p2NTM_15mps_seed1.out
IECDLC1p3ETM	15450	538.413	RootMyc1	out/IECDLC1p3ETM_19mps_seed2.out
IECDLC1p4ECD	15960	56.963	RootMyc3	out/IECDLC1p4ECD_ECD-R.out
IECDLC1p5EWS	11920	46.038	RootMyc2	out/IECDLC1p5EWS_EWSV+11.0.out
IECDLC6p1EWM50	486	251.562	RootMyc3	out/IECDLC6p1EWM50_EWM50+10.out
IECDLC6p3EWM01	406	251.438	RootMyc3	out/IECDLC6p3EWM01_EWM01+10.out

DLC Name	MaxFlapStrain	Occurring at time (sec)	on Channel	in File
IECSweep	2146	404.513	Spn7MLyb1	out/IECSweep_ramp.out
IECDLC1p2NTM	2828	400.1	Spn7MLyb1	out/IECDLC1p2NTM_15mps_seed1.out
IECDLC1p3ETM	3225	538.425	Spn7MLyb1	out/IECDLC1p3ETM_19mps_seed2.out
IECDLC1p4ECD	3502	55.625	Spn7MLyb1	out/IECDLC1p4ECD_ECD-R.out
IECDLC1p5EWS	2590	47.362	Spn7MLyb1	out/IECDLC1p5EWS_EWSV+11.0.out
IECDLC6p1EWM50	2841	252.05	Spn7MLyb1	out/IECDLC6p1EWM50_EWM50+15.out
IECDLC6p3EWM01	1965	252.863	Spn4MLyb1	out/IECDLC6p3EWM01_EWM01+25.out
DLC Name	MaxEdgeStrain	Occurring at time (sec)	on Channel	in File
IECSweep	614	41.263	Spn4MLxb1	out/IECSweep_ramp.out
IECDLC1p2NTM	1158	320.1	Spn4MLxb1	out/IECDLC1p2NTM_23mps_seed6.out
IECDLC1p3ETM	1408	535.125	Spn4MLxb1	out/IECDLC1p3ETM_23mps_seed3.out
IECDLC1p4ECD	836	47.213	Spn4MLxb1	out/IECDLC1p4ECD_ECD-R.out
IECDLC1p5EWS	622	37.388	Spn4MLxb1	out/IECDLC1p5EWS_EWSV+3.0.out
IECDLC6p1EWM50	1154	250.275	Spn4MLxb1	out/IECDLC6p1EWM50_EWM50-15.out
IECDLC6p3EWM01	729	250	Spn4MLxb1	out/IECDLC6p3EWM01_EWM01-15.out
DLC Name	MaxOoPDefl	Occurring at time (sec)	on Channel	in File
IECSweep	6.40	404.7	OoPDefl1	out/IECSweep_ramp.out
IECDLC1p2NTM	8.41	400.175	OoPDefl1	out/IECDLC1p2NTM_15mps_seed1.out
IECDLC1p3ETM	9.72	538.45	OoPDefl1	out/IECDLC1p3ETM_19mps_seed2.out
IECDLC1p4ECD	11.19	57	OoPDefl3	out/IECDLC1p4ECD_ECD-R.out
IECDLC1p5EWS	7.86	46.1	OoPDefl2	out/IECDLC1p5EWS_EWSV+11.0.out
IECDLC6p1EWM50	0.09	251.425	OoPDefl3	out/IECDLC6p1EWM50_EWM50+15.out
IECDLC6p3EWM01	0.16	250.188	OoPDefl1	out/IECDLC6p3EWM01_EWM01-30.out
DLC Name	MaxRotorTh	Occurring at time (sec)	on Channel	in File
IECSweep	822.4	404.9	LSShftFxa	out/IECSweep_ramp.out
IECDLC1p2NTM	971.9	183.75	LSShftFxa	out/IECDLC1p2NTM_19mps_seed4.out
IECDLC1p3ETM	1007.0	543.763	LSShftFxa	out/IECDLC1p3ETM_15mps_seed2.out
IECDLC1p4ECD	966.4	42.812	LSShftFxa	out/IECDLC1p4ECD_ECD-R.out
IECDLC1p5EWS	769.6	42.112	LSShftFxa	out/IECDLC1p5EWS_EWSV-11.0.out
IECDLC6p1EWM50	178.9	251.725	LSShftFxa	out/IECDLC6p1EWM50_EWM50+00.out
IECDLC6p3EWM01	145.5	251.463	LSShftFxa	out/IECDLC6p3EWM01_EWM01+00.out
DLC Name	MinFlapBendingMoment	Occurring at time (sec)	on Channel	in File
IECSweep	1434	30.275	RootMyb2	out/IECSweep_ramp.out
IECDLC1p2NTM	-3169	301.4	RootMyb1	out/IECDLC1p2NTM_23mps_seed5.out
IECDLC1p3ETM	-4834	300.675	RootMyb2	out/IECDLC1p3ETM_23mps_seed5.out
IECDLC1p4ECD	-2765	49.25	RootMyb3	out/IECDLC1p4ECD_ECD+R+2.0.out

IECDLC1p5EWS	-1632	47.075	RootMyb1	out/IECDLC1p5EWS_EWSV+25.0.out
IECDLC6p1EWM50	-11940	250	RootMyb1	out/IECDLC6p1EWM50_EWM50-15.out
IECDLC6p3EWM01	-8062	250.425	RootMyb1	out/IECDLC6p3EWM01_EWM01-30.out
DLC Name	MinRotorFlapBendingMoment	Occurring at time (sec)	on Channel	in File
IECSweep	1434	30.275	RootMyc2	out/IECSweep_ramp.out
IECDLC1p2NTM	-3465	301.375	RootMyc1	out/IECDLC1p2NTM_23mps_seed5.out
IECDLC1p3ETM	-4878	300.663	RootMyc2	out/IECDLC1p3ETM_23mps_seed5.out
IECDLC1p4ECD	-2421	49.175	RootMyc3	out/IECDLC1p4ECD_ECD+R+2.0.out
IECDLC1p5EWS	-1265	46.975	RootMyc1	out/IECDLC1p5EWS_EWSV+25.0.out
IECDLC6p1EWM50	-3357	250	RootMyc1	out/IECDLC6p1EWM50_EWM50+15.out
IECDLC6p3EWM01	-2672	255.887	RootMyc1	out/IECDLC6p3EWM01_EWM01+25.out
DLC Name	MinFlapStrain	Occurring at time (sec)	on Channel	in File
IECSweep	104	32.875	RootMyb1	out/IECSweep_ramp.out
IECDLC1p2NTM	-1140	526.8	Spn7MLyb1	out/IECDLC1p2NTM_23mps_seed4.out
IECDLC1p3ETM	-1383	341.6	Spn7MLyb1	out/IECDLC1p3ETM_23mps_seed6.out
IECDLC1p4ECD	-764	48.263	Spn7MLyb1	out/IECDLC1p4ECD_ECD+R+2.0.out
IECDLC1p5EWS	-907	47.062	Spn7MLyb1	out/IECDLC1p5EWS_EWSV+25.0.out
IECDLC6p1EWM50	-2054	251.488	Spn7MLyb1	out/IECDLC6p1EWM50_EWM50-15.out
IECDLC6p3EWM01	-1331	251.262	Spn7MLyb1	out/IECDLC6p3EWM01_EWM01-15.out
DLC Name	MinEdgeStrain	Occurring at time (sec)	on Channel	in File
IECSweep	-1007	473.1	Spn4MLxb1	out/IECSweep_ramp.out
IECDLC1p2NTM	-1426	205.338	Spn4MLxb1	out/IECDLC1p2NTM_13mps_seed5.out
IECDLC1p3ETM	-1605	162.088	Spn4MLxb1	out/IECDLC1p3ETM_17mps_seed4.out
IECDLC1p4ECD	-1263	61.538	Spn4MLxb1	out/IECDLC1p4ECD_ECD+R.out
IECDLC1p5EWS	-1018	45.25	Spn4MLxb1	out/IECDLC1p5EWS_EWSV+12.0.out
IECDLC6p1EWM50	-288	251.788	Spn4MLxb1	out/IECDLC6p1EWM50_EWM50+05.out
IECDLC6p3EWM01	-194	251.512	Spn4MLxb1	out/IECDLC6p3EWM01_EWM01+05.out
DLC Name	MinOoPDefl	Occurring at time (sec)	on Channel	in File
IECSweep	0.44	999.963	OoPDefl1	out/IECSweep_ramp.out
IECDLC1p2NTM	-2.93	526.812	OoPDefl1	out/IECDLC1p2NTM_23mps_seed4.out
IECDLC1p3ETM	-3.73	280.875	OoPDefl2	out/IECDLC1p3ETM_23mps_seed2.out
IECDLC1p4ECD	-2.04	48.25	OoPDefl1	out/IECDLC1p4ECD_ECD+R+2.0.out
IECDLC1p5EWS	-2.32	47.062	OoPDefl1	out/IECDLC1p5EWS_EWSV+25.0.out
IECDLC6p1EWM50	-1.03	250	OoPDefl1	out/IECDLC6p1EWM50_EWM50+15.out
IECDLC6p3EWM01	-0.73	252.75	OoPDefl1	out/IECDLC6p3EWM01_EWM01+25.out
DLC Name	MinRotorTh	Occurring at time (sec)	on Channel	in File
IECSweep	159.9	30.163	LSShftFxa	out/IECSweep_ramp.out

IECDLC1p2NTM	129.3	526.763	LSShftFxa	out/IECDLC1p2NTM_23mps_seed4.out
IECDLC1p3ETM	81.8	527	LSShftFxa	out/IECDLC1p3ETM_23mps_seed4.out
IECDLC1p4ECD	70.5	48.225	LSShftFxa	out/IECDLC1p4ECD_ECD+R.out
IECDLC1p5EWS	135.5	31.625	LSShftFxa	out/IECDLC1p5EWS_EWSV+3.0.out
IECDLC6p1EWM50	33.2	250	LSShftFxa	out/IECDLC6p1EWM50_EWM50+15.out
IECDLC6p3EWM01	-11.5	298.138	LSShftFxa	out/IECDLC6p3EWM01_EWM01+30.out

Aeroelastic Simulation Outputs – Design 100 low TSR

All values reported here are characteristic values. No safety factors are included in the following table.

DLC Name	MaxFlapBendingMoment	Occurring at time (sec)	on Channel	in File
IECSweep	10990	407.087	RootMyb2	out/IECSweep_ramp.out
IECDLC1p2NTM	15700	400.45	RootMyb1	out/IECDLC1p2NTM_15mps_seed1.out
IECDLC1p3ETM	18810	538.463	RootMyb1	out/IECDLC1p3ETM_19mps_seed2.out
IECDLC1p4ECD	17330	56.8	RootMyb3	out/IECDLC1p4ECD_ECD-R.out
IECDLC1p5EWS	13240	45.625	RootMyb3	out/IECDLC1p5EWS_EWSV+11.0.out
IECDLC6p1EWM50	19310	250	RootMyb1	out/IECDLC6p1EWM50_EWM50+15.out
IECDLC6p3EWM01	13080	250	RootMyb1	out/IECDLC6p3EWM01_EWM01+20.out
DLC Name	MaxRotorFlapBendingMoment	Occurring at time (sec)	on Channel	in File
IECSweep	10990	407.087	RootMyc2	out/IECSweep_ramp.out
IECDLC1p2NTM	15700	400.45	RootMyc1	out/IECDLC1p2NTM_15mps_seed1.out
IECDLC1p3ETM	18810	538.463	RootMyc1	out/IECDLC1p3ETM_19mps_seed2.out
IECDLC1p4ECD	17330	56.8	RootMyc3	out/IECDLC1p4ECD_ECD-R.out
IECDLC1p5EWS	13240	45.625	RootMyc3	out/IECDLC1p5EWS_EWSV+11.0.out
IECDLC6p1EWM50	726	250	RootMyc3	out/IECDLC6p1EWM50_EWM50+10.out
IECDLC6p3EWM01	707	250	RootMyc1	out/IECDLC6p3EWM01_EWM01-30.out
DLC Name	MaxFlapStrain	Occurring at time (sec)	on Channel	in File
IECSweep	1812	404.212	Spn4MLyb1	out/IECSweep_ramp.out
IECDLC1p2NTM	2573	400.45	Spn4MLyb1	out/IECDLC1p2NTM_15mps_seed1.out
IECDLC1p3ETM	3090	538.463	Spn4MLyb1	out/IECDLC1p3ETM_19mps_seed2.out
IECDLC1p4ECD	2870	55.463	Spn4MLyb1	out/IECDLC1p4ECD_ECD-R.out
IECDLC1p5EWS	2111	44.413	Spn4MLyb1	out/IECDLC1p5EWS_EWSV+11.0.out
IECDLC6p1EWM50	3094	250	Spn4MLyb1	out/IECDLC6p1EWM50_EWM50+15.out
IECDLC6p3EWM01	2034	250	Spn4MLyb1	out/IECDLC6p3EWM01_EWM01+20.out
DLC Name	MaxEdgeStrain	Occurring at time (sec)	on Channel	in File
IECSweep	627	34.588	Spn4MLxb1	out/IECSweep_ramp.out
IECDLC1p2NTM	1212	320.138	Spn4MLxb1	out/IECDLC1p2NTM_23mps_seed6.out
IECDLC1p3ETM	1365	282	Spn4MLxb1	out/IECDLC1p3ETM_23mps_seed1.out
IECDLC1p4ECD	863	50.525	Spn4MLxb1	out/IECDLC1p4ECD_ECD+R-2.0.out

IECDLC1p5EWS	636	30.4	Spn4MLxb1	out/IECDLC1p5EWS_EWSV+3.0.out
IECDLC6p1EWM50	1239	250.562	Spn4MLxb1	out/IECDLC6p1EWM50_EWM50-15.out
IECDLC6p3EWM01	694	250	Spn4MLxb1	out/IECDLC6p3EWM01_EWM01-15.out
DLC Name	MaxOoPDefl	Occurring at time (sec)	on Channel	in File
IECSweep	4.19	406.988	OoPDefl2	out/IECSweep_ramp.out
IECDLC1p2NTM	5.91	400.462	OoPDefl1	out/IECDLC1p2NTM_15mps_seed1.out
IECDLC1p3ETM	6.82	538.413	OoPDefl1	out/IECDLC1p3ETM_19mps_seed2.out
IECDLC1p4ECD	6.99	56.825	OoPDefl3	out/IECDLC1p4ECD_ECD-R.out
IECDLC1p5EWS	5.18	45.663	OoPDefl3	out/IECDLC1p5EWS_EWSV+11.0.out
IECDLC6p1EWM50	0.12	250.15	OoPDefl1	out/IECDLC6p1EWM50_EWM50-15.out
IECDLC6p3EWM01	0.21	250	OoPDefl1	out/IECDLC6p3EWM01_EWM01-30.out
DLC Name	MaxRotorTh	Occurring at time (sec)	on Channel	in File
IECSweep	853.4	406.975	LSShftFxa	out/IECSweep_ramp.out
IECDLC1p2NTM	1037.0	191.163	LSShftFxa	out/IECDLC1p2NTM_13mps_seed4.out
IECDLC1p3ETM	1148.0	415.85	LSShftFxa	out/IECDLC1p3ETM_17mps_seed1.out
IECDLC1p4ECD	1032.0	42.75	LSShftFxa	out/IECDLC1p4ECD_ECD-R.out
IECDLC1p5EWS	781.7	49.725	LSShftFxa	out/IECDLC1p5EWS_EWSV+11.0.out
IECDLC6p1EWM50	229.8	250	LSShftFxa	out/IECDLC6p1EWM50_EWM50+00.out
IECDLC6p3EWM01	179.3	250	LSShftFxa	out/IECDLC6p3EWM01_EWM01+00.out
DLC Name	MinFlapBendingMoment	Occurring at time (sec)	on Channel	in File
IECSweep	1488	30.438	RootMyb2	out/IECSweep_ramp.out
IECDLC1p2NTM	-4099	301.462	RootMyb1	out/IECDLC1p2NTM_23mps_seed5.out
IECDLC1p3ETM	-6162	301.312	RootMyb2	out/IECDLC1p3ETM_23mps_seed5.out
IECDLC1p4ECD	-3991	49.15	RootMyb3	out/IECDLC1p4ECD_ECD+R+2.0.out
IECDLC1p5EWS	-2354	46.975	RootMyb1	out/IECDLC1p5EWS_EWSV+25.0.out
IECDLC6p1EWM50	-14800	250.675	RootMyb1	out/IECDLC6p1EWM50_EWM50-15.out
IECDLC6p3EWM01	-10280	250	RootMyb1	out/IECDLC6p3EWM01_EWM01-30.out
DLC Name	MinRotorFlapBendingMoment	Occurring at time (sec)	on Channel	in File
IECSweep	1488	30.438	RootMyc2	out/IECSweep_ramp.out
IECDLC1p2NTM	-4442	301.4	RootMyc1	out/IECDLC1p2NTM_23mps_seed5.out
IECDLC1p3ETM	-6529	301.263	RootMyc2	out/IECDLC1p3ETM_23mps_seed5.out
IECDLC1p4ECD	-3538	49.1	RootMyc3	out/IECDLC1p4ECD_ECD+R+2.0.out
IECDLC1p5EWS	-1944	46.875	RootMyc1	out/IECDLC1p5EWS_EWSV+25.0.out
IECDLC6p1EWM50	-4116	250	RootMyc1	out/IECDLC6p1EWM50_EWM50+15.out
IECDLC6p3EWM01	-3384	250	RootMyc1	out/IECDLC6p3EWM01_EWM01+25.out
DLC Name	MinFlapStrain	Occurring at time (sec)	on Channel	in File
IECSweep	105	918.362	Spn7MLyb1	out/IECSweep_ramp.out
IECDLC1p2NTM	-744	452.013	Spn4MLyb1	out/IECDLC1p2NTM_23mps_seed2.out
IECDLC1p3ETM	-928	453	Spn4MLyb1	out/IECDLC1p3ETM_23mps_seed2.out
IECDLC1p4ECD	-620	48.025	Spn4MLyb1	out/IECDLC1p4ECD_ECD+R+2.0.out

IECDLC1p5EWS	-545	46.963	Spn7MLyb1	out/IECDLC1p5EWS_EWSV+25.0.out
IECDLC6p1EWM50	-2159	250.05	Spn4MLyb1	out/IECDLC6p1EWM50_EWM50-15.out
IECDLC6p3EWM01	-1484	250	Spn4MLyb1	out/IECDLC6p3EWM01_EWM01-30.out
DLC Name	MinEdgeStrain	Occurring at time (sec)	on Channel	in File
IECSweep	-1079	409.825	Spn4MLxb1	out/IECSweep_ramp.out
IECDLC1p2NTM	-1404	302.525	Spn4MLxb1	out/IECDLC1p2NTM_23mps_seed5.out
IECDLC1p3ETM	-1561	415.913	Spn4MLxb1	out/IECDLC1p3ETM_17mps_seed1.out
IECDLC1p4ECD	-1239	57.725	Spn4MLxb1	out/IECDLC1p4ECD_ECD-R.out
IECDLC1p5EWS	-1084	45.125	Spn4MLxb1	out/IECDLC1p5EWS_EWSV+12.0.out
IECDLC6p1EWM50	-301	250	Spn4MLxb1	out/IECDLC6p1EWM50_EWM50+05.out
IECDLC6p3EWM01	-204	250	Spn4MLxb1	out/IECDLC6p3EWM01_EWM01+05.out
DLC Name	MinOoPDefl	Occurring at time (sec)	on Channel	in File
IECSweep	0.58	999.612	OoPDefl3	out/IECSweep_ramp.out
IECDLC1p2NTM	-2.01	301.513	OoPDefl1	out/IECDLC1p2NTM_23mps_seed5.out
IECDLC1p3ETM	-2.50	301.325	OoPDefl2	out/IECDLC1p3ETM_23mps_seed5.out
IECDLC1p4ECD	-1.41	49.225	OoPDefl3	out/IECDLC1p4ECD_ECD+R+2.0.out
IECDLC1p5EWS	-1.57	46.925	OoPDefl1	out/IECDLC1p5EWS_EWSV+25.0.out
IECDLC6p1EWM50	-0.98	250	OoPDefl1	out/IECDLC6p1EWM50_EWM50+15.out
IECDLC6p3EWM01	-0.68	250	OoPDefl1	out/IECDLC6p3EWM01_EWM01+20.out
DLC Name	MinRotorTh	Occurring at time (sec)	on Channel	in File
IECSweep	162.9	30.013	LSShftFxa	out/IECSweep_ramp.out
IECDLC1p2NTM	84.1	526.788	LSShftFxa	out/IECDLC1p2NTM_23mps_seed4.out
IECDLC1p3ETM	38.5	526.663	LSShftFxa	out/IECDLC1p3ETM_23mps_seed4.out
IECDLC1p4ECD	67.7	48.737	LSShftFxa	out/IECDLC1p4ECD_ECD+R.out
IECDLC1p5EWS	161.4	39.513	LSShftFxa	out/IECDLC1p5EWS_EWSV+3.0.out
IECDLC6p1EWM50	65.2	250	LSShftFxa	out/IECDLC6p1EWM50_EWM50+15.out
IECDLC6p3EWM01	17.2	250	LSShftFxa	out/IECDLC6p3EWM01_EWM01+25.out

Aeroelastic Simulation Outputs – Design 100 low TSR flexible

All values reported here are characteristic values. No safety factors are included in the following table.

DLC Name	MaxFlapBendingMoment	Occurring at time (sec)	on Channel	in File
IECSweep	10750	407.188	RootMyb2	out/IECSweep_ramp.out
IECDLC1p2NTM	15420	415.225	RootMyb2	out/IECDLC1p2NTM_15mps_seed1.out
IECDLC1p3ETM	17860	538.463	RootMyb1	out/IECDLC1p3ETM_19mps_seed2.out
IECDLC1p4ECD	17340	55.6	RootMyb1	out/IECDLC1p4ECD_ECD-R.out
IECDLC1p5EWS	12810	45.725	RootMyb3	out/IECDLC1p5EWS_EWSV+11.0.out
IECDLC6p1EWM50	19210	250	RootMyb1	out/IECDLC6p1EWM50_EWM50+15.out
IECDLC6p3EWM01	13040	250	RootMyb1	out/IECDLC6p3EWM01_EWM01+20.out

DLC Name	MaxRotorFlapBendingMoment	Occurring at time (sec)	on Channel	in File
IECSweep	10740	407.138	RootMyc2	out/IECSweep_ramp.out
IECDLC1p2NTM	15420	415.225	RootMyc2	out/IECDLC1p2NTM_15mps_seed1.out
IECDLC1p3ETM	17860	538.463	RootMyc1	out/IECDLC1p3ETM_19mps_seed2.out
IECDLC1p4ECD	17340	55.6	RootMyc1	out/IECDLC1p4ECD_ECD-R.out
IECDLC1p5EWS	12810	45.725	RootMyc3	out/IECDLC1p5EWS_EWSV+11.0.out
IECDLC6p1EWM50	692	250	RootMyc3	out/IECDLC6p1EWM50_EWM50+10.out
IECDLC6p3EWM01	694	250	RootMyc1	out/IECDLC6p3EWM01_EWM01-30.out
DLC Name	MaxFlapStrain	Occurring at time (sec)	on Channel	in File
IECSweep	1900	404.225	Spn4MLyb1	out/IECSweep_ramp.out
IECDLC1p2NTM	2640	400.488	Spn4MLyb1	out/IECDLC1p2NTM_15mps_seed1.out
IECDLC1p3ETM	3180	538.487	Spn4MLyb1	out/IECDLC1p3ETM_19mps_seed2.out
IECDLC1p4ECD	3197	55.575	Spn4MLyb1	out/IECDLC1p4ECD_ECD-R.out
IECDLC1p5EWS	2212	44.5	Spn4MLyb1	out/IECDLC1p5EWS_EWSV+11.0.out
IECDLC6p1EWM50	3333	250	Spn4MLyb1	out/IECDLC6p1EWM50_EWM50+15.out
IECDLC6p3EWM01	2195	250	Spn4MLyb1	out/IECDLC6p3EWM01_EWM01+20.out
DLC Name	MaxEdgeStrain	Occurring at time (sec)	on Channel	in File
IECSweep	417	34.788	Spn4MLxb1	out/IECSweep_ramp.out
IECDLC1p2NTM	714	526.225	Spn4MLxb1	out/IECDLC1p2NTM_23mps_seed4.out
IECDLC1p3ETM	936	281.7	Spn4MLxb1	out/IECDLC1p3ETM_23mps_seed1.out
IECDLC1p4ECD	573	47.15	Spn4MLxb1	out/IECDLC1p4ECD_ECD-R.out
IECDLC1p5EWS	422	51.463	Spn4MLxb1	out/IECDLC1p5EWS_EWSV-3.0.out
IECDLC6p1EWM50	872	250.137	Spn4MLxb1	out/IECDLC6p1EWM50_EWM50-15.out
IECDLC6p3EWM01	546	250	Spn4MLxb1	out/IECDLC6p3EWM01_EWM01-15.out
DLC Name	MaxOoPDefl	Occurring at time (sec)	on Channel	in File
IECSweep	5.62	407.025	OoPDefl2	out/IECSweep_ramp.out
IECDLC1p2NTM	7.77	400.525	OoPDefl1	out/IECDLC1p2NTM_15mps_seed1.out
IECDLC1p3ETM	8.91	538.45	OoPDefl1	out/IECDLC1p3ETM_19mps_seed2.out
IECDLC1p4ECD	9.85	55.6	OoPDefl1	out/IECDLC1p4ECD_ECD-R.out
IECDLC1p5EWS	6.91	45.775	OoPDefl3	out/IECDLC1p5EWS_EWSV+11.0.out
IECDLC6p1EWM50	0.27	250.5	OoPDefl1	out/IECDLC6p1EWM50_EWM50-15.out
IECDLC6p3EWM01	0.33	250	OoPDefl1	out/IECDLC6p3EWM01_EWM01-30.out
DLC Name	MaxRotorTh	Occurring at time (sec)	on Channel	in File
IECSweep	847.7	407.062	LSShftFxa	out/IECSweep_ramp.out
IECDLC1p2NTM	1019.0	415.263	LSShftFxa	out/IECDLC1p2NTM_15mps_seed1.out
IECDLC1p3ETM	1108.0	192.413	LSShftFxa	out/IECDLC1p3ETM_13mps_seed4.out
IECDLC1p4ECD	1025.0	42.788	LSShftFxa	out/IECDLC1p4ECD_ECD-R.out
IECDLC1p5EWS	775.7	49.938	LSShftFxa	out/IECDLC1p5EWS_EWSV-11.0.out
IECDLC6p1EWM50	227.2	250	LSShftFxa	out/IECDLC6p1EWM50_EWM50+00.out
IECDLC6p3EWM01	177.0	250	LSShftFxa	out/IECDLC6p3EWM01_EWM01+00.out

DLC Name	MinFlapBendingMoment	Occurring at time (sec)	on Channel	in File
IECSweep	1425	30.962	RootMyb2	out/IECSweep_ramp.out
IECDLC1p2NTM	-4084	301.462	RootMyb1	out/IECDLC1p2NTM_23mps_seed5.out
IECDLC1p3ETM	-5963	301.238	RootMyb2	out/IECDLC1p3ETM_23mps_seed5.out
IECDLC1p4ECD	-3293	49.125	RootMyb3	out/IECDLC1p4ECD_ECD+R+2.0.out
IECDLC1p5EWS	-2335	46.975	RootMyb1	out/IECDLC1p5EWS_EWSV+25.0.out
IECDLC6p1EWM50	-14700	250	RootMyb1	out/IECDLC6p1EWM50_EWM50-15.out
IECDLC6p3EWM01	-10250	250	RootMyb1	out/IECDLC6p3EWM01_EWM01-30.out
DLC Name	MinRotorFlapBendingMoment	Occurring at time (sec)	on Channel	in File
IECSweep	1425	30.962	RootMyc2	out/IECSweep_ramp.out
IECDLC1p2NTM	-3972	301.462	RootMyc1	out/IECDLC1p2NTM_23mps_seed5.out
IECDLC1p3ETM	-5768	301.212	RootMyc2	out/IECDLC1p3ETM_23mps_seed5.out
IECDLC1p4ECD	-2927	49.075	RootMyc3	out/IECDLC1p4ECD_ECD+R+2.0.out
IECDLC1p5EWS	-1931	46.888	RootMyc1	out/IECDLC1p5EWS_EWSV+25.0.out
IECDLC6p1EWM50	-4102	250	RootMyc1	out/IECDLC6p1EWM50_EWM50+15.out
IECDLC6p3EWM01	-3407	250	RootMyc1	out/IECDLC6p3EWM01_EWM01+25.out
DLC Name	MinFlapStrain	Occurring at time (sec)	on Channel	in File
IECSweep	102	33.013	RootMyb1	out/IECSweep_ramp.out
IECDLC1p2NTM	-1002	452.05	Spn7MLyb1	out/IECDLC1p2NTM_23mps_seed2.out
IECDLC1p3ETM	-1179	342.312	Spn7MLyb1	out/IECDLC1p3ETM_23mps_seed2.out
IECDLC1p4ECD	-625	48	Spn4MLyb1	out/IECDLC1p4ECD_ECD+R+2.0.out
IECDLC1p5EWS	-808	46.975	Spn7MLyb1	out/IECDLC1p5EWS_EWSV+25.0.out
IECDLC6p1EWM50	-2317	250.4	Spn4MLyb1	out/IECDLC6p1EWM50_EWM50-15.out
IECDLC6p3EWM01	-1599	250	Spn4MLyb1	out/IECDLC6p3EWM01_EWM01-30.out
DLC Name	MinEdgeStrain	Occurring at time (sec)	on Channel	in File
IECSweep	-751	409.788	Spn4MLxb1	out/IECSweep_ramp.out
IECDLC1p2NTM	-953	161.538	Spn4MLxb1	out/IECDLC1p2NTM_15mps_seed4.out
IECDLC1p3ETM	-1036	162.188	Spn4MLxb1	out/IECDLC1p3ETM_17mps_seed4.out
IECDLC1p4ECD	-834	44.538	Spn4MLxb1	out/IECDLC1p4ECD_ECD-R-2.0.out
IECDLC1p5EWS	-752	56.987	Spn4MLxb1	out/IECDLC1p5EWS_EWSV+12.0.out
IECDLC6p1EWM50	-231	250	Spn4MLxb1	out/IECDLC6p1EWM50_EWM50+05.out
IECDLC6p3EWM01	-156	250	Spn4MLxb1	out/IECDLC6p3EWM01_EWM01+05.out
DLC Name	MinOoPDefl	Occurring at time (sec)	on Channel	in File
IECSweep	0.61	999.588	OoPDefl3	out/IECSweep_ramp.out
IECDLC1p2NTM	-2.71	342.587	OoPDefl3	out/IECDLC1p2NTM_23mps_seed2.out
IECDLC1p3ETM	-3.31	621.812	OoPDefl1	out/IECDLC1p3ETM_19mps_seed3.out
IECDLC1p4ECD	-1.75	48.1	OoPDefl1	out/IECDLC1p4ECD_ECD+R+2.0.out
IECDLC1p5EWS	-2.20	46.975	OoPDefl1	out/IECDLC1p5EWS_EWSV+25.0.out
IECDLC6p1EWM50	-1.19	250	OoPDefl1	out/IECDLC6p1EWM50_EWM50+15.out
IECDLC6p3EWM01	-0.80	250	OoPDefl1	out/IECDLC6p3EWM01_EWM01+20.out

DLC Name	MinRotorTh	Occurring at time (sec)	on Channel	in File
IECSweep	160.6	30.038	LSShftFxa	out/IECSweep_ramp.out
IECDLC1p2NTM	92.4	526.788	LSShftFxa	out/IECDLC1p2NTM_23mps_seed4.out
IECDLC1p3ETM	47.0	591.713	LSShftFxa	out/IECDLC1p3ETM_5mps_seed2.out
IECDLC1p4ECD	87.8	48.325	LSShftFxa	out/IECDLC1p4ECD_ECD+R.out
IECDLC1p5EWS	159.0	32.875	LSShftFxa	out/IECDLC1p5EWS_EWSV+3.0.out
IECDLC6p1EWM50	65.2	250	LSShftFxa	out/IECDLC6p1EWM50_EWM50+15.out
IECDLC6p3EWM01	14.2	250	LSShftFxa	out/IECDLC6p3EWM01_EWM01+25.out

Computed Fatigue Damage – Design 80

Fatigue damage computations include safety factors as listed in Table 16.

	E-LT-5500(UD)	Newport 307 Carbon Prepreg (UD)
RootMxb1	1.569E-09	
Spn1MLxb1	2.050E-08	
Spn2MLxb1	7.682E-08	
Spn3MLxb1	9.460E-07	
Spn4MLxb1	2.975E-04	
Spn5MLxb1	5.352E-05	
Spn6MLxb1	1.753E-06	
Spn7MLxb1	4.399E-07	
Spn8MLxb1	8.793E-08	
Spn9MLxb1	5.075E-09	
RootMyb1		4.111E-09
Spn1MLyb1		7.129E-07
Spn2MLyb1		1.813E-07
Spn3MLyb1		1.919E-07
Spn4MLyb1		5.778E-06
Spn5MLyb1		3.689E-04
Spn6MLyb1		1.601E-04
Spn7MLyb1		4.030E-04
Spn8MLyb1		1.124E-03
Spn9MLyb1		4.019E-04
Max. damage value	2.975E-04	1.124E-03
Extrapolated life (years)	67233	17788

Computed Fatigue Damage – Design 100 high TSR

Fatigue damage computations include safety factors as listed in Table 16.

	E-LT-5500(UD)	Newport 307 Carbon Prepreg (UD)
RootMxb1	1.3155E-09	
Spn1MLxb1	2.2528E-08	
Spn2MLxb1	1.4439E-07	
Spn3MLxb1	4.9625E-06	
Spn4MLxb1	1.7908E-04	
Spn5MLxb1	4.3355E-05	
Spn6MLxb1	1.2636E-06	
Spn7MLxb1	2.2270E-07	
Spn8MLxb1	3.9396E-08	
Spn9MLxb1	1.8205E-09	
RootMyb1		6.4515E-10
Spn1MLyb1		1.2626E-07
Spn2MLyb1		5.6592E-08
Spn3MLyb1		1.3468E-06
Spn4MLyb1		1.1753E-04
Spn5MLyb1		2.0100E-05
Spn6MLyb1		5.6312E-06
Spn7MLyb1		6.9543E-06
Spn8MLyb1		5.8632E-06
Spn9MLyb1		4.6010E-06
Max. damage value	1.7908E-04	1.1753E-04
Extrapolated life (years)	111683	170173

Computed Fatigue Damage – Design 100 high TSR flexible

Fatigue damage computations include safety factors as listed in Table 16.

	E-LT-5500(UD)	Newport 307 Carbon Prepreg (UD)
RootMxb1	5.135E-11	
Spn1MLxb1	7.218E-10	
Spn2MLxb1	7.768E-09	
Spn3MLxb1	6.474E-07	
Spn4MLxb1	7.117E-05	
Spn5MLxb1	2.005E-05	
Spn6MLxb1	8.879E-07	
Spn7MLxb1	2.249E-07	
Spn8MLxb1	7.621E-08	
Spn9MLxb1	1.706E-08	
RootMyb1		2.208E-10

Spn1MLyb1		3.778E-08
Spn2MLyb1		3.097E-08
Spn3MLyb1		1.360E-06
Spn4MLyb1		2.534E-04
Spn5MLyb1		1.934E-04
Spn6MLyb1		7.446E-04
Spn7MLyb1		5.110E-03
Spn8MLyb1		9.340E-03
Spn9MLyb1		9.187E-03
Max. damage value	7.117E-05	9.340E-03
Extrapolated life (years)	281006	2141

Computed Fatigue Damage – Design 100 low TSR

Fatigue damage computations include safety factors as listed in Table 16.

	E-LT-5500(UD)	Newport 307 Carbon Prepreg (UD)
RootMxb1	2.988E-09	
Spn1MLxb1	3.960E-08	
Spn2MLxb1	2.131E-07	
Spn3MLxb1	7.273E-06	
Spn4MLxb1	6.549E-04	
Spn5MLxb1	4.971E-05	
Spn6MLxb1	9.703E-07	
Spn7MLxb1	1.738E-07	
Spn8MLxb1	3.826E-08	
Spn9MLxb1	4.114E-09	
RootMyb1		1.957E-08
Spn1MLyb1		2.934E-06
Spn2MLyb1		2.719E-06
Spn3MLyb1		1.014E-04
Spn4MLyb1		4.576E-03
Spn5MLyb1		3.599E-04
Spn6MLyb1		4.176E-05
Spn7MLyb1		2.520E-05
Spn8MLyb1		3.559E-05
Spn9MLyb1		1.288E-05
Max. damage value	6.549E-04	4.576E-03
Extrapolated life (years)	30541	4371

Computed Fatigue Damage – Design 100 low TSR flexible

Fatigue damage computations include safety factors as listed in Table 16.

	E-LT-5500(UD)	Newport 307 Carbon Prepreg (UD)
RootMxb1	9.365E-10	
Spn1MLxb1	1.127E-08	
Spn2MLxb1	3.270E-08	
Spn3MLxb1	4.358E-07	
Spn4MLxb1	1.255E-05	
Spn5MLxb1	9.123E-07	
Spn6MLxb1	1.661E-08	
Spn7MLxb1	3.591E-09	
Spn8MLxb1	2.009E-09	
Spn9MLxb1	3.282E-09	
RootMyb1		1.004E-08
Spn1MLyb1		1.467E-06
Spn2MLyb1		1.660E-06
Spn3MLyb1		8.661E-05
Spn4MLyb1		6.786E-03
Spn5MLyb1		1.093E-03
Spn6MLyb1		7.574E-04
Spn7MLyb1		3.761E-03
Spn8MLyb1		2.012E-02
Spn9MLyb1		1.331E-02
Max. damage value	1.255E-05	2.012E-02
Extrapolated life (years)	1593254	994

APPENDIX E - BILL OF MATERIALS AND MATERIAL COST

Early cost models were based on scaling approaches. A commonly referenced scaling approach is outlined in Reference [27] in which scaling was primarily driven by rotor size.

The weight of individual dry fabrics and resin are used to compute blade material costs (Table 26) in a higher fidelity approach as demonstrated by Griffith [15]. Rows 1, 2, 3, 4, 8, 9 and 11 in Table 26 are material weights computed directly from the ANSYS models of the blades. Assumed fiber volume fractions and material densities were used to infer the mass of actual fiber (rows 6 and 7) and resin (row 10). The triaxial material used for root buildup and skins was assumed to be made from a combination of unidirectional fiber (row 6) and double-bias fiber (row 7). No parasitic resin was assumed in these designs. Materials costs were taken from Griffith. Blade three dimensional areas were computed by NuMAD and represent the total wetted area of the blade skins (row 12). Cost of kitting and materials for the core material (rows 13-17) was computed based on skin area.

The approach in Griffith [15] was used to estimate labor and tooling costs of these blades; results are found in the report in Table 4. The blade costs do not include considerations for labor and tooling. Labor and tooling costs are expected to be relatively consistent across all the designs.

Table 26: Blade bills of material and costs

					Design 80		Design 100 low TSR		Design 100 high TSR		Design 100 low TSR flexible		Design 100 high TSR flexible	
		Raw material cost ($/kg)	Fiber volume fraction	Triax composition, %uni	kg	% blade mass	kg	% blade mass	kg	% blade mass	kg	% blade mass	kg	% blade mass
(1)	Blade mass (kg)				16068		16423		17590		15611		14607	
(2)	(TE-Reinf.) E-LT-5500 Uni,wet (kg)		0.540		779		957		1987		1562		1319	
(3)	(SW) Saertex DB,wet (kg)		0.440		888.3		838.6		692.9		841.7		692.9	
(4)	(Root & Skins) Triax, wet (kg)		0.492	51.89%	9006		8922		7990		8922		7985	
(5)	Parasitic Resin (kg)				0		0		0		0		0	
(6)	E-LT-5500 Uni fiber	$ 2.97			2,552	15.9%	2,628	16.4%	2,964	18.4%	2,955	18.4%	2,602	16.2%
(7)	Saertex DB fiber	$ 2.97			2,690	16.7%	2,646	16.5%	2,344	14.6%	2,648	16.5%	2,343	14.6%
(8)	(Core) Foam				2899.8	18.0%	2693	16.8%	1561	9.7%	2308	14.4%	1619	10.1%
(9)	(Gelcoat)	$ 14.00			26.48	0.2%	26.59	0.2%	21.90	0.1%	26.59	0.2%	21.90	0.1%
(10)	Total Resin	$ 4.65			5,432	33.8%	5,443	33.9%	5,362	33.4%	5,723	35.6%	5,052	31.4%
(11)	(Spar Cap) Newport 307 Prepreg (incl. resin)	$ 26.40			2468	15.4%	2986	18.6%	5336	33.2%	1951	12.1%	2969	18.5%
	Blade material cost estimation													
(12)	Blade 3D area (m^2, HP and LP)				428		430		356		430		356	
(13)	Foam kitting cost ($/m^2)				$ 20.00		$ 20.00		$ 20.00		$ 20.00		$ 20.00	
(14)	Foam kitting cost ($)				$ 8,560		$ 8,600		$ 7,120		$ 8,600		$ 7,120	
(15)	Foam effective thickness, t_eff (mm)				33.9		31.3		21.9		26.8		22.7	
(16)	Foam cost based on t_eff ($/m^2)				$ 16.94		$ 15.66		$ 10.96		$ 13.42		$ 11.37	
(17)	Total foam cost, kitting + matl				$15,809.50		$ 15,332.50		$ 11,022.50		$ 14,370.00		$ 11,167.50	
(18)	Total blade material cost				$ 122,170		$ 135,511		$ 192,897		$ 109,501		$ 128,034	
(19)	Effective blade material cost ($/kg)				$ 7.60		$ 8.25		$ 10.97		$ 7.01		$ 8.77	

DISTRIBUTION

1	MS0899	Technical Library	9536 (electronic copy)


Sandia National Laboratories